Airflow and Aerosol Concentration in a Ribbed Smoked Sheet Rubber Cooperative and Improvement of Ventilation

Lasman Parulian Purba

A Thesis Submitted in Fulfillment of the Requirements for the Degree of
Master of Engineering in Mechanical Engineering
Prince of Songkla University

2009

Thesis Title	**Airflow and Aerosol Concentration in a Ribbed Smoked Sheet Rubber Cooperative and Improvement of Ventilation**
Author	Mr. Lasman Parulian Purba
Major Program	**Master of Engineering in Mechanical Engineering**

Major Advisor

……
(Assoc. Prof. Dr. Perapong Tekasakul)

Co-advisor

……
(Dr. Kittinan Maliwan)

Examining Committee:

…….Chairperson
(Asst. Prof. Dr. Suchart Limkatanyu)

……..…Committee
(Assoc.Prof. Dr. Masami Furuuchi)

……..Committee
(Dr. Nakorn Tippayawong)

…….Committee
(Dr. ……)

The Graduate School, Prince of Songkla University, has approved this thesis as partial fulfillment of the requirements for the Master of Engineering Degree in Mechanical Engineering.

……
(Assoc. Prof. Dr. Krerkchai Thongnoo)
Dean of Graduate School

Thesis Title	**Airflow and Aerosol Concentration in a Ribbed Smoked Sheet Rubber Cooperative and Improvement of Ventilation**
Author	Mr. Lasman Parulian Purba
Major Program	Master of Engineering in Mechanical Engineering
Academic Year	2008

ABSTRACT

A computational fluid dynamics (CFD) method was used to investigate the velocity, temperature, particles trajectories, and particles concentration distribution in a present natural rubber sheet smoking cooperative, to improve a ventilation system (for airflows as well as aerosol particles). The measured velocity and temperature data at various locations were used as boundary conditions and to validate the CFD model. Simulation was performed using turbulent free convection flows where the Rayleigh number was found to be between 5.3838×10^{10} and 33.2003×10^{10}. A total of 2,159,347 mesh volumes were applied to the entire ribbed smoked sheet rubber Cooperative. It was found that the results from the CFD simulation and experiment are in good agreement. The air contains particles flows naturally from ventilating lids of the smoking room to the roof. Experimental and simulation results show that the thick cloud of smokes has a long residence time in the roof area. The smoke particles follow the airflow fields where some of them leave the junction of the roof and the others deposit onto the walls. The smoke particles that leave the junction of the roof then travel to the workplace areas which then make the workers feel uncomfortable and irritable. Aerosol particle ventilation could be satisfactorily improved by appropriate roof ridge vent.

Keywords: Computational fluid dynamics, Flow simulation, Aerosol concentration, Free convection, Rubber smoking-cooperative, Ventilation of airflow.

ACKNOWLEDGEMENTS

Several people played important roles in accomplishment of this thesis. I would like to acknowledge them here.

Assoc. Prof. Dr. Perapong Tekasakul as the main advisor. Without his advice, the thesis would have not been completed. His directions are the best things to do or follow.

Dr. Kittinan Maliwan as a co-advisor. Without his contribution, the thesis would have not been powerful.

Assoc. Prof. Dr. Masami Furuuchi as the second co-advisor for useful advice.

Asst. Prof. Dr. Suchart Limkatanyu for his availability about my thesis defense.

Dr. Nakorn Tippayawong for his useful comments about my thesis.

Dr. Chayut Nuntadusit for the colourful comments at the thesis progress examination.

Dr. Jeerapa Sookgaew for the comments at the thesis progress examination.

Asst. Prof. Dr. Charoenyut Dechwayukul as the Head of Mechanical Engineering Department for his supported comments about my study.

Besides them, there are Mr. Teerapol Chanwarin my best partner, and SAMO crew, Mr. Werachai Kao-ien, and all graduate students of Mechanical Engineering. Thanks also go to Mr. Phoungthong Khamphe, Mr. Mason Sandkhamanee, Mrs. Jirapon Chomanee, Ms. Thitiworn Choosong, and Asst. Prof. Dr. Surajit Tekasakul for support during measurements.

To perform the administrative work about my study, Ms. Nutcha Pankaew, Mrs. Pranom Pakdeerugeerat, Mrs. Puchalee Thongcharoen, Ms. Arisa Prasompong, Mrs. Kingkarn Tonnayopas, and Ms. Kuttiyaporn Chaisawat are very helpful.

Mr. Chalad Yuenyao, Mr. Naret Jindapet, Mr. Wacharapong Innupat, and Mr. Banyat Niyomvas are also helpful until I finish this thesis writing.

Least but not last, I would like to thank my wife (Evi Thelia Sari) and my son (Mercidominick F. C. M. Purba alias Nico) for their snacks, love and understanding.

It's is not enough to write all of the persons who ever help me until I finish the thesis: thanks a lot.

Lasman Parulian Purba, Mr. (Lasman)

List of Tables

List of Figures

List of Figures (continued)

Figures of Velocity Fields

Figures of Temperature Field

Figures of Particle Trajectory

List of Figures (continued)

Figures of Particles Concentration

Figures of Ventilation Improvement

Figures of Case 2

List of Figures (continued)

Figures of Case 3

Figures of Case 4

List of Figures (continued)

List of Abbreviations and Symbols

Abbreviations

AHU	Air Handling Unit
CBNP	Chemical & Biological Nonproliferation Program
CFD	Computational Fluid Dynamics
DPM	Discrete Phase Model
EPA	Environmental Protection Agency
FVM	Finite-Volume Method
GDE	General Differential Equation
GEV	General Exhaust Ventilation
LEV	Local Exhaust Ventilation
MMAD	Mass Median Aerodynamics Diameter
PAH	Polycyclic Aromatic Hydrocarbon
RSP	Respirable Suspended Particle
RSSC	Rubber Sheet Smoked Cooperative
SD	Standard Deviation
SPE	Species Module of FLUENT
VOC	Volatile Organic Compound

Symbols

C_c	The Cunningham Correction Factor
C_P	Specific Heat, J/(kg.K)
D_i	The Diffusion Coefficient
d_p	The Particle Diameter, m

G_b	The Generation of k Buoyancy
g_i	Gravitational Vector (Force), m/s^2
G_k	The Generation of k due to The Mean Velocity Gradient
H	Height, m
k	Turbulent Kinetic Energy
p	Pressure, Pascal, Pa
Pr_t	The Turbulent Prandtl Number for Energy
Ra	Rayleigh Number
S_i	The Source/Sink Term
S_k	User-Defined Source Terms for k
S_ε	User-Defined Source Terms for ε
T	Temperature, ^{o}C
t	Time, second
u	Velocity Vector, (u, v, w), m/s
u_p	The Particle Velocity, m/s
X_i	The Mass Fraction
x_i	Coordinate Axis (x, y, z)
Y_M	The Contribution of The Fluctuating Dilatation in Compressible Turbulence to The Overall ε

Greek Symbols

α	Thermal Diffusivity, m^2/s
β	Thermal Expansion Coefficient, K^{-1}
ε	Turbulent Dissipation Rate

θ	Temperature Profiles
λ	The Molecular Mean Free Path
μ	Viscosity, kg/(m.s)
μ_t	The Turbulent (or Eddy) Viscosity
v	Kinematic Viscosity, m^2/s
ρ	Density, kg/m^3
ρ_p	The Density of The Particle, kg/m^3
σ_k	The Turbulent Prandtl Numbers for k
σ_ε	The Turbulent Prandtl Numbers for ε

Contents

Contents (continued)

Chapter 1

Introduction

1.1 Rubber Sheet Smoking

Thailand is the largest natural rubber (*Hevea brasiliensis*) producer in the world (Ministry of Commerce Thailand, 2007). One of the main products is the ribbed smoked sheet rubber. Currently, production of ribbed smoked sheet is shifted from large factories to small-scale community-based ribbed smoked sheet rubber cooperatives. Currently, in total there are about 500 rubber cooperatives in Thailand. In general, there are two models of ribbed smoked sheet rubber cooperative, the 1994 and 1995 models. These two models differ in the size of smoking rooms and hence, the capacity for the rubber sheets. For the 1994 model, the size of the rubber sheet smoking room is 2.5 m (width) x 4.0 m (height) x 6.0 m (depth), one half of that for the 1995 model. In the ribbed smoked sheet production, rubber-wood is burned to supply heat and smoke to the rubber sheets in a smoking room (Promtong and Tekasakul, 2007; Tekasakul and Promtong, 2008). Burning of woods generates a large portion of fine smoke aerosol particles. This is potentially harmful to workers in the factories as part of the particles is allowed to flow into the workplace area in the ribbed smoked sheet rubber cooperative (Fig 1.1). Improvement of the airflow is then necessary to reduce the risk to workers' health by exposure to these smoke particles. Some particle concentration data have recently been obtained (Choosong et al., 2007). However, no studies of airflow inside the workplace area have been conducted so far. Therefore, it is necessary to study the airflow, particle trajectories and concentration

inside the workplace area of ribbed smoked sheet rubber which leads to an appropriate way in controlling or ventilating the particles.

The research is started with simulation of airflow distribution (velocity and temperature distributions) and particle concentration inside of the ribbed smoked sheet rubber cooperative as well as smoke particle trajectories. FLUENT CFD package with GAMBIT will be used, to perform the simulation of airflow as well as aerosol transport in the current smoking cooperative. Experimental verification of particle concentration will be performed. Then improvement of airflow inside the cooperative will be studied by CFD simulation.

Fig 1.1 Workplace area of the ribbed smoked sheet rubber cooperative.

1.2 Objectives

1. To study airflow and aerosol transport in a ribbed smoked sheet rubber cooperative.

2. To improve airflow in the cooperative to lessen risk of workers exposed to a large portion of smoke aerosol particles.

1.3 Scope of Study

1. CFD Simulation of airflow and aerosol concentration in a current ribbed smoked sheet rubber cooperative.
2. Experimental measurements of source concentration and workplace concentration in the cooperative.
3. CFD Simulation to improve airflow in the cooperative.

1.4 Organization of the Thesis

Chapter 2 focuses on literature review of several topics relevant to the scope of the thesis. Chapter 3 presents the domain of problem, measurements setup including apparatus for measurement of temperature, velocity, aerosol concentration, and CFD Simulation details includes system/boundary conditions, grid generation and verification, and turbulent model used. Results and discussions are presented in Chapter 4 following by the Conclusion in Chapter 5.

Chapter 2

Literature Review

This chapter presents a literature review of the topics related to this thesis work: aerosol and its effects, fluid flow, the standard $k-\varepsilon$ turbulence model, aerosol transport, ventilation, and CFD technique.

2.1 Aerosol Transport and Its Effects

An aerosol is defined in its simplest form as a collection of solid or liquid particles suspended in a gas (Seinfeld and Pandis, 1998; Hinds, 1999). Since the early 1970s, aerosol particles have been distinguished as fine and coarse (Whitby, 1978). Coarse particles refer to particulate matters larger than 2.5 micrometers in diameter, while fine particles refer to particulate matters smaller than 2.5 micrometers. Aerosol particles smaller than 1.0 micrometer are known as submicron particles. However, Nazaroff (2004) classified particles according to their diameter into three size modes; ultra-fine (smaller than 0.1 micrometer), accumulation (0.1 to 2 micrometer), and coarse (larger than 2 micrometer). Smoke particles generated from burning of rubber-wood considered in this work are mostly in an accumulation mode having mass median aerodynamics diameter (MMAD) of 0.95 micrometer (Kalasee et al., 2003)

Smoke is a visible aerosol resulting from incomplete combustion or pyrolysis (British Standards BS4422, 1987; ISO 8421-1, 1987; Hinds, 1999). It is known that the airflow pattern plays a fundamental role in the deposition, migration and distribution of aerosol particles (Lu and Howarth, 1996). Choosong et al., (2007)

studied indoor air quality of working environment in a rubber sheet smoking factory in Thailand. Working environment in a ribbed smoked sheet rubber cooperative has been monitored focusing on polycyclic aromatic hydrocarbons (PAHs) pollutants in particular. Personal exposure to particle-bound PAHs was sampled by using a personal sampler, while size fractionated particles were sampled by an Andersen Sampler. The summary of their investigation by using respiratory symptom questionnaire, there were symptoms which very likely to be related to pollutants in the workplace. From the summary of experiment; the worker's main discomforts were smoke and odor, the average PAHs concentration in the workplace area was more than 5 times larger than in the ambient.

Kanaoka et al. (2006) investigated numerically the flow and dust concentration distributions in the work area of a mountain tunnel under construction. Flow patterns, dust concentration profile, and particle motion were also investigated numerically. CFD Package FLUENT 5.2 was used in the numerical simulation of flow through the traffic tunnel. The aerosol particle concentration distributions were calculated by assuming the dust-laden air to be a fluid having the same density as air. The results show that the dust concentration near the working face was extremely high and was too spatially variable to be accurately described by the average dust concentration in the area between the working face and the air inlet.

Loomans et al. (2002) described three approaches for the calculation of the particle contaminant distribution in a room using CFD. The approaches were tested for two types of flow problem; comparison uses particle measurement results from literature for clean room ventilation conditions, comparison uses new measurement

results obtained from bio aerosol measurements in an office room. The results indicate that the Eulerian approach, in which only the particle settling velocity is incorporated, presents an attractive alternative to the Lagrangian approach. The Passive Scalar approach should not be used to calculate the particle distribution in a room.

Lu et al. (1996) presented a method using a single phase to represent air and particle flow. The Eulerian approach regarding the flow medium as a continuous fluid (air) was used to solve the whole set of equations for the continuum at all control volumes and obtain the results of fluid velocity over the whole flow field. Besides the Eulerian methods for solving the continuous fluid, a discrete trajectory approach (Lagrangian Method) was employed in the particle tracking model. The Lagrangian approach splits the particle phase into a representative set of individual particles and tracks these particles separately through the airflow domain by solving the equations of particle movement.

Indicator of contamination of aerosol particles in a closed space or indoor air is the contaminant concentration, i.e. the mass of contaminant per unit volume of air, mass concentration (measured in mg/m^3). Sometimes it is shown in number of contaminant per unit volume of air, number concentration (measured in $number/m^3$). In this work, the definition of mass concentration will be used.

Mathematical models and theory involved in aerosol particle transport are presented in this section. Aerosol technology is the study of properties, behavior, and physical principles of aerosols and application of this knowledge to their measurement and control. The particulate phase of an aerosol represents only a very

small fraction of its total mass and volume, less than 0.0001%. Bulk properties of aerosols, such as viscosity and density, differ imperceptibly from those of pure air. Consequently, to study the properties of aerosols, one must adopt a microscopic point of view (Hinds, 1999).

In the presence of a velocity field, the conservation equation for a chemical species *i* take the following form:

$$\frac{\partial}{\partial t}(\rho X_i) + \nabla \cdot (\rho \mathbf{u} X_i) = \nabla \cdot (\rho D_i \nabla X_i) + S_i \tag{1}$$

where $\mathbf{u}$ is the velocity, X_i is the mass fraction, D_i is the diffusion coefficient, and S_i is the source/sink term.

By assuming particle flow as continuum, aerosol particle trajectory can be known by representing them in the discrete phase. This phase can be modeled by using the discrete phase model (DPM) of FLUENT. The trajectory of a discrete phase particles is predicted by integrating the force balance on the particle, which is written in a Lagrangian frame of reference. This force balance equates the particle inertia with the forces acting on the particle, and can be written (for the *x* direction in Cartesian coordinates) as (Chow et al., 2003):

$$\frac{du_p}{dt} = F_D(u - u_p) + \frac{g_x(\rho_p - \rho)}{\rho_p} + F_x \tag{2}$$

where F_D is the Stokes' law drag force for submicron particles defined as

$$F_D = \frac{18\mu}{\rho_p d_p^2 C_c} \tag{3}$$

Here, u is the fluid phase velocity, u_p is the particle velocity, μ is the molecular viscosity of the fluid, ρ is the fluid density, ρ_p is the density of the particle, and d_p is the particle diameter. C_c is the Cunningham correction to Stokes' drag law to a spherical particle, which can compute from,

$$C_c = 1 + \frac{2\lambda}{d_p}\left(1.257 + 0.4e^{-\left(\frac{1.1 d_p}{2\lambda}\right)}\right) \tag{4}$$

where λ is the molecular free path.

When a temperature gradient is established in a gas, an aerosol particle in that gas experiences a force, thermophoretic force, in the direction of decreasing temperature (Hinds, 1999). Thermal force and aerosol particle motion are always in the direction of decreasing temperature. In this work, thermophoretic force on particles is not included as the additional force term, F_x (Eqs. 5), because the flow containing aerosol particles has a small temperature gradient:

$$F_x = -D_{th}\frac{1}{m_p T}\frac{\partial T}{\partial x} \tag{5}$$

where D_{th} is the thermophoretic coefficient.

The Discrete Phase Model (DPM) is primarily used to simulate the transport of large, individual particles. Large super micron particles are usually formed by mechanical processes. Submicron particles are usually formed by chemical processes. The DPM in FLUENT is primarily useful for simulating the dynamics of super micron particles. It can be used to simulate the transport of particles. In this study, the DPM is used to simulate dynamics of smoke aerosol particles.

2.2 Fluid Flow

Since the work in this research involves simulation of air flow, particle trajectories and concentration in a workplace area of a ribbed smoked sheet rubber cooperative, theoretical background of fluid flow will be presented.

The numerical solution of fluid flow, and other related processes can begin with the laws governing these processes expressed in mathematical forms, generally in terms of differential equations (Patankar, 1980). The individual equations describe a certain conservation principle. Each equation employs a certain physical property as its dependent variable. The dependent variables are usually specific extensive properties, i.e., properties expressed on a unit-mass basis. Examples are: mass fractions, velocity (momentum per unit mass), specific enthalpy, particle concentration per unit mass (Stratman et al., 2006).

From fluid dynamics, the continuity equation describing mass conservation can be written as:

$$\frac{\partial \rho}{\partial t} + \nabla \cdot (\rho \mathbf{u}) = 0 \tag{6}$$

If the flow under consideration is steady flow the first term on the left-hand side of Eqs. (6) simply varnishes.

The differential equations for the conservation of momentum for an incompressible flow, or the Navier-Stokes Equations, take the following form:

$$\nabla \cdot (\rho \mathbf{u} u) = \nabla \cdot (\mu \nabla \mathbf{u}) - \nabla p \tag{7}$$

where μ is the viscosity [kg/(m.s)], $\mathbf{u}$ is the velocity [m/s], and p is the pressure [Pa].

The energy equation can be written as:

$$\rho C_P \frac{DT}{Dt} = k\nabla^2 T + \mu\theta \tag{8}$$

where:

$$\theta = 2\left[\left(\frac{\partial u}{\partial x}\right)^2 + \left(\frac{\partial v}{\partial y}\right)^2 + \left(\frac{\partial w}{\partial z}\right)^2\right] + \left[\left(\frac{\partial u}{\partial y} + \frac{\partial v}{\partial x}\right)^2 + \left(\frac{\partial v}{\partial z} + \frac{\partial w}{\partial y}\right)^2 + \left(\frac{\partial w}{\partial x} + \frac{\partial u}{\partial z}\right)^2\right] - \frac{2}{3}\left(\frac{\partial u}{\partial x} + \frac{\partial v}{\partial y} + \frac{\partial w}{\partial z}\right)^2 \tag{9}$$

Here $\nabla^2 T$ is the Laplacian term and k is the thermal conductivity.

Patankar (1980), White (1988) and many researchers use the general differential equation (GDE) which can denote the dependent variable as Φ in the form of Eulerian conservation equation:

$$\frac{\partial}{\partial t}(\rho\Phi) + \nabla\cdot(\rho u\Phi) = \nabla\cdot(\Gamma_\Phi \nabla\Phi) + S_\Phi \tag{10}$$

where $\partial(\rho\Phi)/\partial t$ is the unsteady term, $\nabla\cdot(\rho u\Phi)$ is the convective heat transfer term, $\nabla\cdot(\Gamma_\Phi\nabla\Phi)$ is the diffusive term, and S_Φ is the generalized source/sink. Here Φ is the variety of different quantities, such as the mass component, the turbulence kinetics energy, or a turbulence length scale, which is given in detail in Table 3.2.

2.3 Turbulence Model

The flow, in general, in a workplace of the ribbed smoked sheet rubber cooperative is natural and it is turbulent with the Rayleigh number, $Ra = g\beta(T_s - T_\infty)H^3/\nu\alpha$ lies between 5.38 x 10^{10} to 33.20 x 10^{10} (for ΔT between 1.2 to 7.4ºC). The critical value of Ra is 10^9. When heat is added to a fluid and the fluid density varies with temperature, a flow can be induced due to the buoyancy

force. To consider if the flow is mixed convection or only natural (free) convection, calculation of the ratio between Grashoff number and squared Reynold numbers $\left(Gr/\mathrm{Re}^2 = g\beta\Delta TH/V^2\right)$ needs to be performed. According to the real measurement, values of velocity near the walls is always zero, and about 0.01 m/s at about 10 cm from the vertical walls, and average value of 0.08 m/s for free stream flows, so the fluid flows to be modeled and solved behave as natural convection and a mixed convection. In our case, Gr is 6.7584 x 10^{10} and Re is 10580.43 so that Gr/Re^2 is 63.876. Since $Gr/\mathrm{Re}^2 > 1$, the flow is strongly influenced by buoyancy. In the calculation, β is 0.0032/K, ΔT is 1.2ºC. There are various turbulent models developed to date. In this work, the most widely used standard $k-\varepsilon$ turbulent model will be used. Robustness, economy, and reasonable accuracy for a wide range of turbulent flows explain its popularity in industrial flow and heat transfer simulations. It is a semi-empirical model, and the derivation of the model equations relies on phenomenological considerations and empiricism. Therefore, its principle and details will be presented here.

The standard k-ε model is a model transport equations for the turbulence kinetic energy (k) and its dissipation rate (ε). The model transport equation for k is derived from the exact equation, while the model transports equation for ε was obtained using physical reasoning and it bears little resemblance to its mathematically exact counterpart. In the derivation of the k-ε model, the assumption is that the flow is fully turbulent, and the effects of molecular viscosity are negligible. The standard k-ε model is therefore valid only for fully turbulent flows (Launders and Spalding, 1972; White, 1988).

The turbulence kinetic energy, k, and its rate of dissipation, ε, are obtained from the following transport equations:

$$\frac{\partial}{\partial x_i}(\rho k u_i) = \frac{\partial}{\partial x_j}\left[\left(\mu + \frac{\mu_t}{\sigma_k}\right)\frac{\partial k}{\partial x_j}\right] + G_k + G_b - \rho\varepsilon - Y_M + S_k \tag{11}$$

and

$$\frac{\partial}{\partial x_i}(\rho \varepsilon u_i) = \frac{\partial}{\partial x_j}\left[\left(\mu + \frac{\mu_t}{\sigma_k}\right)\frac{\partial \varepsilon}{\partial x_j}\right] + C_{1\varepsilon}\frac{\varepsilon}{k}(G_k + C_{3\varepsilon}G_b) - C_{2\varepsilon}\rho\frac{\varepsilon^2}{k} + S_\varepsilon \tag{12}$$

In these equations, G_k represents the generation of turbulence kinetic energy due to the mean velocity gradients, G_b is the generation of turbulence kinetic energy due to buoyancy, Y_M represents the contribution of the fluctuating dilatation in compressible turbulence to the overall dissipation rate, $C_{1\varepsilon}$, $C_{2\varepsilon}$ and $C_{3\varepsilon}$ are constants, σ_k and σ_ε are the turbulent Prandtl numbers for k, and ε, respectively, S_k and S_ε are user-defined source terms. The turbulent (or eddy) viscosity, μ_t, is computed by combining k and ε as follows:

$$\mu_t = \rho C_\mu k^2 / \varepsilon \tag{13}$$

where C_μ is a constant. The model constants $C_{1\varepsilon}$, $C_{2\varepsilon}$, C_μ, σ_k, and σ_ε have the following default values (Launders and Spalding, 1972):

$$C_{1\varepsilon} = 1.44 \quad C_{2\varepsilon} = 1.92 \quad C_\mu = 1.92 \quad \sigma_k = 1.0 \quad \sigma_\varepsilon = 1.0$$

These default values have been determined from experiments with air and water for fundamental turbulent shear flows including homogeneous shear flows and decaying isotropic grid turbulence. They have been found to work fairly well for a wide range

of wall-bounded and free shear flows. However, the default values of the model constants are the standard ones most widely accepted.

The generation of turbulence due to buoyancy G_b is given by:

$$G_b = \beta g_i \frac{\mu_t}{\mathrm{Pr}_t} \frac{\partial T}{\partial x_i} \tag{14}$$

where Pr_t is the turbulent Prandtl number for energy and g_i is the component of the gravitational vector in the i-th direction. For the standard k -ε models, the default value of Pr_t is 0.85. The coefficient of thermal expansion, β, is defined as

$$\beta = -\frac{1}{\rho}\left(\frac{\partial \rho}{\partial T}\right)_p \tag{15}$$

The transport equations for k (Eqs. 11) shows that the turbulence kinetic energy tends to be increased (G_b>0) in unstable stratification and for stable stratification, buoyancy tends to suppress the turbulence (G_b<0).

The effects of buoyancy on the generation of k are always included when a non-zero gravity field and a non-zero temperature (or density) gradient are present simultaneously. While the buoyancy effects on the generation of k are relatively well understood, the effect on ε is less clear. The buoyancy effects on ε are neglected simply by setting G_b to zero in the transport equation for ε (Eqs. 12).

The degree to which ε is affected by the buoyancy is determined by the constant $C_{3\varepsilon}$. In FLUENT, $C_{3\varepsilon}$ is not specified, but is instead calculated according to the following relation (Henkes et al., 1991):

$$C_{3\varepsilon} = \tanh \left| \frac{v}{u} \right| \tag{16}$$

where v is the component of the flow velocity parallel to the gravitational vector and u is the component of the flow velocity perpendicular to the gravitational vector. In this way, $C_{3\varepsilon}$ will become 1 for buoyant shear layers for which the main flow direction is aligned with the direction of gravity. For buoyant shear layers that are perpendicular to the gravitational vector, $C_{3\varepsilon}$ will become zero. The contribution of the fluctuating dilatation in compressible turbulence to the overall dissipation rate (Y_M) equals zero for the incompressible flow.

2.4 Ventilation

Ventilation is defined as one of the most important engineering controls available to the industrial hygienist for improving or maintaining the quality of the air in the occupational work environment. It is a method of controlling the environment with air flow, the intentional movement of air from outside a building to the inside. Ventilation is used for providing acceptable indoor air quality. When humans are present in buildings, ventilation air is necessary to dilute odors and limits the concentration of harmful materials, such as carbon dioxide, carbon monoxide, and airborne pollutants such as respirable suspended particles (RSPs), volatile organic compounds (VOCs) and also PAHs. Ventilation air is often delivered to spaces by mechanical systems which may also heat, cool, humidify and dehumidify the space. Air movement into buildings can occur due to uncontrolled infiltration of outside air through the building fabric or the use of deliberate natural ventilation strategies.

Vincent (1995), Gant et al., (2006), Xu (2003) attempted to study the reduction of risk to industrial hygienist workers associated with exposure to aerosol. It is clear that ventilation (Vincent, 1995), and aerosol properties (Gant et al., 2006) are the major components affecting aerosol transport around the room.

Xu (2003) showed that ventilation plays an active role in exhausting contaminants, diluting potentially contaminated indoor air, as well as controlling the indoor humidity and temperature. He also described two ways of ventilation in houses, mechanical ventilation which is independent from the building shell, and natural ventilation which relies on leakages or openings, such as windows and doors.

Mechanical or forced ventilation systems circulate fresh air using ducts and fans, rather than relying on airflow through small holes or cracks in a home's walls, roof, or windows. It can be implemented through an air handling unit (AHU) of an air-conditioning system or direct injection to a space by a fan. A local exhaust fan can enhance infiltration or natural ventilation, thus increasing the ventilation air flow rate. If the mechanical ventilation operates constantly and consistently, it will be good for indoor environment. Of course, this will lead to more energy consumption.

Local exhaust ventilation (LEV) is one of the techniques used in industrial hygiene process (Vincent, 1995). This technique involves the capture of airborne contaminants released from industrial processes before they can become widely dispersed into the workplace environment.

Natural ventilation is used to be the most common ventilation method in allowing fresh outdoor air to replace indoor air. Natural ventilation occurs when the air in a space is changed with outdoor air without the use of mechanical systems, such

as a fan. Natural ventilation occurs when there is uncontrolled air movement or infiltration through cracks, holes between indoor environment and outdoor environment. Opening windows and doors also provides natural ventilation. Natural ventilation depends on air tightness, outdoor temperatures, wind, and other factors. Infiltration is separate from ventilation, but is often used to provide ventilation air.

General exhaust ventilation (GEV), also called dilution ventilation (Vincent, 1995; Occupational Safety & Health Administration, 2007) is a form of exposure control that involves providing enough air in the workplace to dilute the concentration of airborne contaminants to acceptable levels.

Poor ventilation will lead to high relative humidity values and therefore create a good environment for the development of micro-organism and house mites. Thus increasing the risk of allergic reactions of dwellers. Poor ventilation also leads to high level of carbon and elevated risks of odour nuisance. That is why in this thesis, study of airflow improvement as a way to improve ventilation system to the ribbed smoked sheet cooperative to lessen risk of worker's exposure to smoke particles will be performed. Results of airflow improvement inside the cooperative will be displayed in the form of airflow fields (velocity vectors and temperatures contours).

2.5 CFD Technique

Computational Fluid Dynamics (CFD) has been used as a universal tool to predict indoor airflows since early 1970s and it gained popularity among researchers in the field of fluid dynamics in the last few decades as a result of advancement in the computing power (Einberg, 2005; Hussein et al., 2005; Gant et al., 2006; Sohn et al.,

2007; Zang and Chen, 2006). CFD has usually been used to simulate air movement and contaminant dispersion. Applications include internal environment of large spaces, such as atriums, museum, theaters, or coliseums. Such are capable of simulating the stratification of air and the diffusion of contaminants in a conditioned environment. The most significant advantage of CFD is the possibility to test different system configurations virtually without real construction.

Generally speaking, CFD is a mathematical modeling procedure whereby the fluid parameters of velocity, temperature, pressure, turbulence, and contaminant concentrations are calculated by solving the governing partial differential equations for fluid flow, heat transfer, and conservation of species [Section 2.2, Eqs. (10); Section 2.1, Eqs. (1)]. These differential equations describe a three-dimensional viscous fluid flow field. Due to the non-linearity of these equations, they generally cannot be solved analytically. The CFD approach is to transform these differential equations into a set of discrete algebraic equations and solve the algebraic equations by an iterative procedure (Sohn et al., 2004).

In the 1980s, Cray supercomputers were used to process CFD simulations, with solution times taking days. The same simulations may now be run on a personal laptop computer in a matter of hours. CFD modeling has been continually validated since its inception against many known fluid phenomena. It is considered a very useful tool for engineers and scientists working on fluid flow problems across many disciplines (Sohn et al., 2004).

Chemical & Biological Nonproliferation Program (CBNP) Transport & Fate Team (Los Alamos National Laboratory, 2007) reported five-types of CFD computer

codes that are already used in the world to model transport and fate phenomenon. These include CFD models for flow around building, building interior flow and transport models, mesoscale atmospheric models, plume dispersion models, and subway system & interior flow models.

Chapter 3

Methodology

3.1. Domain of the Problem

This thesis focuses on investigating airflow field (velocity distribution and temperature distribution), aerosol flow (trajectory of the smoke particles and the smoke particles concentration), and airflow improvement in a natural ribbed smoked sheet rubber cooperative using a CFD technique. Experimental data of velocity, temperature, and aerosol concentration are used as boundary conditions for the CFD simulation, and validation of the CFD results.

The ribbed smoked sheet rubber cooperative used in this study is the Saikao Cooperative located in Tambon Toongwang, Muang district, Songkhla province. It is about 30 kms north east of Hat Yai down town as shown in Fig 3.1.

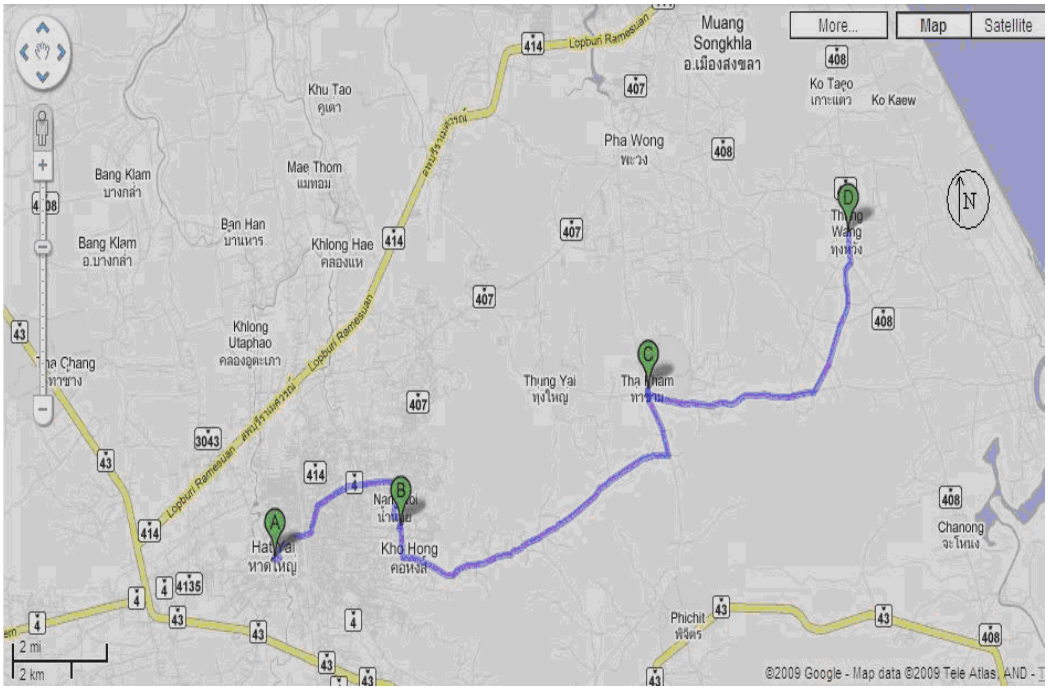

Fig 3.1 Map of the cooperative used in this work.

Layout of the rubber sheet smoked cooperative to be studied in this thesis work (Model 1995) is shown in Fig 3.2. The cooperative contains four identical rubber smoking rooms (A-D) in which the fresh rubber sheets are dried by heat from rubber-wood combustion. Each rubber smoke room has a wood burner at the back side. Hot gas containing smoke particles is induced from the burner to the smoke room via openings on the floor. Dimension of each room is 5.0 m x 4.0 m x 6.0 m. These rooms are the source of smoke emission to the workplace area and atmospheric environment. Smoke enters the workplace area via the ventilating lids on top of each smoking room before escaping to atmospheric environment. Each smoking room contains two 60 cm x 60 cm ventilating lids. These lids are fully opened in the first day of rubber smoking process and partially opened or closed in the following days depending on moisture and temperature in the smoking room. In generally, it takes 3-4 days to complete drying process of the rubber sheets. The rubber latex receiving platform is on the bottom left corner of the layout where the fresh latex is collected

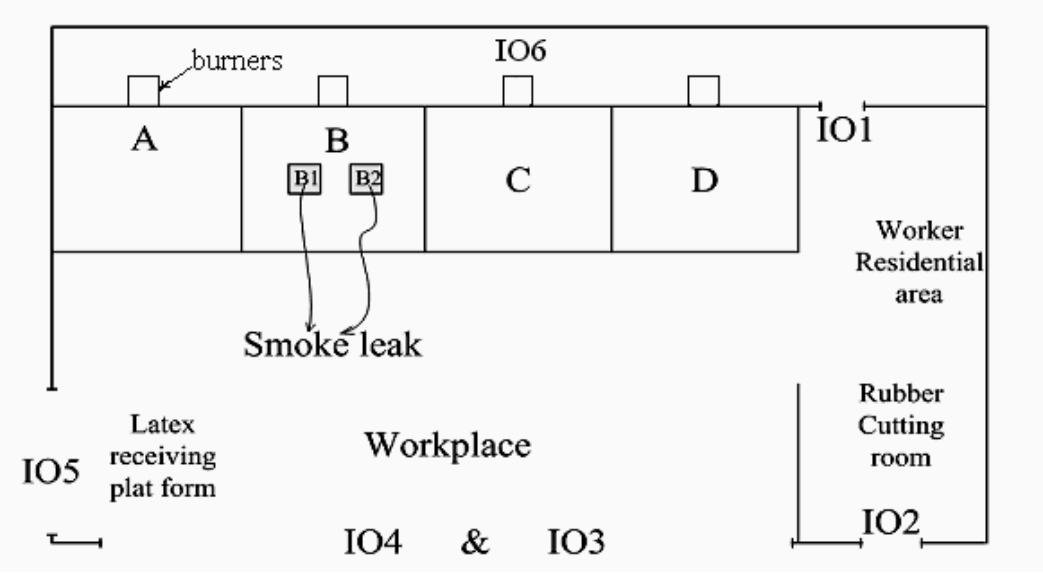

Fig 3.2 Schematic diagram of the rubber sheet smoked cooperative, model 1995.

from members of the cooperative. The rubber solidification and sheet forming are performed in the workplace area where workers generally work during the day time. The area at the bottom right corner is used for the workers to remove defect from the dried rubber sheets (rubber cutting area) while the remaining area at the top right corner is used as the residential area for all the workers in the cooperative. Generally speaking, the workers spend most of the time, day and night, in the cooperative and are directly exposed to the smoke emission from the rubber-wood burning.

3.2. Experimental Parameters and Apparatus

In this work, experiments will be conducted for two purposes. First, some measurement data will be used as boundary conditions for the CFD study. Second, since results from the CFD study need to be validated, some additional measurement data will be obtained. The data to be used as boundary conditions includes velocity and temperature of the smoke flowing out of the ventilating lids which are considered as inlets to the system domain, velocity and temperature at other boundaries of the system and wall, and particle concentration will be measured inside the smoking room and diameter of the particle of interest was assumed to be uniform. Measurement data used for CFD validation includes velocity and temperature at various locations in the cooperative, and workplace concentration at 3 heights at one location (point P). All the measurement locations are shown in Figs. 3.2. – 3.5. The particle concentrations in the workplace are measured at 1.5 m (P1), 3.0 m (P2), and 4.5 m (P3) from ground, point P indicated in Fig 3.3. This is to study the variation of particle concentration at different height.

Velocity and temperature measurement probes were installed in the positions shown in Fig 3.3. Details of openings around the cooperative, IO2, IO3, IO4 and IO6 are shown in Figs. 3.4 and 3.5. IO1 and IO2 are the entrance /exit openings on the back and front sides of the cooperative, respectively. IO3 is the opening above the front wall designed for ventilation. It is divided into 16 partitions for velocity and temperature measurement purpose, as shown in Fig 3.4. Measurement position is located at the center of each partition. IO4 is the opening above IO3 and below the roof edge designed for ventilation purpose as well. It is divided into 5 partitions as shown in Fig 3.4.

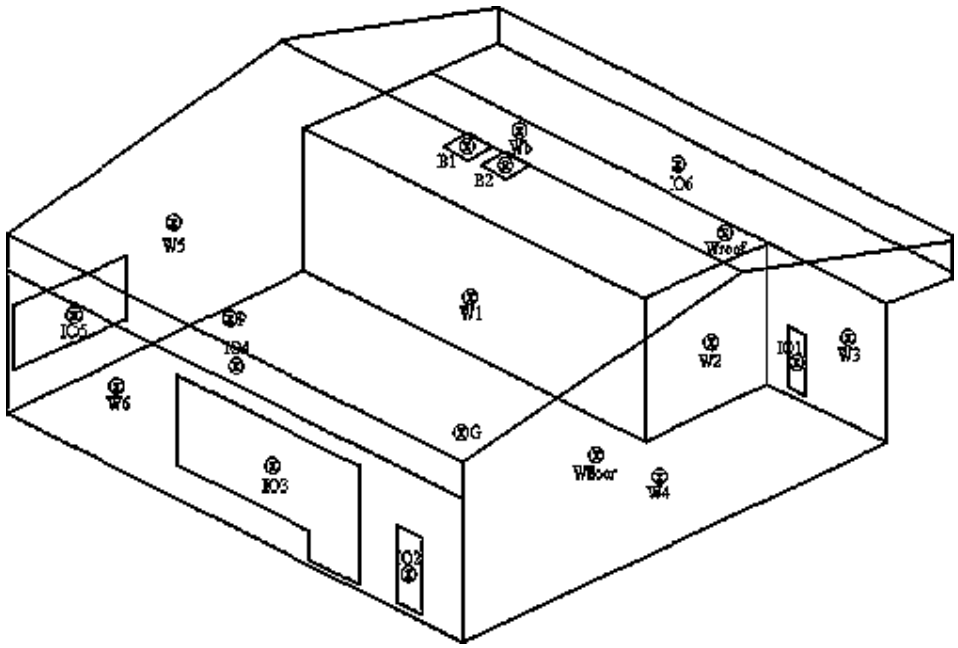

⊗ indicates measurement point (locations)

Fig 3.3 Positions of velocity and temperature measurements in the ribbed smoked sheet rubber cooperative.

IO5 is the entrance to the cooperative, 1.3 m above the workplace ground, for farmers to deliver the rubber latex. IO6 is the ventilation opening on the rear side just behind, and on the same level of the ceiling of the rubber smoking room as shown in Fig 3.5.

The walls inside the cooperative are divided into 6 sections, W1 to W6, as shown in Fig 3.3. Other solid boundaries include the roof (Wroof), the smoke room ceiling (Wb) and the floor (Wfloor).

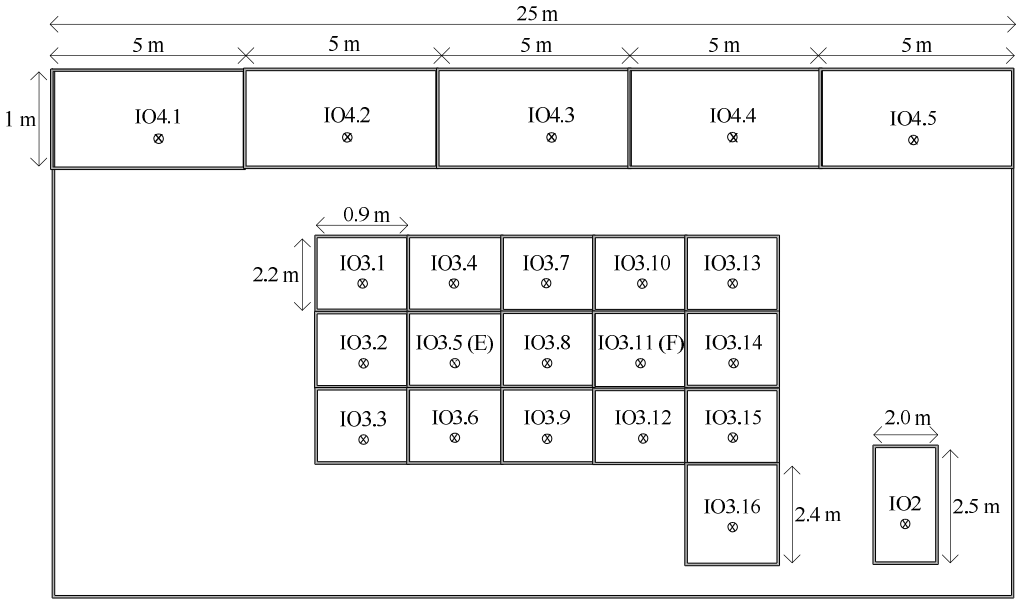

Fig 3.4 Layout of a plane (+Z direction) showing partitioning and measurement positions of IO2, IO3, and IO4.

Full details of measurement parameters are given in Table 3.1. Number of ribbed smoked sheet produced (2,600 pieces) and fuel (rubber-wood) used in each room (2,100 kg) are also recorded for reference. A log sheet used in the record of the measurement data is given in Appendix A.

Each smoking room has 2 ventilating lids on the ceiling. Smoke particles are released to the workplace area through these ventilating lids when the room is used for rubber sheet smoking. During 9 months of measurement, we never experienced the operation when all 4 rooms were used simultaneously. The data set used for

simulation is the case when one room (B) is under operation and ventilating lid B1 and B2 are opened.

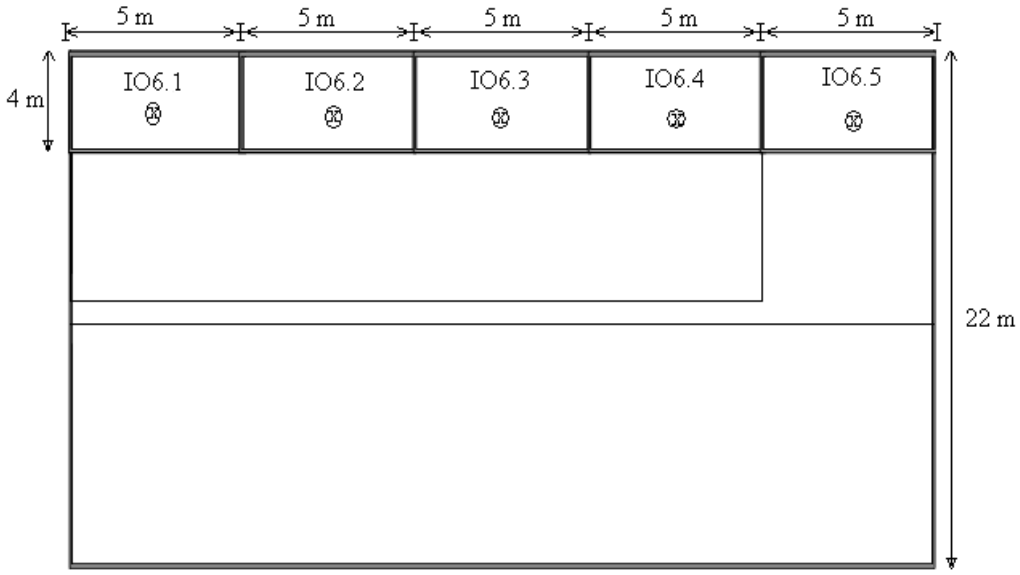

Fig 3.5 Layout of a plane (+Y direction) showing partitioning and measurement positions of IO6.

The velocity of air is measured by hot-wire type anemometers (Airflow Instrumentation, TA400T and Testo, 405-V1) and the temperature of air is recorded by a data logger (DataTaker, DT605). The velocity measurement range is 0 – 2 m/s for TA400T and 0 - 10 m/s for 405-V1. Temperature at each location in the ribbed smoked sheet rubber cooperative is measured by a type-K thermocouple. The same data logger (DataTaker, DT 605) is also used to record the temperature at every 3-second interval to ensure continuous reading for about 3 hours of measurement. Then all of the data from all of the measurements is averaged. The average data will be used as the values for boundary condition to the simulation (the data in details of

Table 3.1 Measurement parameters.

Description	Measurement Parameter	Location	Purpose
Inlet of smoke aerosol from ventilating lids	V (m/s)	B1, B2	Boundary conditions
	T (^{o}C)	B1, B2	Boundary conditions
Ambient Condition in the workplace (1-m above ground)	V (m/s)	E, F, G, P	Validation
		IO1, IO2, IO3, IO4, IO5, IO6	Boundary conditions
	T (^{o}C)	E, F, G, P	Validation
		IO1, IO2, IO3, IO4, IO5, IO6	Boundary conditions
Wall temperature	T (^{o}C)	W1, W2, W3, W4, W5, W6, WB, Wroof, Wfloor	Boundary conditions
Source Concentrations	C (mg/m^{3})	B1, B2	Boundary conditions
Workplace concentration	C (mg/m^{3})	P1 (1.5 m from ground) P2 (3.0 m from ground) P3 (4.5 m from ground)	Validation
Number of rubber sheets in each room	-	Rooms A, B, C, D	Reference data
Fuel used in each room	-	Rooms A, B, C, or D	Reference data

measurements is shown in Appendix B). The particles concentration is measured by self-made air sampler, shown schematically in Fig 3.6. The filters were conditioned in a controlled environment (25^{o}C, 50% RH) for 48hr prior to and after samplings. Difference of mass of the filter after sampling indicates amount of particles collected which is then used for calculation of particle concentration.

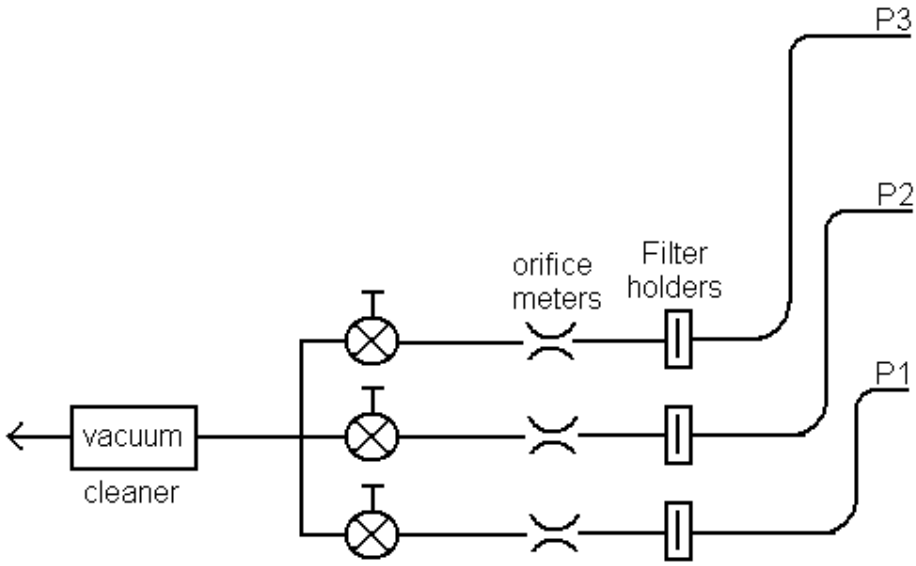

Fig 3.6 The self-made air sampler.

Firewood (rubber-wood) of known mass (measured by a scale) is fed to the burner. Samples of firewood were used to determine the moisture content on a dry basis by drying it in a laboratory oven at 105°C until totally dried.

3.3 CFD Simulation

Flow modeling using a CFD technique can save time otherwise spent on conventional design and troubleshooting methods. No existing study of CFD

simulation of airflow in the ribbed smoked sheet rubber cooperative has been presented so far. However, there are two existing studies of CFD simulation of airflow inside the rubber sheet smoking room which is the source of smoke particles released to the workplace area (Promtong and Tekasakul, 2007; Tekasakul and Promtong, 2008). CFD technique was used to investigate the temperature and velocity distribution in a smoking-room in attempt to improve airflow distribution.

This section presents a methodology for validation study to determine the accuracy of the simulation results, to investigate airflow and aerosol concentration, and to improve ventilation in a ribbed smoked sheet rubber cooperative. First of all, the finite volume discretization scheme used in this work is described. The system boundary conditions and grid setting will subsequently be explained.

In the result analysis, four parameters will be used as a representation of the results in the simulation:

1. Velocity fields (flow pattern distribution) of the airflows containing smokes in the ribbed smoked sheet rubber cooperative. Results will be displayed in the form of velocity vectors followed by comparison between measurement and simulation.

2. Temperature fields (temperature distribution) of the airflows containing smokes in the ribbed smoked sheet rubber cooperative. Results will be displayed in the form of contours of temperature and comparison between simulation and measurement.

3. Particle trajectory distributions of the airflows containing smokes start from ventilating lids to anywhere inside the ribbed smoked sheet rubber cooperative.

4. Particles concentration distributions of the airflow contain smokes, namely workplace concentrations. Results will be displayed in the form of contours or image of particle concentration inside the cooperative. Comparison of the values at different heights at one location will be made.

In order to lessen risk of workers exposed to a large portion of smoke aerosol particles, improvement of ventilation system by addition of natural ventilation at the middle of the roof is presented. Flow improvement will be indicated by velocity vectors, temperature contours, and particle concentration. Four cases will be investigated in order to determine the appropriate modification. Results will be used for recommendation to the implementation for improvement of smoke ventilation. All of the results and validation will be presented in Chapter 4.

3.3.1 The Finite Volume Scheme

In this thesis work a control-volume-based technique, Finite Volume Methods, is used in representing discretization. Steps for this technique include:

- Division of the domain into discrete control volumes using a computational grid.
- Integration of the governing equations on the individual control volumes to construct algebraic equations for the discrete dependent variables ("unknowns") such as velocity, pressure, temperature, and conserved scalars.
- Linearization of the discretized equations and solution of the resultant linear equation system to yield updated values of the dependent variables.

The finite-volume method (FVM) is largely employed for solution of CFD problems in engineering. FVM is characterized by the partitioning of the spatial domain in to a finite number of elementary volumes for which the balances of mass, momentum and energy are applied. The standard $k-\varepsilon$ two-equation model of turbulence will be used in this work with natural convection airflows, Newtonian, steady, and incompressible fluid, Eqs. (10) become

$$\nabla \cdot (\rho u \Phi) = \nabla \cdot (\Gamma_{\Phi} \nabla \Phi) + S_{\Phi} \tag{17}$$

where the term on the left hand side represents the convective heat transfer term, the first term on the right hand side represents the diffusive term, and S_{Φ} represents the source/sink term. Here Φ is the generalized variable representing a variety of different quantities, such as the mass component, velocity, enthalpy, turbulence kinetics energy, or turbulence length scale, and Γ_{Φ} is the generalized diffusion coefficient. Table 3.2 describes Eqs. (17) for different Φ.

The kinetic energy generation rate (G_s) can be expressed as:

$$G_s = 2\mu_e\left[\left(\frac{\partial u}{\partial x}\right)^2+\left(\frac{\partial v}{\partial y}\right)^2+\left(\frac{\partial w}{\partial z}\right)^2\right]+\mu_e\left[\left(\frac{\partial u}{\partial y}+\frac{\partial v}{\partial x}\right)^2+\left(\frac{\partial v}{\partial z}+\frac{\partial w}{\partial y}\right)^2+\left(\frac{\partial w}{\partial x}+\frac{\partial v}{\partial z}\right)^2\right] \tag{18}$$

Here, μ_e is the effective viscosity, defined by $\mu_e = \mu + \mu_t$, μ is molecular viscosity, and $\mu_t = C_\mu \rho k^2 / \varepsilon$, $C_{1\varepsilon}=1.44$, $C_{2\varepsilon}=1.92$, $C_\mu=0.09$, $\sigma_k=1.0$, $\sigma_\varepsilon=1.3$. The terms F_x, F_y, and F_z, represent the momentum transfer per unit volume between the continuous phase and particles. The movement of the particles in this work is driven by drag force of the surrounding air and, gravity of the particles. If neglecting these momentum transfer, $F_x = F_y = F_z = 0$. u is velocity component for x-direction, v is

velocity component for y-direction, *w* is velocity component for z-direction, and P is pressure respectively.

Table 3.2 Source terms in the conservation equation written in the cartesian coordinates.

Balance Equation	Φ	Γ_Φ	S_Φ
Mass	1	0	0
x-momentum	u	μ_e	$-\frac{\partial P}{\partial x}+\frac{\partial}{\partial x}(\mu_e\frac{\partial u}{\partial x})+\frac{\partial}{\partial y}(\mu_e\frac{\partial v}{\partial x})+\frac{\partial}{\partial z}(\mu_e\frac{\partial w}{\partial x})+F_x$
y-momentum	v	μ_e	$-\frac{\partial P}{\partial y}+\frac{\partial}{\partial x}(\mu_e\frac{\partial u}{\partial x})+\frac{\partial}{\partial y}(\mu_e\frac{\partial v}{\partial x})+\frac{\partial}{\partial z}(\mu_e\frac{\partial w}{\partial x})+F_y$
z-momentum	w	μ_e	$-\frac{\partial P}{\partial z}+\frac{\partial}{\partial x}(\mu_e\frac{\partial u}{\partial x})+\frac{\partial}{\partial y}(\mu_e\frac{\partial v}{\partial x})+\frac{\partial}{\partial z}(\mu_e\frac{\partial w}{\partial x})+F_z$
Kinetic energy	k	$\frac{\mu_e}{\sigma_k}$	$G_s-\rho\varepsilon$
Dissipation rate	ε	$\frac{\mu_e}{\sigma_\varepsilon}$	$C_1\frac{\varepsilon}{k}G_s-C_2\rho\frac{\varepsilon^2}{k}$

In this method, the discretized equations represent the flow problem in each control volume. A commercial CFD Packages FLUENT Version 6.3 will be employed for simulation throughout. Detail of this method includes the following procedure:

Discretization - Discretization means integration process of Eqs. (10) or Eqs. (17) over a cubic volume of dimension *dx, dy, dz* and over time (interval between *t* and *t* + *dt*). By default, FLUENT stores discrete values of the scalar Φ at the cell. However, its face values are required for the convection terms and must be interpolated from the cell center values. This is accomplished using an upwind scheme. Up-winding means that the face value of the scalar Φ is derived from quantities in the cell upstream, or "upwind," relative to the direction of the normal velocity v_n. A detail of the discretization refers to Appendix C. The discretization in this work employed a cubic volume shape and first order upwind scheme was used.

Solver - FLUENT allows us to choose one of the two numerical methods: pressure-based solver, or density-based solver. The density-based approach was mainly used for high-speed compressible flows (ANSYS FLUENT, 2006). In the density-based approach, the velocity field is obtained from the momentum equations while the pressure field is determined from the equation of state. On the other hand, the pressure field is extracted by solving a pressure or pressure correction equation which is obtained by manipulating continuity and momentum equations. Using the method, FLUENT solves the governing integral equations for the conservation of mass and momentum, and (when appropriate) for energy and other scalars such as turbulence. Gradients are needed not only for constructing values of a scalar at the cell faces, but also for computing secondary diffusion terms and velocity derivatives. The gradient $\nabla\Phi$ of a given variable Φ is used to discretize the convection and diffusion terms in the flow conservation equations. The gradients are computed in FLUENT according

to the following methods: Green-Gauss Cell-Based, Green-Gauss Node-Based, and Least Squares Cell-Based.

In this work, the pressure-based approach will be used because the problem under study is low-speed incompressible (ANSYS FLUENT, 2006). Recently, however, both methods have been extended and reformulated to solve and operate for a wide range of flow conditions beyond their traditional or original intent.

FLUENT allows us to choose the discretization scheme for the convection terms of each governing equation. Second-order accuracy is automatically used for the viscous terms. When the pressure-based solver is used, all equations are, by default, solved using the first-order upwind discretization for convection.

Convergence - Because of the non-linearity of the problem, the solution process is controlled via relaxation factors. A relaxation factor controls the change of a variable as calculated at each iteration. The convergence is checked by several criteria: the mass and heat conservation should be balanced; the residuals of the discretized conservation equations must steadily decrease; and the change in field values between two iterations should be very small. The convergence criteria were 10^{-3} for continuity-, momentum- and standard k-ε model- equations, and 10^{-6} for energy equation.

This thesis work uses Eulerian method to solve the continuous fluid (airflow containing smoke particles) without considering the aerosol particles transport on the set of conservation equations. After convergent CFD simulation results on the air flow equations are achieved, the particle transport will be taken into account by the Lagrangian approach (Lagrangian frame of reference) in order to study particles

trajectories released from ventilating lids to the workplace area. By using the interphase exchange of momentum, heat, and mass determined during the previous particle calculation, the continuous phase flow field and the discrete phase trajectories were modified in order to obtaining particle trajectories. These modifications is repeated until a converged solution is achieved in which both the continuous phase flow field and the discrete phase particle trajectories are unchanged with each additional calculation.

Modeling particle concentration can be achieved by using the concept of mixture materials which can be used to model species diffusion in the energy equation. This is called the “species transport”. Capability of the species transport (species module) includes an ability to calculate multi-species transport either non-reacting or reacting (ANSYS FLUENT, 2006). In this work, the calculation of non-reacting aerosol species transport is used to obtain aerosol concentration distribution (in the form of contours or images) in the ribbed smoked sheet rubber cooperative. Carbon monoxide is selected as a representative of aerosol species (Furuuchi et al., 2008). All the details of the calculation species module are shown in Appendix D. Comparison between particle concentration simulation and measurement will be performed to verify the proposed flow field model.

3.3.2 Grid Generation

The grid generation program, GAMBIT, is used to construct the grid system prior to the calculation by FLUENT CFD package version 6.3 run on a PC 2.79 GHz.

The result of meshing process of the domain of the ribbed smoked sheet rubber cooperative geometry is shown in Table 3.3.

Grid verification which is generated by GAMBIT is essential to ensure that CFD can be used with confidence. Kickinger et al. (1999) and Anderson et al. (1999) used the unstructured meshing techniques and adaptive (automatically) grid refinement to ensure what of their grid. It was found that the unstructured meshing will be dense at relevant regions and coarse elsewhere. TGrid is a robust and highly automated unstructured volume mesh generator which uses wrapper for generating triangle surface mesh. It includes tools for repairing and improving boundary mesh. It can also generate many shape meshes including tetrahedral, hexahedral core, prisms and pyramids mesh. Using Delaunay Triangulation for triangle/ tetrahedral, and Advancing Layer Method for prism. It includes tools to manipulate face/cell zones (Fluent Inc., 1997). The equisize skew of TGrid scheme is less than 0.97 (Fluent Incorporated, 2004).

The results is supported by Kleven et al. (2005) who already tested their cells quality in TGrid, to ensure a proper grid for the simulations by comparing the cell's shape to an equilateral cell of equivalent volume. It was found that the degree of skewness lies in the range between zero and one, where zero skewness is optimal and a skewness of one indicates a degenerate cell. Meshing TGrid results of these thesis works is shown in Fig 3.7, respectively. More detail of the meshing process of the thesis work domain geometry is shown in Appendix E.

Table 3.3 Result of volume meshing process.

Elements	Tet/Hybrid
Type	TGrid
Size	0.2 (m)
Mesh volumes generated	2,159,347

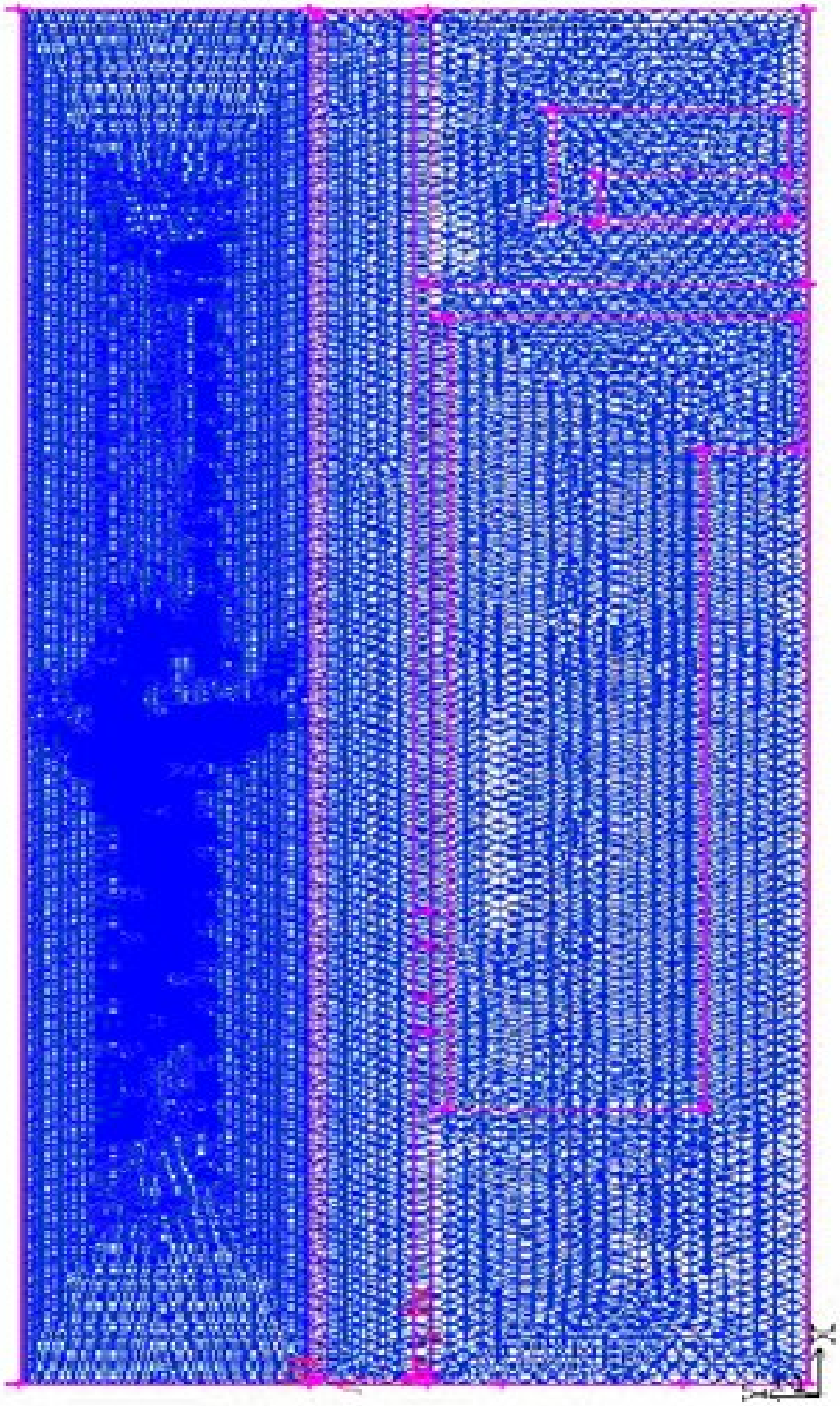

Fig 3.7 The meshing of the ribbed smoked sheet rubber cooperative using GAMBIT: view from direction +Z of Fig. 3.3 at Z = 22 m.

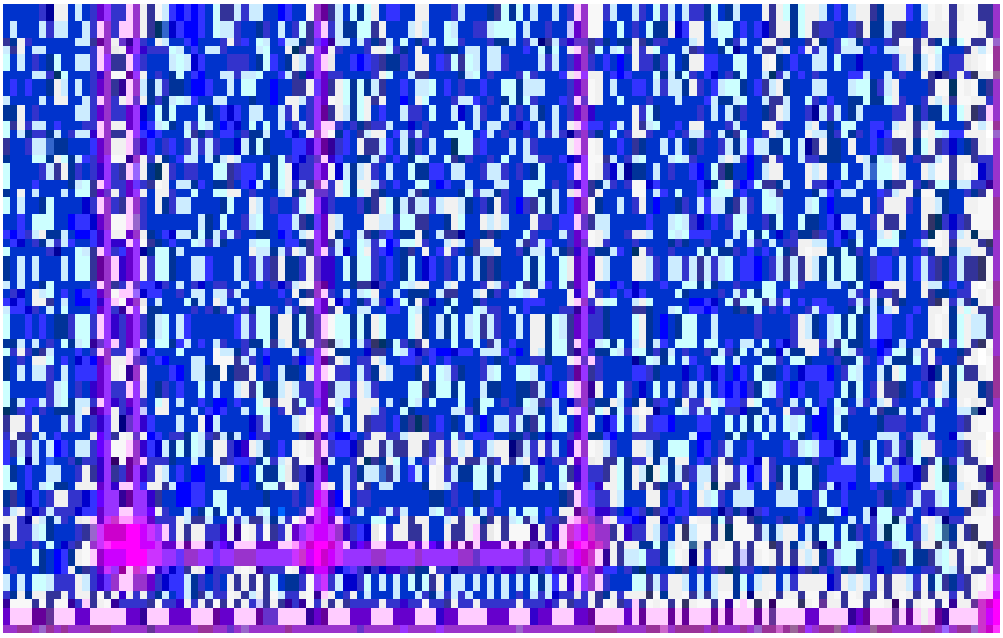

Fig 3.7a The meshing of the ribbed smoked sheet rubber cooperative using GAMBIT: cut and enlarge at the lower right side of Fig 3.7.

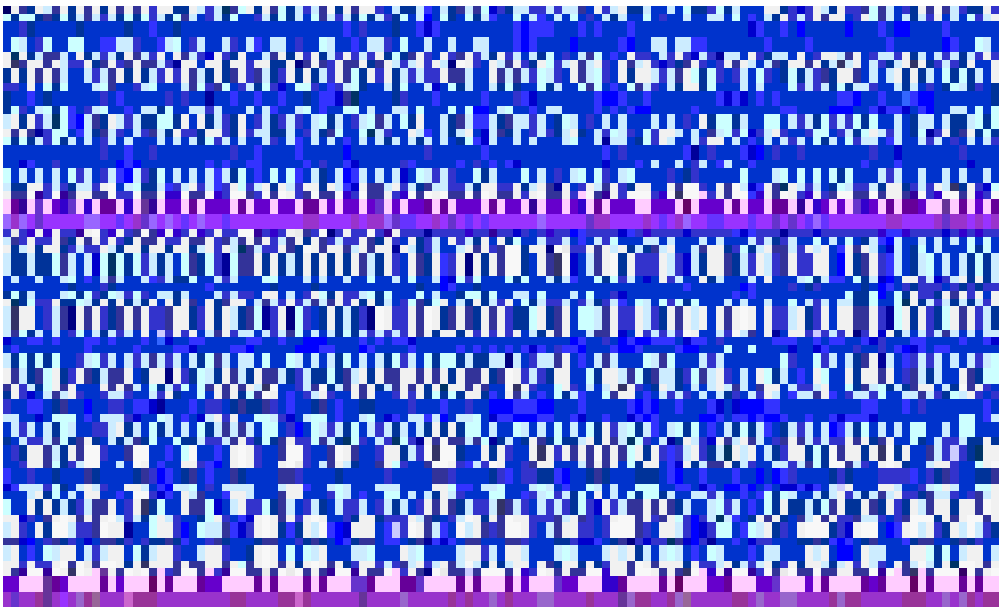

Fig 3.7b The meshing of the ribbed smoked sheet rubber cooperative using GAMBIT: cut and enlarge at the lower middle side of Fig 3.7.

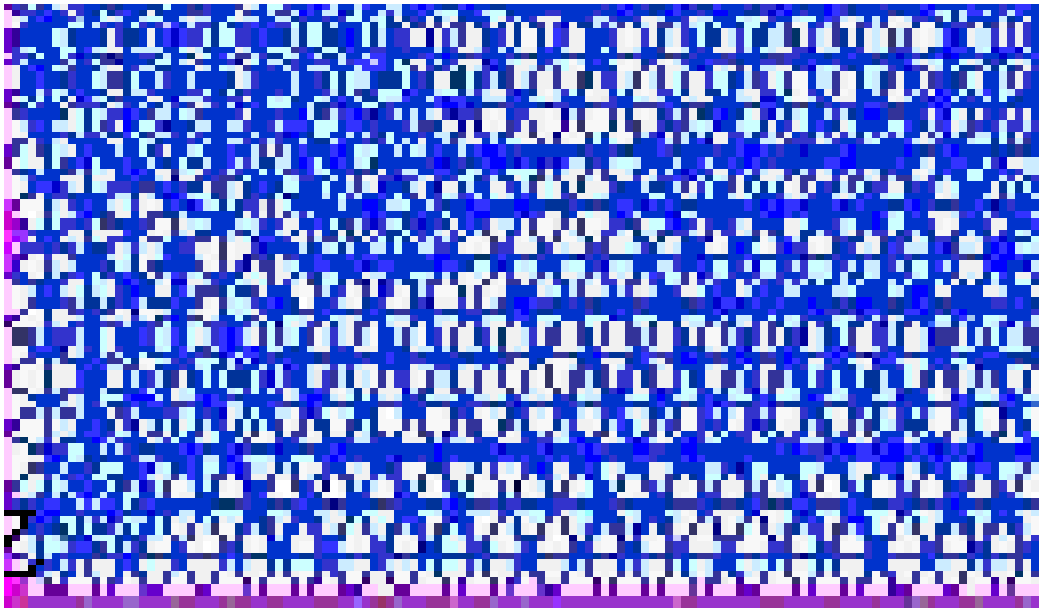

Fig 3.7c The meshing of the ribbed smoked sheet rubber cooperative using GAMBIT: cut and enlarge at the lower left side of Fig 3.7.

Fig 3.7d The meshing of the ribbed smoked sheet rubber cooperative using GAMBIT: cut and enlarge at the middle part of the middle side of Fig 3.7.

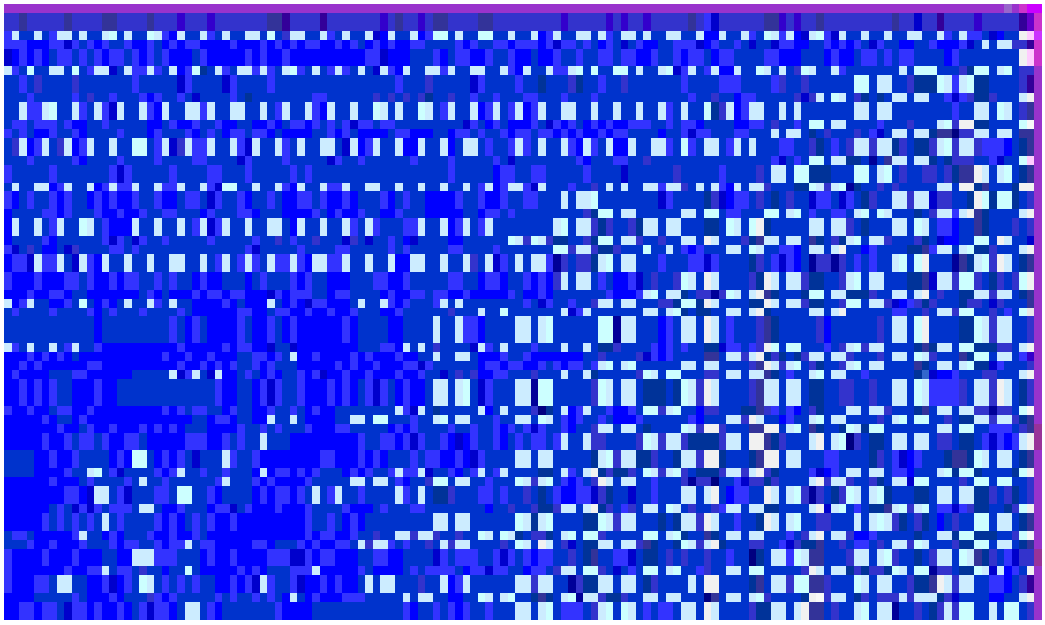

Fig 3.7e The meshing of the ribbed smoked sheet rubber cooperative using GAMBIT: cut and enlarge at the upper right side of Fig 3.7.

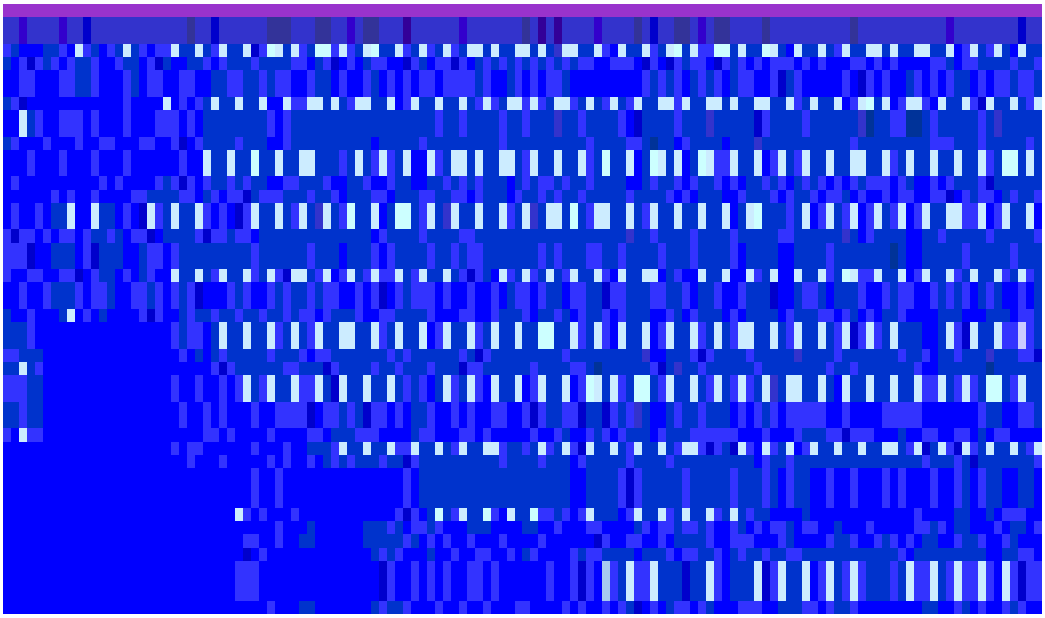

Fig 3.7f The meshing of the ribbed smoked sheet rubber cooperative using GAMBIT: cut and enlarge at the middle upper side of Fig 3.7.

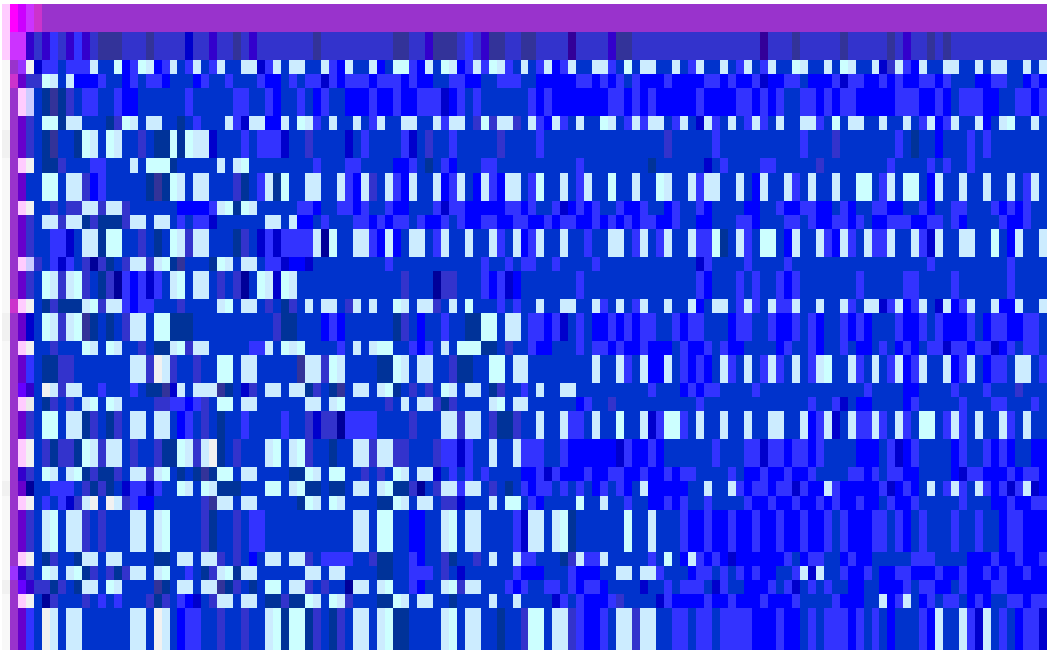

Fig 3.7g The meshing of the ribbed smoked sheet rubber cooperative using GAMBIT: cut and enlarge at the upper left side of Fig 3.7.

Chapter 4

Results and Discussions

4.1 Boundary Conditions

Data of velocity and temperature from measurements used for boundary conditions in CFD are presented in Table 4.1. The data at locations IO3, IO4 and IO6 are average values from 16, 5 and 5 measuring points, respectively. Moreover, value from each measuring point represents an average value from 10 measurements. Details of data from all measuring points are shown in Appendix B.

Static pressure boundary condition which is used to represent the system surroundings was a constant value of zero gauge pressure. Ambient temperature was 33.2^{o}C.

4.2. Computation and Representations

CFD simulation was performed on a desktop computer (Pentium 4, CPU 2.79 GHz and 2 GB of RAM). GAMBIT 2.2 was used to generate the mesh while the calculation was achieved by FLUENT 6.3. The computation using grid setting described in Sec. 3.3.2 was found to converge after 350 iterations as shown in Fig 4.1. The convergence criteria were 10^{-3} for continuity-, momentum- and standard k-ε model- equations, and 10^{-6} for energy equation.

Velocity vectors of flow pattern in the cooperative are displayed in 5 planes shown in Fig 4.2 in order to understand the flow behavior inside the domain.

Table 4.1 Average results of measurement data for velocity and temperature used as boundary condition.

Location	Velocity (m/s)	Temperature (^{o}C)
B1	1.03	48.7
B2	1.02	48.5
IO1	0.79	31.5
IO2	0.49	31.6
IO3	0.32	32.3
IO4	0.35	33.9
IO5	0.35	31.4
IO6	0.01	35.0
W1	0.0	47.6
W2	0.0	44.1
W3	0.0	33.9
W4	0.0	42.2
W5	0.0	32.1
W6	0.0	32.1
Wb	0.0	36.4
Wfloor	0.0	32.5
Wroof	0.0	39.8

Planes $A-A'$, $B-B'$ and $C-C'$ are the Y-Z planes cut along the X – axis at X = 1.0, 6.7 and 8.3 m, respectively. Plane $A-A'$ is near the left wall of the cooperative and it includes the sampling points P1, P2 and P3.

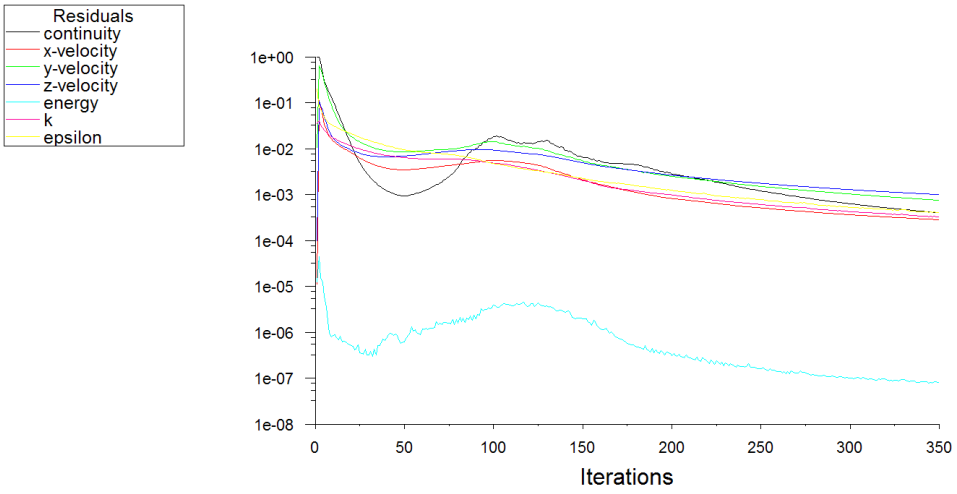

Fig 4.1 Scaled residuals of the calculation showing convergence after 350 iterations.

Plane $B-B'$ is cut through the center of the ventilating lid B1, while plane $C-C'$ is cut through the center of the ventilating lid B2. Planes $D-D'$ and $E-E'$, are the X-Y planes cut along Z – axis at Z = 7.0, and Z = 11.0 m, respectively. Plane $D-D'$ is cut through the centers of all ventilating lids, while plane $E-E'$ is cut through the center of the factory. From all of the 5 planes, the whole flow patterns, temperature distributions and particle concentration contours in the ribbed smoked sheet rubber cooperative can be understood. The average running time per case was about 4 hours depending on the number of elements.

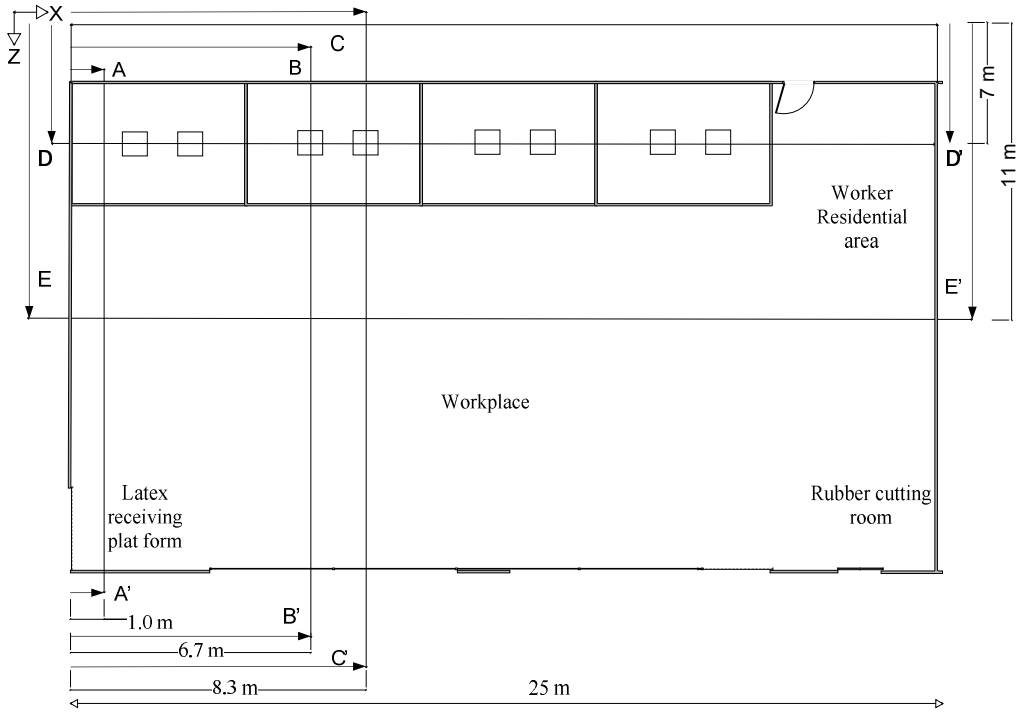

Fig 4.2 Top view of layout of the cooperative describing planes to display the velocity and temperature distributions.

4.3 Velocity Fields

The velocity of air at the plane A – A' is displayed in Fig 4.3. The air from the left side of the figure (IO6) flows up to the rubber smoking room ceiling and then moves upward to the roof. This flow swirls because the air that flows towards inside of the factory is accumulated with the other flow near the floor. At the right side of the figure, the flow from the opening window (IO4) is combined with the flow from the opening window at the entrance on the second floor (IO5). This combination results in a vortex-like flow. The flow then leaves the cooperative at IO3 on the right.

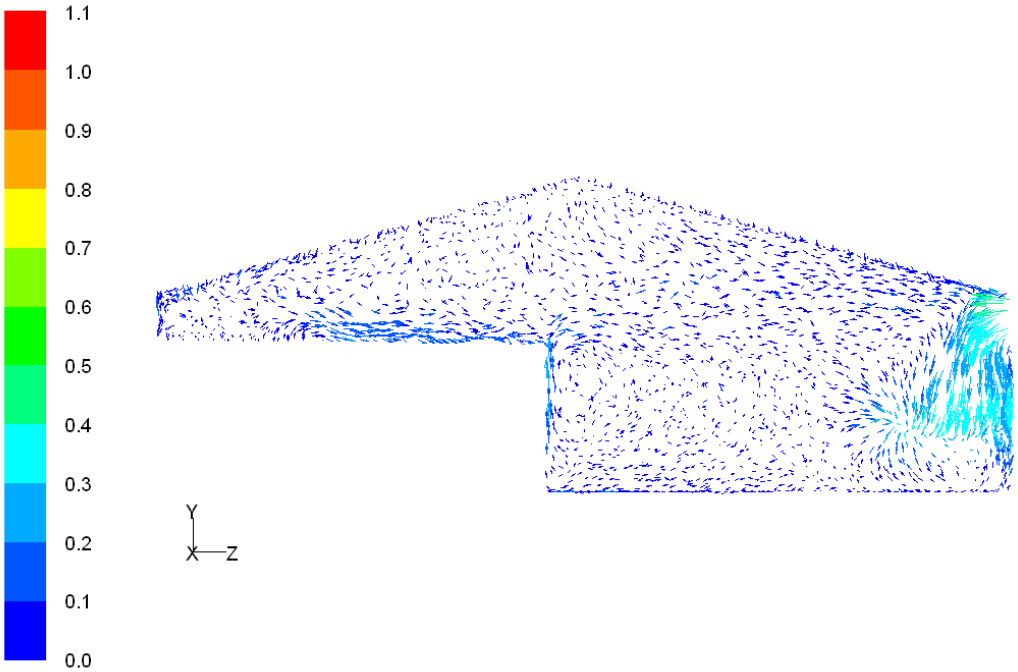

Fig 4.3 Velocity vectors at the plane A – A'.

Velocity vector on the plane B – B' cut through the center of B1 is shown in Fig 4.4. The higher velocities are located around the exit of the ventilating lid B1. The figure shows that the air from the ventilating lid B1 flows upward to the roof area. When it hits the roof, the flow is divided into two streams; to the left and right sides. At the opening on the right side, airflow blows into the domain from the upper part (IO4) and leaves the factory through the same opening at the lower part (IO3). A part of the flow from the roof of the factory is induced and leaves the factory at the same location (IO3). The magnitudes of velocity at the right side of the figure range from 0.03 to 0.12 m/s, and at the bottom part of the figure (bottom-left side of the figure) the velocity is as low as 0.07 m/s.

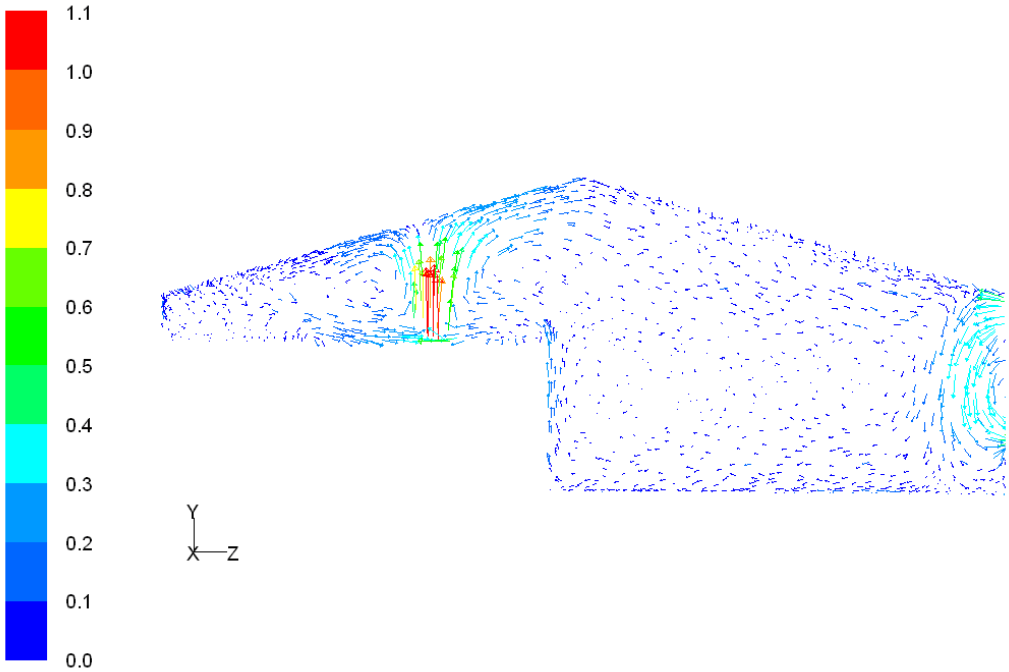

Fig 4.4 Velocity vectors at the plane $B-B'$.

Velocity vector on the plane $C-C'$ cut through the center of B2 is shown in Fig 4.5. The flow pattern is similar to that of plane $B-B'$. However, the magnitudes of velocity near the roof on top of B2 are higher than at IO3. The magnitudes near IO3 range from 0.07 to 0.10 m/s.

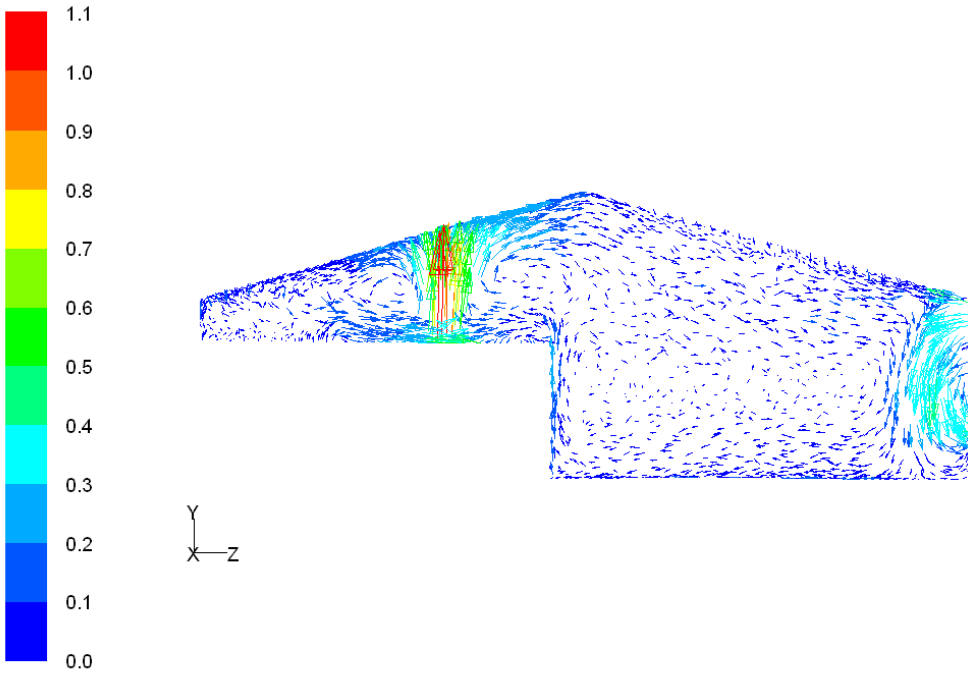

Fig 4.5 Velocity vectors at the plane $C-C'$.

The airflow in plane $D-D'$ is shown in Fig 4.6. It shows that the flow from ventilating lids B1 and B2 blows to the roof area and when it hits the roof, the flow is divided into two streams, to the left and the right sides. On the left side, the flow around the ceiling of the rubber smoking room and the roof of the cooperative was influenced by the flow from the opening at the bottom-left side (IO6), causing a swirl in the counter-clockwise direction. On the right side, the flow around the ceiling of the ventilating lids and the roof of the cooperative was in opposite direction.

When considering with the flow characteristics in planes $A-A'$ and $B-B'$, it can be concluded that when the flows from sources B1 and B2 hit the roof, they spread in all directions. They also combine with the flow entering the cooperative via

IO6 and cause swirls. A portion of the flow merges with that entering via IO4 and leaves the workplace at IO3 below.

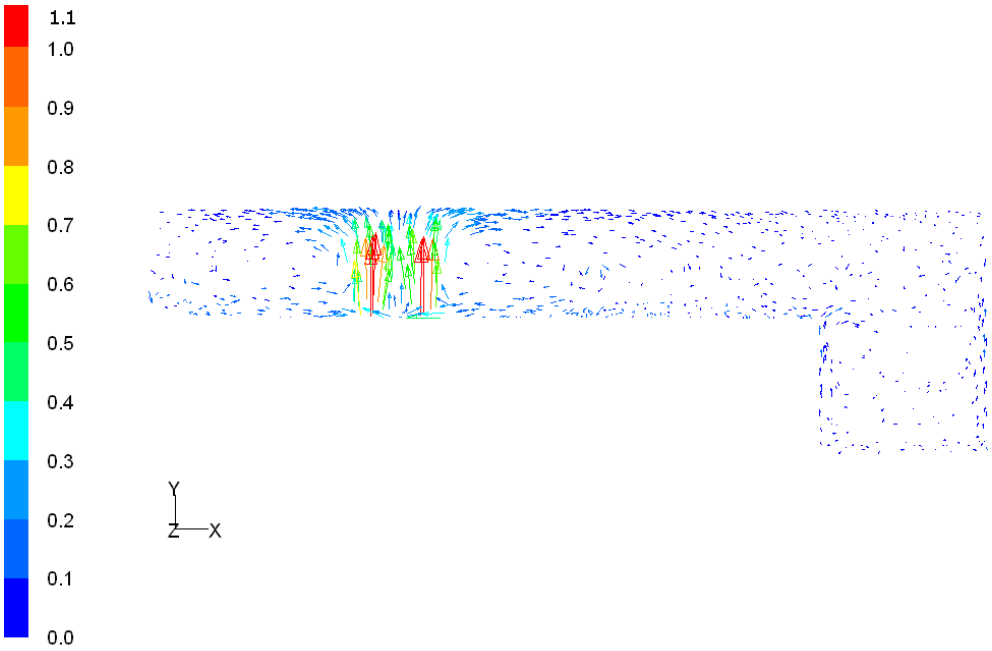

Fig 4.6 Velocity vectors at the plane D – D'.

The flow in the center of the cooperative (plane E – E') is shown in Fig 4.7. It shows non-uniform velocity vectors in the middle part. It can be seen that at the height around one third from the roof, the flow is influenced by the flows from the ventilating lids B1 and B2. However, the magnitudes of the velocity are low. The maximum velocity magnitude is approximately 0.19 m/s at the area around one-third of the height (at the left side) from the roof. Most of the flow circulates inside the workplace without exiting. This indicates improper ventilation of air (or smoke) inside the workplace. Therefore an improvement of ventilation is necessary to enhance air quality in the workplace area.

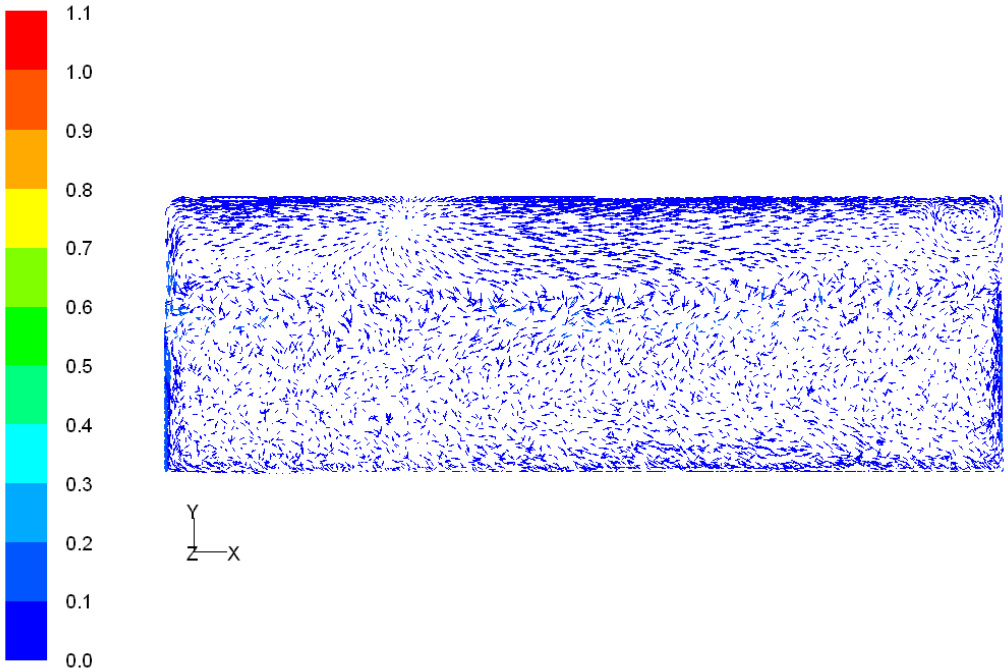

Fig 4.7 Velocity vectors at the plane $E - E'$

Comparison of velocity between simulation and measurement

Comparison of velocity between simulation and experiment at various locations are shown in Fig 4.8 and Table 4.2. Error of velocity between measurement and simulation at location P is high because sometimes there were many workers and peoples came to deliver their rubber latex at the opening around the second floor (IO5) near point P. This could cause disturbance to the airflow when measurement was performed. Errors at a few more locations are also high because it was measured in real situation and was uncontrollable. Error was calculated from

$$\text{Error} \quad (\%) \quad = \frac{\left| X_{mea} - X_{sim} \right|}{X_{mea}} \times 100 \tag{19}$$

where X_{mea} and X_{sim} represent values from measurement and simulation, respectively. In general, results show a sufficiently good agreement with average error less than 22 % considering the condition is uncontrollable. This indicates a proper simulation scheme.

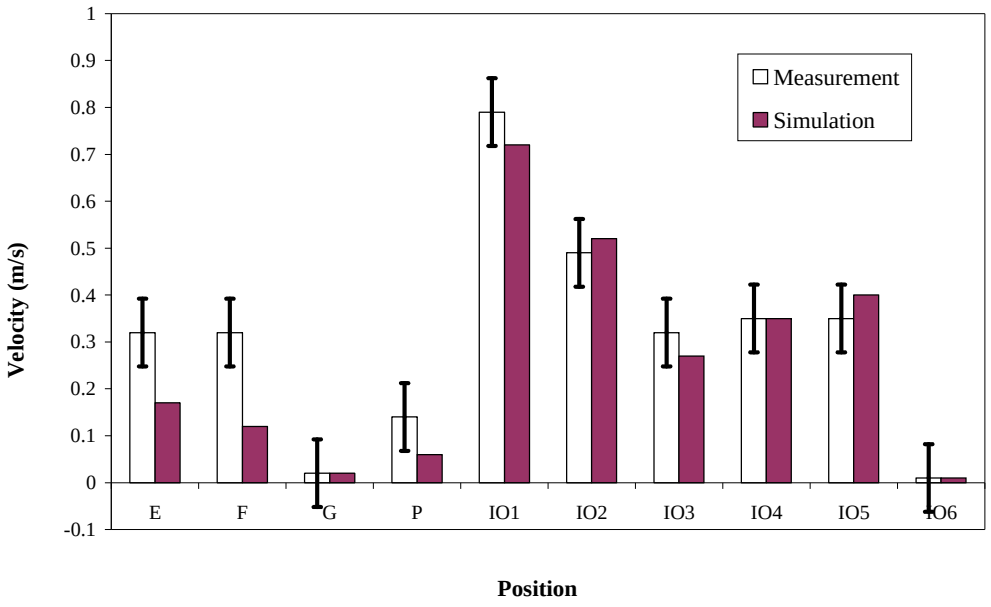

Fig 4.8 Comparison of velocity from measurement and simulation.

4.4 Temperature Fields

Data of temperature from measurements used as boundary condition in CFD simulation is also presented in Table 4.1. The details of data from all measuring points are shown in Appendix B.

Temperature distribution on $A - A'$ plane is shown in Fig 4.9. It shows that the highest temperature in this plane (39.0^{o}C) is located at the front door surface of the smoke room. This is influenced by the heat transfer from the smoking room through the wall. The lowest temperature takes place at the right side near the ground

Table 4.2 Data comparison between results from measurement (Mea) and simulation (Sim) of velocities.

Location	Velocity (m/s)		S.D.
	Mea	Sim	
E	0.32	0.17	0.15
F	0.32	0.12	0.04
G	0.02	0.02	0.01
P	0.14	0.06	0.01
IO1	0.79	0.72	0.08
IO2	0.49	0.52	0.08
IO3	0.32	0.27	0.10
IO4	0.35	0.35	0.06
IO5	0.35	0.40	0.03
IO6	0.01	0.01	0.01

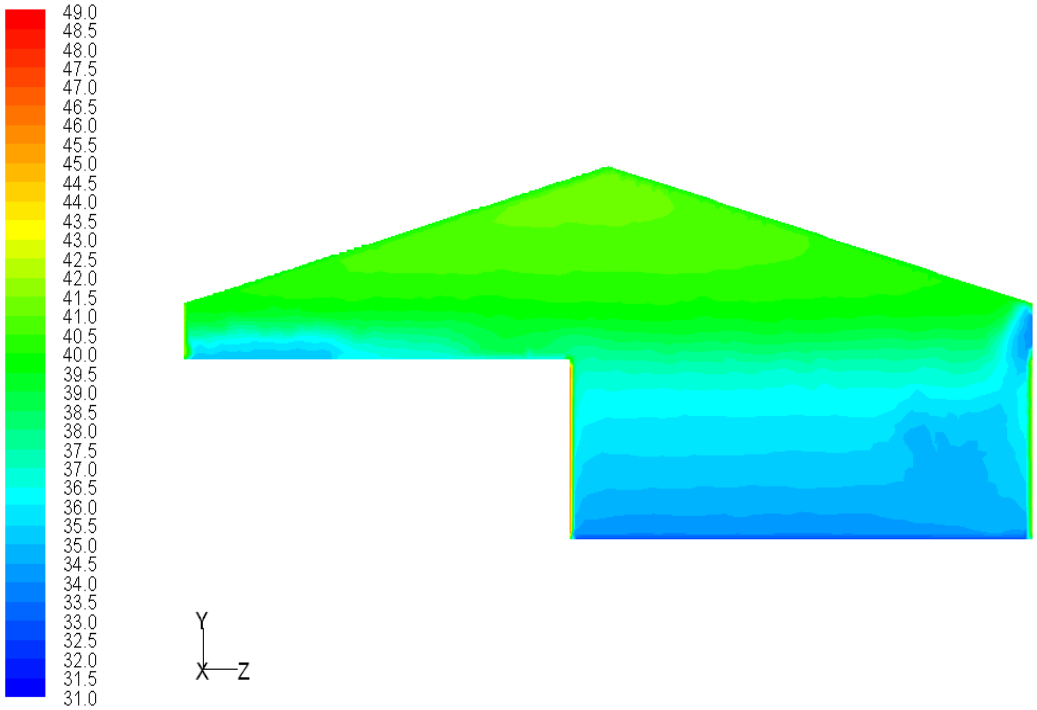

Fig 4.9 The contours of temperature (^{o}C) at the plane A – A' .

area (31.6°C). The separation between the temperature above and below the height of the smoke room ceiling is clear. Temperature above the ceiling is high because of the natural convection of heat from the smoke room and the heat released from the ventilating lids to the roof.

The temperature contours at the plane $B-B'$ is shown in Fig 4.10. It shows that the high temperature areas, around 48.5°C, are at the ventilating lid B1 and solid boundary between workplace and ventilating lids (located at the middle of the figure). The moderately low temperature (32.8°C) area is located around the upper part of the right opening (upper part of the IO4) and the lower part of the right opening of the picture (lower part of the IO3). The lowest temperature in this plane (31.5°C) takes place at the middle part of the right side of the picture (IO3) followed by the ground and the second opening of the right side (IO4). This distribution is caused by the

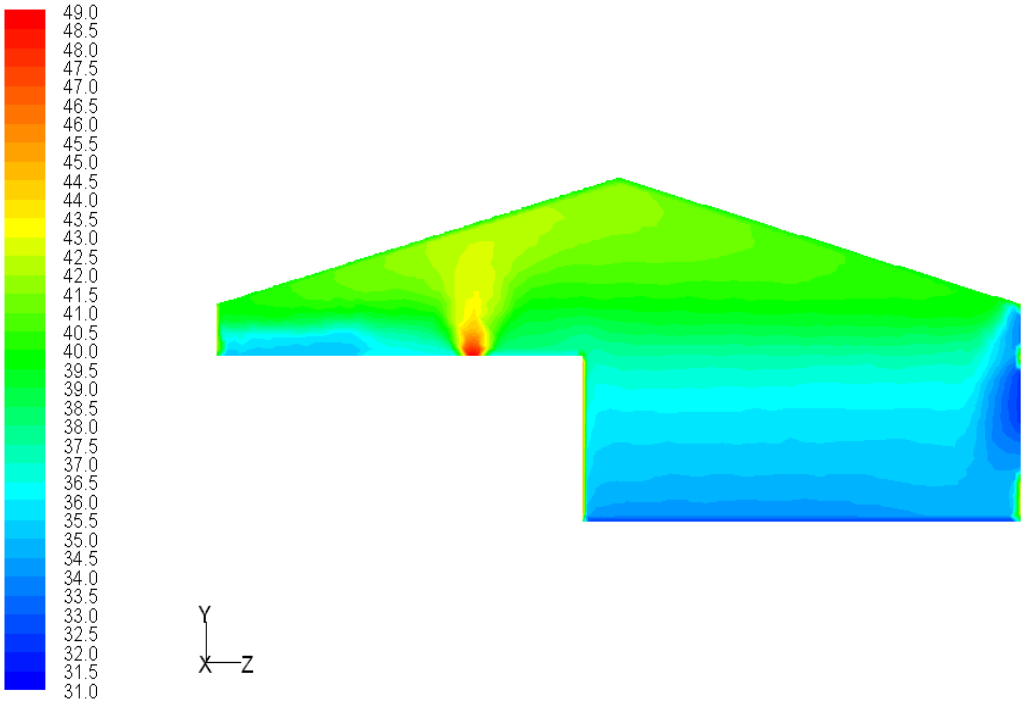

Fig 4.10 The contours of temperature (°C) at the plane $B-B'$.

moderately high velocity of the air flowing to the factory. Cooling effect of the air near the interface between outdoor environment and indoor environment takes place because of inlet air flowing into the workplace.

The temperature contours at the plane $C-C'$ is shown in Fig 4.11. It is similar to that in plane $B-B'$ showing that the highest temperature is located at ventilating lid B2 (48.3^{o}C). The lowest temperature in this plane (31.5^{o}C) is in the middle part of the right side of the figure (IO3) followed by the area near the ground and the second opening of the right side (IO4). The temperature in the large area in the workplace ranges from 32.2 to 35.7^{o}C.

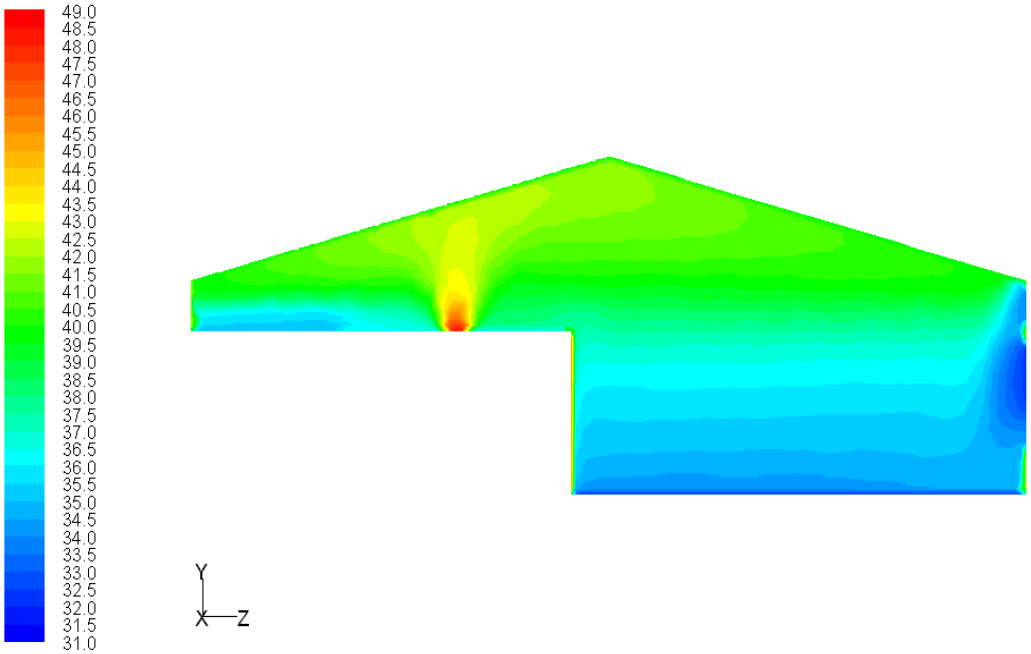

Fig 4.11 The contours of temperature (^{o}C) at the plane $C-C'$.

The temperature contours at the plane $D-D'$ is shown in Fig 4.12. The highest temperature area is located at the ventilating lids B1 and B2 and above as

expected. The separation of low and high temperature regions is also clear. The lowest temperature in this plane is located near the floor area on the bottom-right side of the figure.

The impact of high temperature which comes from B1 and B2 is clearly shown in Fig 4.13. The area at the height of one third from the roof shows the highest temperature profile in the range of 39.8 to 40.5^{o}C. It also shows that the lowest temperature is located near the ground and the left side of the cooperative because it is the area far away from the heat source (smoke room and ventilating lids). Overall, the temperature is reduced downward as one may expect because of the buoyancy effect.

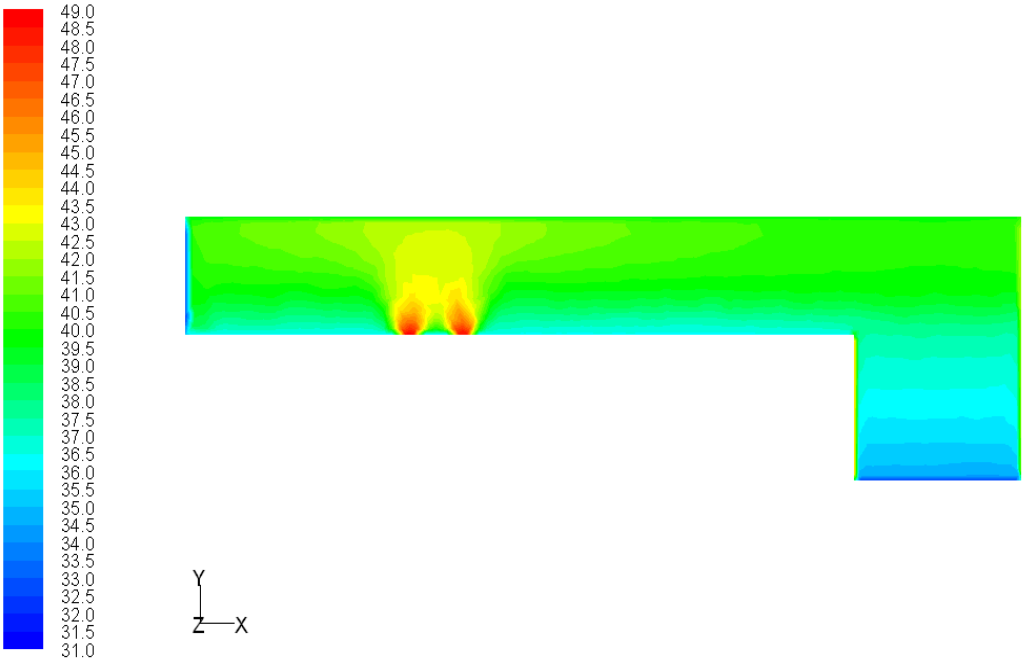

Fig 4.12 The contours of temperature (^{o}C) at the plane D – D' .

Comparison of temperature between simulation and measurement

Comparison of temperature between simulation and experiment at various locations are shown in Fig 4.14 and Table 4.3. The results show a good agreement between the measurement and simulation values with error less than 6 %. This indicates a proper simulation scheme.

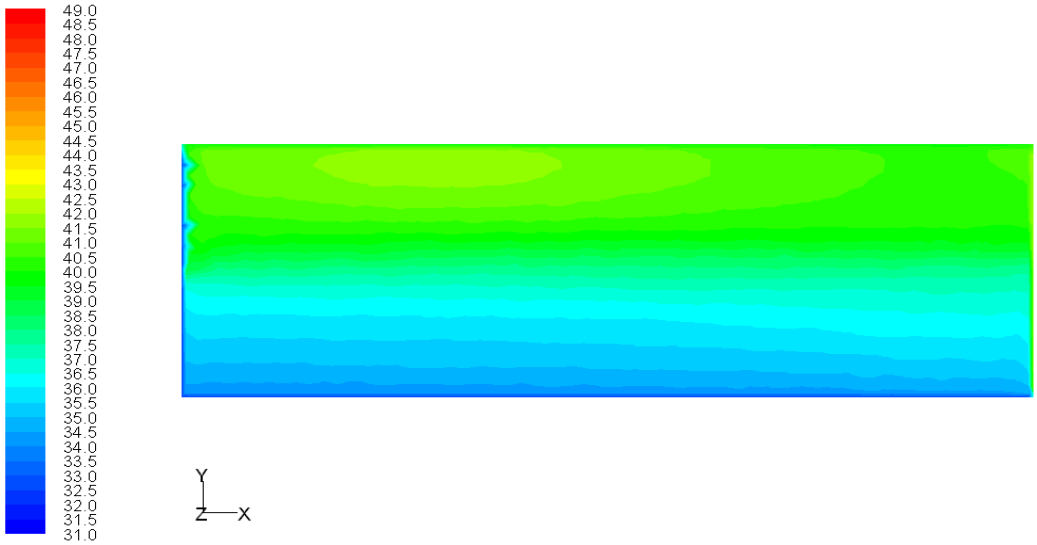

Fig 4.13 The contours of temperature (^{o}C) at the plane E – E'.

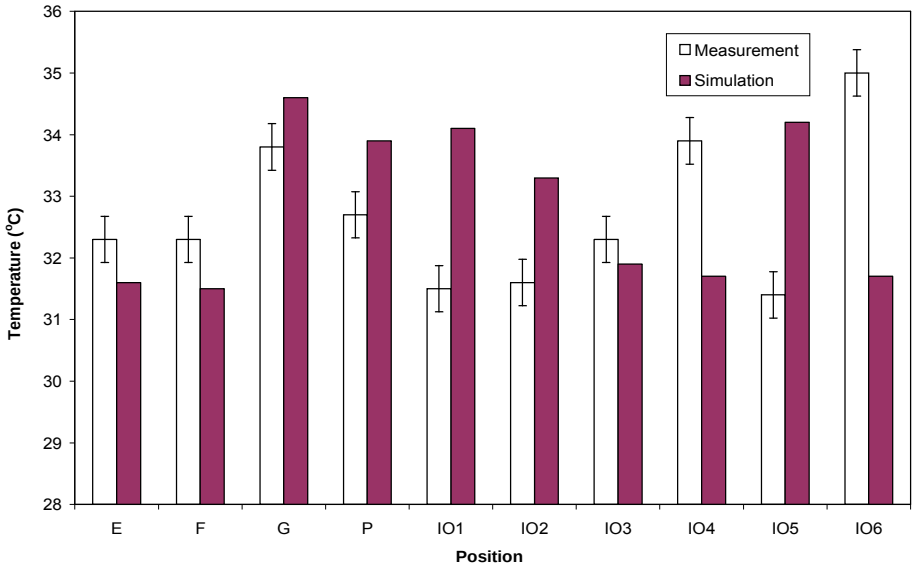

Fig 4.14 Comparison of temperature from measurement and simulation.

Table 4.3 Data comparison between results from measurement (Mea) and simulation (Sim) of temperatures.

Parameters	Temperature (^{o}C)		S.D.
	Mea	Sim	
E	32.3	31.6	0.29
F	32.3	31.5	1.90
G	33.8	34.6	5.59
P	32.7	33.9	1.33
IO1	31.5	34.1	2.03
IO2	31.6	33.3	2.08
IO3	32.3	31.9	1.34
IO4	33.9	31.7	1.23
IO5	31.4	34.2	2.00
IO6	35.0	31.7	1.29

4.5 Particle Trajectory

The trajectories of particles released from the surfaces of the opened ventilating lids B1 and B2 are shown in Fig 4.15. The particles were released normal to boundaries and would reflect if they collide with the walls. There are 18 sampled particles released (displayed in the Fig 4.15 as the particle number 0, particle number 1, particle number 2, particle number 3, … , particle number 17), 9 particles from each ventilating lid. The particle diameter was assumed to be uniform of 1.0

micrometer, because smoke particles under consideration are resulted from burning of rubber-wood (Kalasee et al., 2003).

The average velocity of every particle is 1.025 m/s, the temperature is 48.6^{o}C, and the aerosol concentration is 4.178 mg/m^{3} (Purba et al., 2008). This results in the aerosol mass flow rate of 4.178 x 10^{-6} (kg/m^{3}) x 1.025 (m/s) x 0.6 (m) x 0.6 (m) = 1.5416 x 10^{-6} kg/s. The smoke particles follow the airflow fields where some of them leave the junction of the roof and some of them deposit onto the walls. The particles seem to be congested near the roof area before vented out of the cooperative. One particle escapes via IO5 (the entrance to the cooperative) on the left side of the figure and the other 17 particles are still contained inside of the RSS cooperative for a given specific number of step of simulation, after total traveling distance of about 200 m.

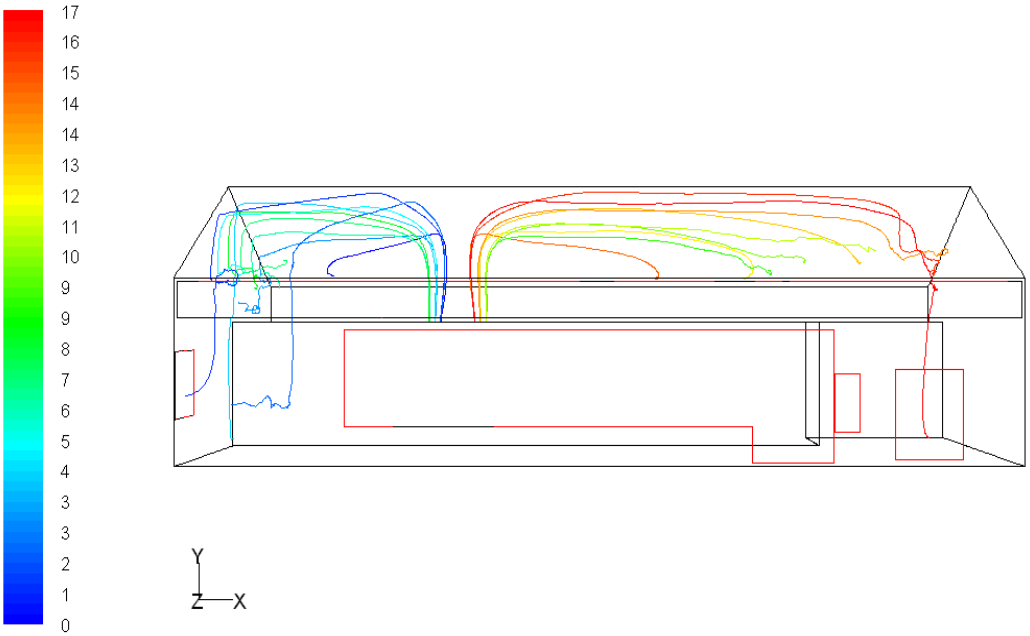

Fig 4.15 Trajectories of smoke particles with diameter of 1 micrometer released from B1 and B2 by using Discrete Phase Model of FLUENT (average traveling distance of about 200 m).

4.6 Particle Concentration

The calculation of concentrations of aerosol particles was achieved by assuming the aerosol as a gas phase. The species module was used in this calculation. Carbon monoxide was used as a representative of aerosol species. The gas was then assumed to be a mixture of air and carbon monoxide. Boundary values of species mass fraction were needed in the calculation. It was calculated from species mass fraction = mass of aerosol particles/ (mass of aerosol particles + mass of air).

Considering 1 m^3 of volume, mass of air at 20.0^oC is 1.225 kg and mass of aerosol particles at the inlet boundary (B1 and B2) is 4.178 mg (concentration at inlet boundary is 4.178 mg/m^3 from measurement). Therefore the mass fraction of aerosol species at the inlet is 3.41 x 10^{-6} which was then used as a boundary condition.

The resultant particle concentrations at P1, P2, and P3 from the species module simulation were compared with those obtained from measurements as a verification method. Detail of this simulation steps is shown in Appendix D. Mass fraction of particles for outlet boundaries (assumption) was assumed to be 0.0, and set to be zero diffusive flux for solid boundaries. Mean reaction between wall and particles was not taken into account. Others boundary conditions are as given in the Table 4.1.

It is clearly seen from Fig 4.16 that particle concentration distribution at the plane $A-A'$ at the working height is quite small but it keeps increasing along the height to the roof, ranging from 0.8896 mg/m^3 at the smoking room ceiling height to 1.6019 mg/m^3 below the roof wall. From Fig 4.17 and Fig 4.18, the particle concentrations at the working height in planes $B-B'$ and $C-C'$ are also small

compared to those above ceiling as shown in Figs. 4.17 and 4.18. The concentrations at the ventilating lid exits are highest as these points serve as the sources of aerosol particles.

Fig 4.19 shows the particle concentration distribution at the plane $D - D'$. The particles from B1 and B2 propagate to the workplace area following the streamlines while other lids (A1, A2, C1, C2, D1 and D2) are closed. The highest particle concentrations are located at the vicinity above the ventilating lids B1 and B2. The lowest one is located at the worker residential area.

Particle concentration distribution at the coordinate $Z = 11.0$ (plane $E - E'$) is shown in Fig 4.20. Particle concentration is high on the upper left side of the workplace compared to the right side. This is because the aerosol flow from ventilating lid B1 cannot easily escape from the workplace as the boundary is a solid wall and small opening, while the particles from B2 have longer range to travel to the right side. This results in lower concentration near the residential and rubber cutting areas.

From Fig 4.19 and Fig 4.20, the particle concentrations at the workplace area are small, when compared with the values near the roof. This is because the aerosol flows upward with the air due to buoyancy force. However, the concentration at the workplace height is high enough to cause health problem of workers who usually work and live inside the cooperative. This reiterate the need for better ventilation of air and smoke particles inside the workplace area of the cooperative.

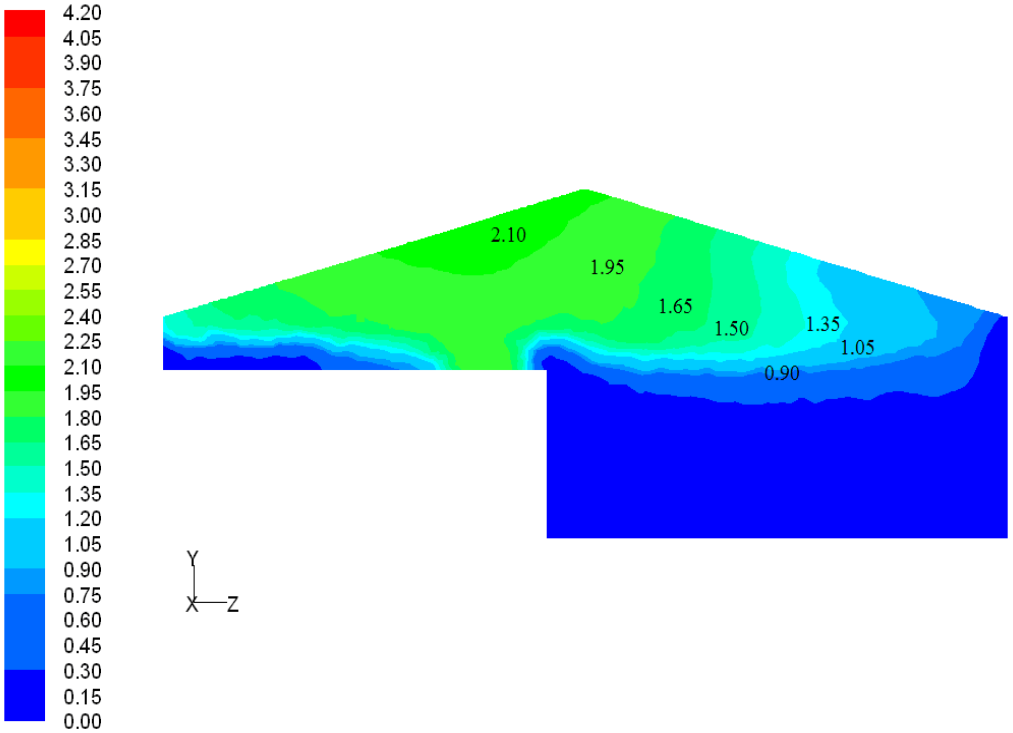

Fig 4.16 Contours of particle-concentrations (mg/m^3) at the plane A – A' .

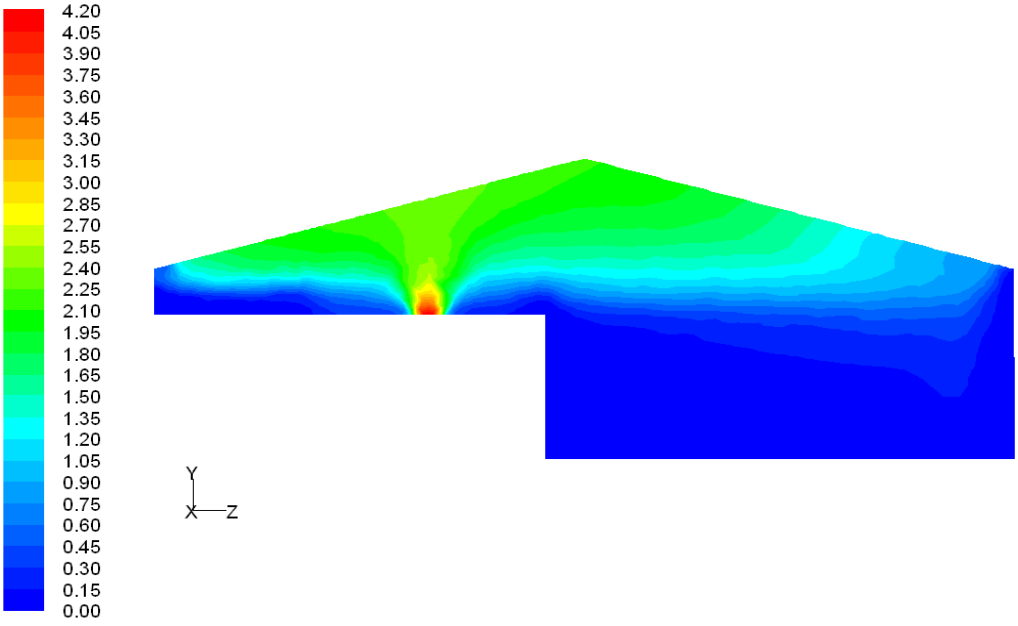

Fig 4.17 Contours of particle-concentrations (mg/m^3) at the plane B – B' .

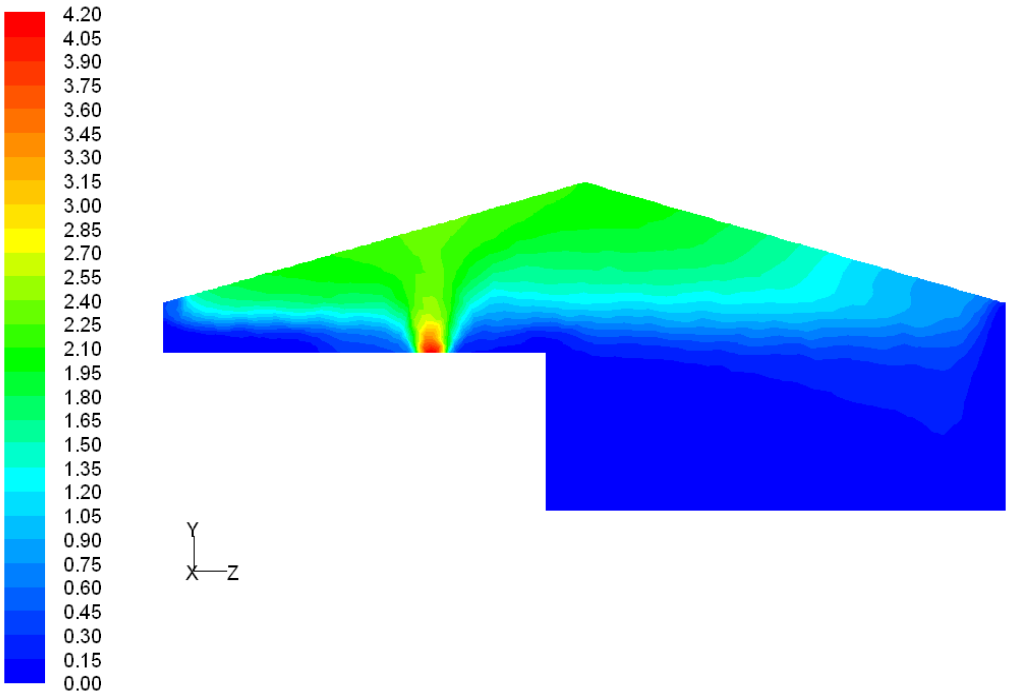

Fig 4.18 Contours of particle-concentrations (mg/m^3) at the plane C – C' .

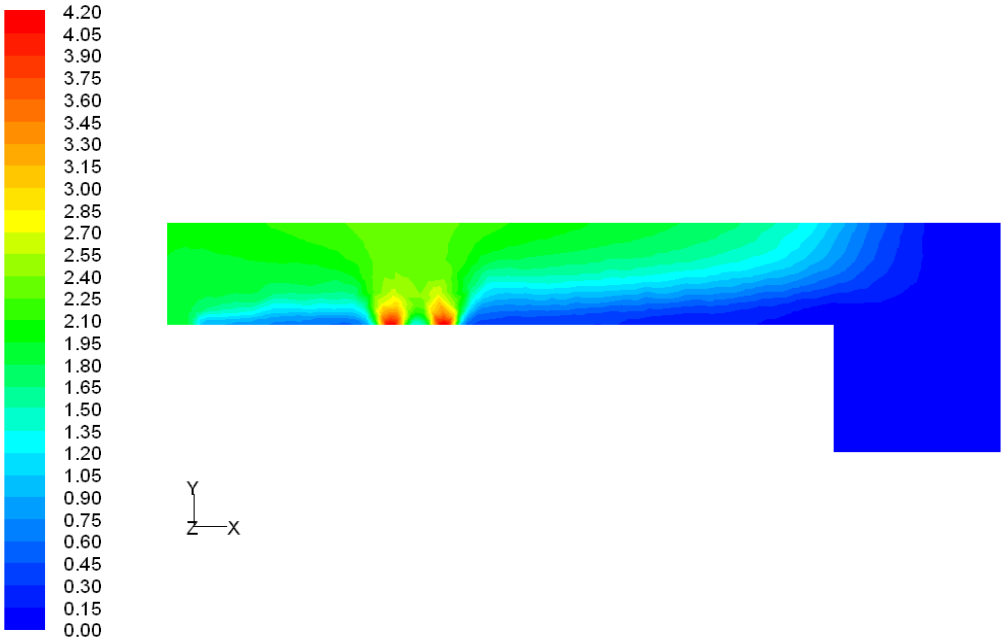

Fig 4.19 Contours of particle-concentrations (mg/m^3) at the plane D – D' .

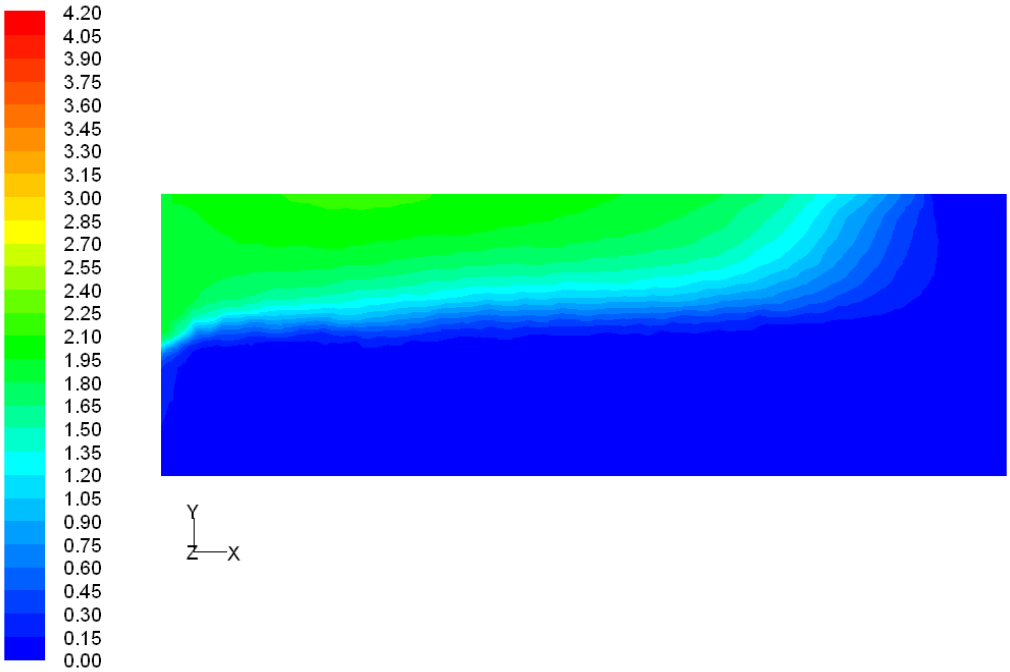

Fig 4.20 Contours of particle-concentrations (mg/m^3) at the plane E – E'.

Comparison of concentration between simulation and measurement

Comparison between simulation and measurement results of particle concentration at 3 positions (P1, P2 and P3) are shown in Fig 4.21 and Table 4.4. Agreement is quite well (average error less than 31 %) considering the difficulty in the measurement where condition was uncontrollable. It can be concluded that particle concentration is increased along the height. Concentration above the ceiling of the smoke rooms is more than three times as high as that at the working level. This does make sense considering the particle trajectories shown previously.

Summary about particle concentration

Simulation results of contours or images of particles concentration show that

the highest particle concentration is located at ventilating lids B1 and B2 as these are the sources of aerosol particles to the workplace. The particles flow up to the roof following air streamlines and leave the workplace through the openings along with the air. The concentration is reduced along the downward direction of the height. Agreement of the simulation and measurement results is acceptable, considering the difficulties in measurement. Although the concentration at the workplace is not very high, the particles are congested in the area above the workplace. If all the smoke rooms are in use, it is possible that the concentration at the working height can be escalated. Hence, proper ventilation of these smoke particles is required.

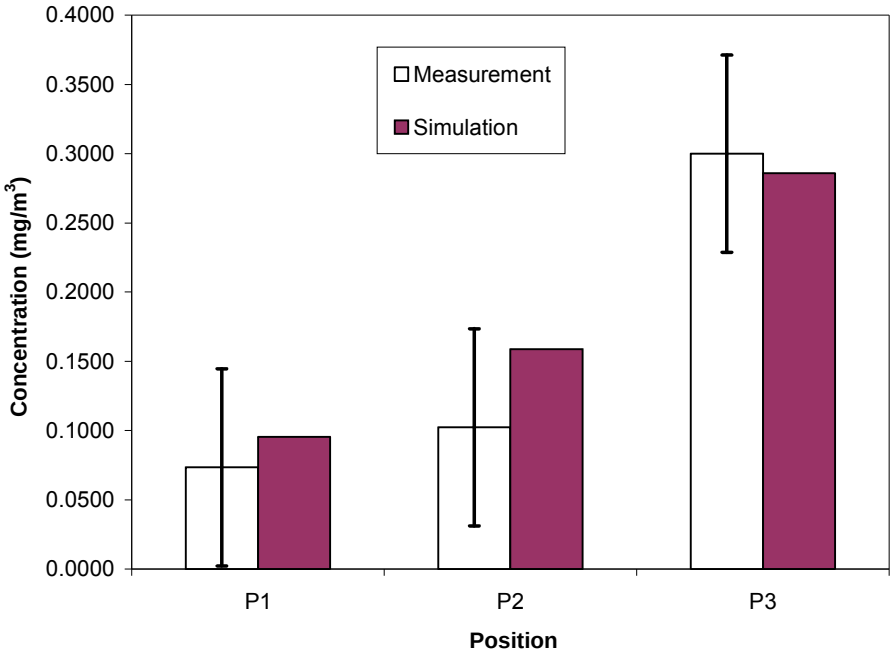

Fig 4.21 Comparison of particle distribution from measurement and simulation.

Table 4.4 Comparison of particle distribution between measurement and simulation in a ribbed smoked sheet rubber cooperative.

Location	Concentration (mg/m^3)		Standard Deviation (SD)
	Measurement	Simulation	
P1	0.0733	0.0953	0.0166
P2	0.1022	0.1588	0.0276
P3	0.3000	0.2858	0.0810

4.6 Ventilation Improvement

In order to lessen risk of workers exposes to a high concentration of smoke aerosol particles, study of airflow to improve ventilation system for the ribbed smoked sheet rubber cooperative is needed.

There are many alternatives possible for the improvement of ventilation of smoke particles in the RSS rubber cooperative. Forced convection is an effective means to ventilate air but it involves use of energy to drive the ventilation devices usually suction fans or blowers. Natural convection is an appropriate way for ventilation in the cooperative as no cost of energy is required. In this work, natural convection of heat and ventilation of smoke particles out of the cooperative roof will be considered. By modifying the roof top to include spaces for ventilation or roof ridge vent, smoke particles can be released through these spaces. The configuration considered in this work is shown in Fig 4.22 and the dimensions to be varied are

shown in Table 4.5. Variation of the dimensions *a*, *b* and *c* will be conducted in 4 cases to compare ventilation capability. Here *a* is the dimension of horizontal span of improved roof, *b* is the dimension of the opening height (vertical span) in the vertical direction, and *c* is the dimension of span according to variation of the spans *a* and *b*. Positions *L*, *M* and *N* are the monitoring points for velocity, temperature and aerosol concentration. These values will be used for discussion of ventilation improvement.

Table 4.5 Parameters of dimensions varied in the ventilation improvement simulation.

Improvement	*a* (m)	*b* (m)	*c* (m)
Case 1	3	1	3.6
Case 2	3	0.5	1.8
Case 3	2	1	3.6
Case 4	2	0.5	1.8

Case 1

The calculation was converged after 583 iterations. The residual of the convergent case is shown in Fig 4.23. The velocity vectors in Fig 4.24 show that a major part of the smoke released from a ventilating lid escapes the cooperative through the opening on the roof top. A small part of the smoke escapes via the opening on the back side (left side of the figure, IO6). Some fresh air induced to the cooperative via the opening IO4 (upper right) moves along the ground to the front door surface of the smoke room and leave the cooperative via the opening on the roof top along with the smoke particles.

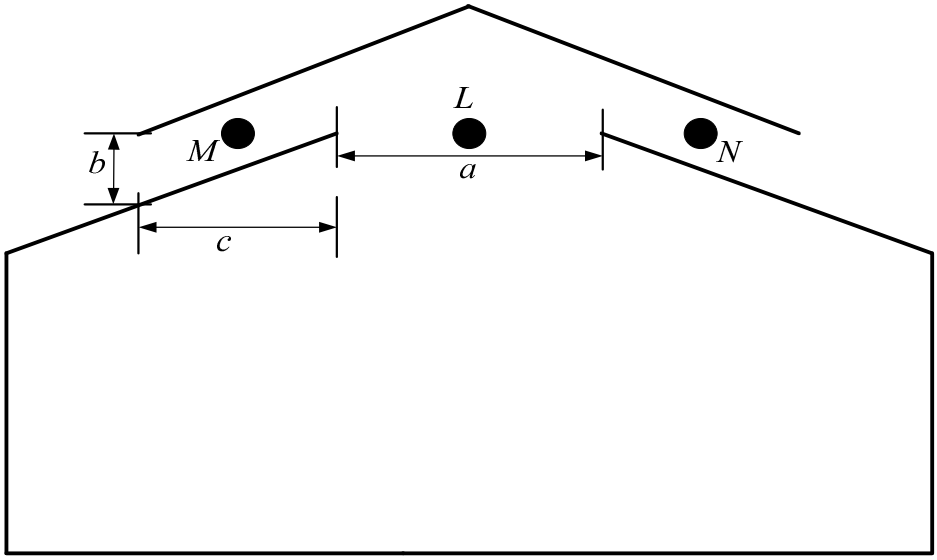

Fig 4.22 Dimension of the improved cooperative including roof ridge vent.

The remaining portions of the air entering IO4 and the top part of IO3 leave at the bottom part of IO3. Escaping velocities at the centers of the roof openings on the left (point *M*) and right (point *N*) sides are 0.20 and 0.38 m/s, respectively. The velocity at the center of span *a* (point *L*) is 0.17 m/s. Since most of the smoke particles are vented, the temperature in the cooperative is significantly reduced as shown in Fig 4.25. The temperature at the center of span *a* (point *L*) is 39.5^{o}C. The particle concentration at this position is 1.463 mg/m^3, while the concentration at P1, P2 and P3 are 0.024, 0.023 and 0.060 mg/m^3, respectively. The contour plot of aerosol concentration in Fig 4.26 indicates the distinguished layers between the top part (high concentration) and the bottom part (low concentration).

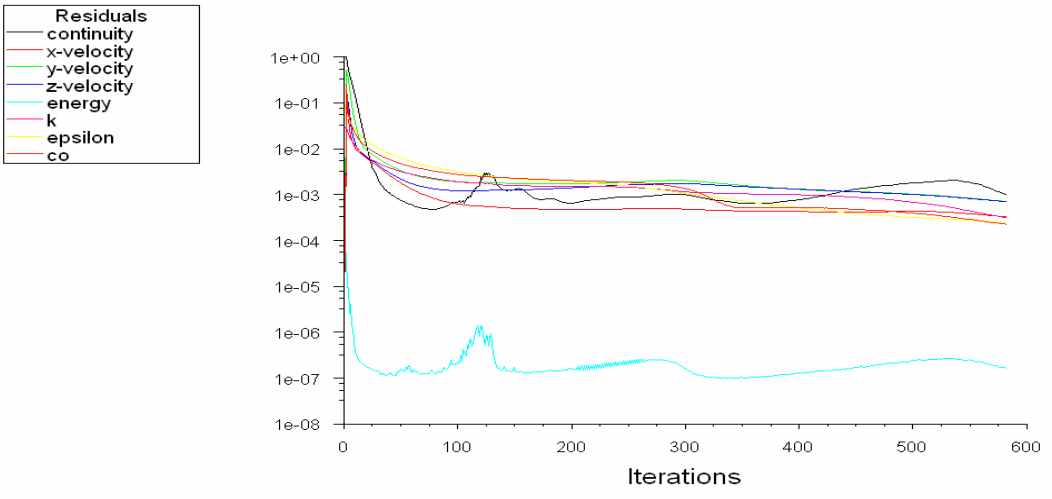

Fig 4.23 Scaled residuals of the calculation after convergence for 583 iterations (improvement Case 1).

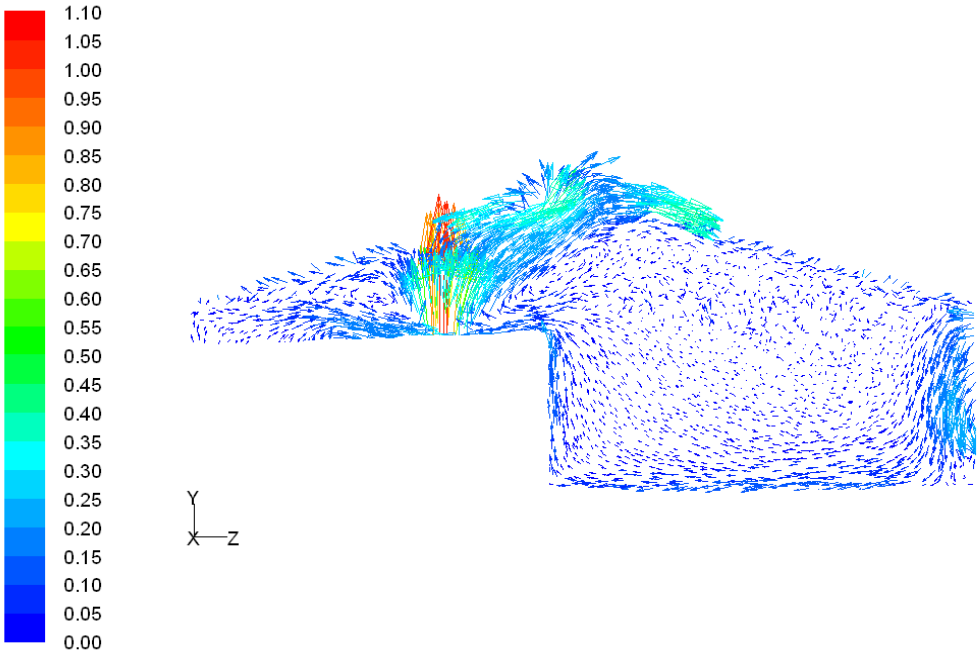

Fig 4.24 Vector of velocity magnitude at the plane cut across the center of B2 (improvement Case 1).

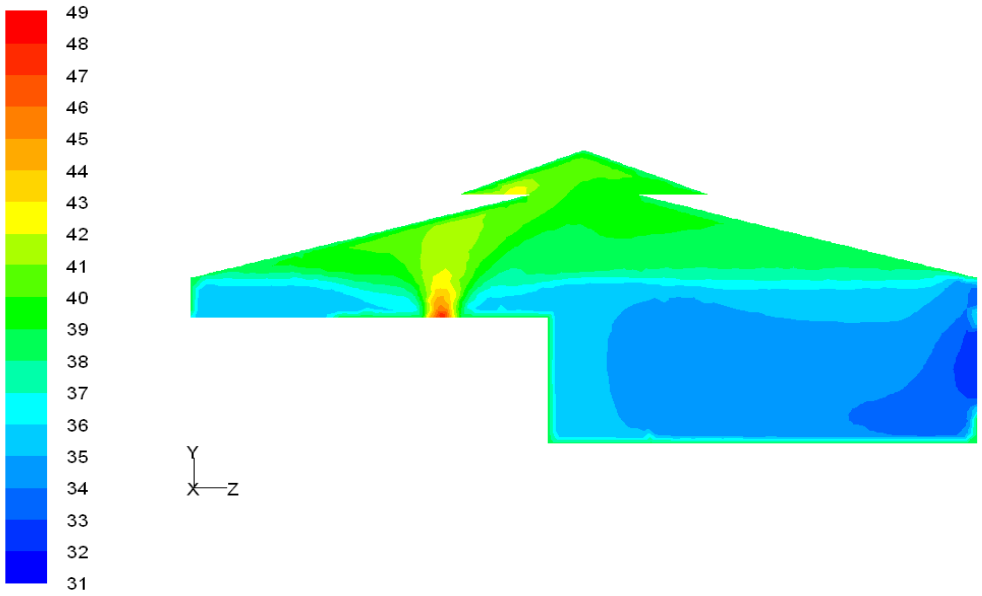

Fig 4.25 Contours of temperature at the plane cut across the center of B2 (improvement Case 1).

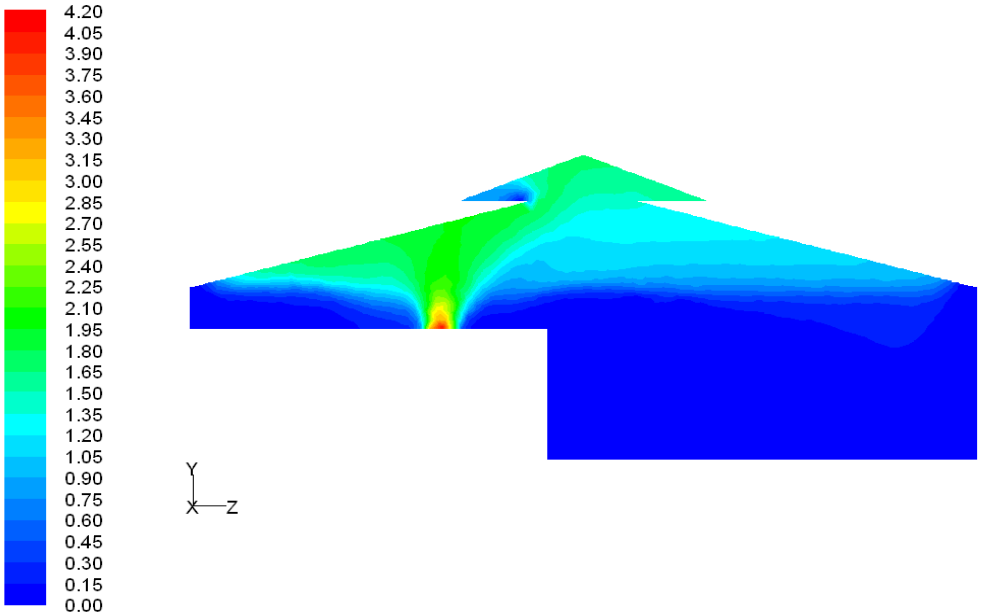

Fig 4.26 The contours of particle concentrations at the plane cut across the center of B2 (improvement Case 1).

Case 2

In this case the opening height in the vertical direction (*b*) and the span (*c*) of an improved roof are reduced in half as given in Table 4.5. The calculation was converged after 550 iterations. The residual of the convergent case is shown in Fig 4.27. The velocity vectors in Fig 4.28 show that a major part of the smoke released from a ventilating lid escapes the cooperative through the opening on the roof top as in Case 1 although their velocities are quite small. Velocities at the centers of roof openings on the left (point *M*) and right (point *N*) sides are 0.00 and 0.09 m/s, respectively. The velocity at the center of span *a* (point *L*) is 0.07 m/s. A small part of the smoke escapes via the opening on the back side (left side of the figure, IO6). Some fresh air induced to the cooperative via the opening IO4 (upper right), moves along the ground to the front door surface of the smoke room and leave the cooperative via the opening on the roof top along with the smoke particles. The remaining portions of the air entering IO4 and the top part of IO3 leave at the bottom part of IO3 as in Case 1. The temperature at the center of the span *a* (point *L*) is 44.1^{o}C which is almost 5^{o}C higher than Case 1. The particle concentration at this position is 1.681 mg/m^{3}, while the concentration at P1, P2 and P3 are 0.074, 0.493 and 0.654 mg/m^{3}, respectively, significantly higher than those in Case 1. The temperature and aerosol concentration contours, shown in Fig 4.29 and Fig 4.30, indicate same behaviors as in Case 1 but the values are higher.

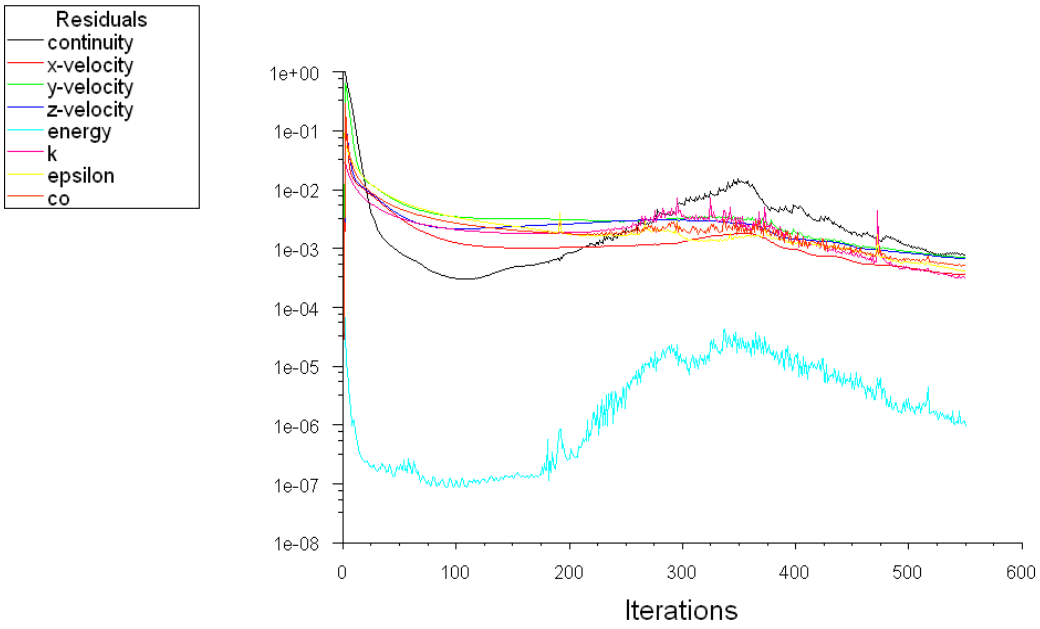

Fig 4.27 Scaled residuals of the calculation after convergence for 550 iterations (improvement Case 2).

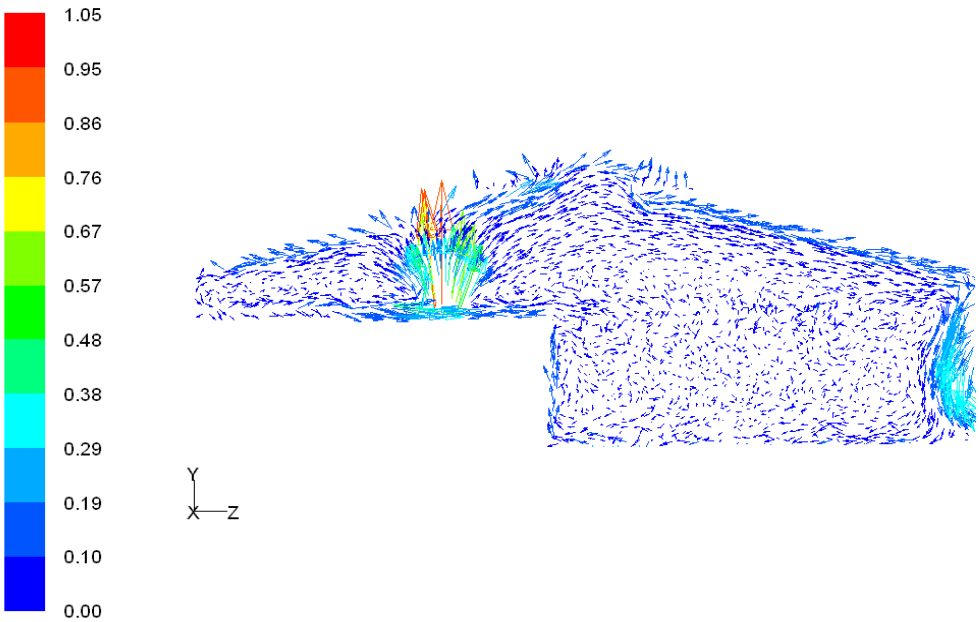

Fig 4.28 Vector of velocity magnitude at the plane cut across the center of B2 (improvement Case 2).

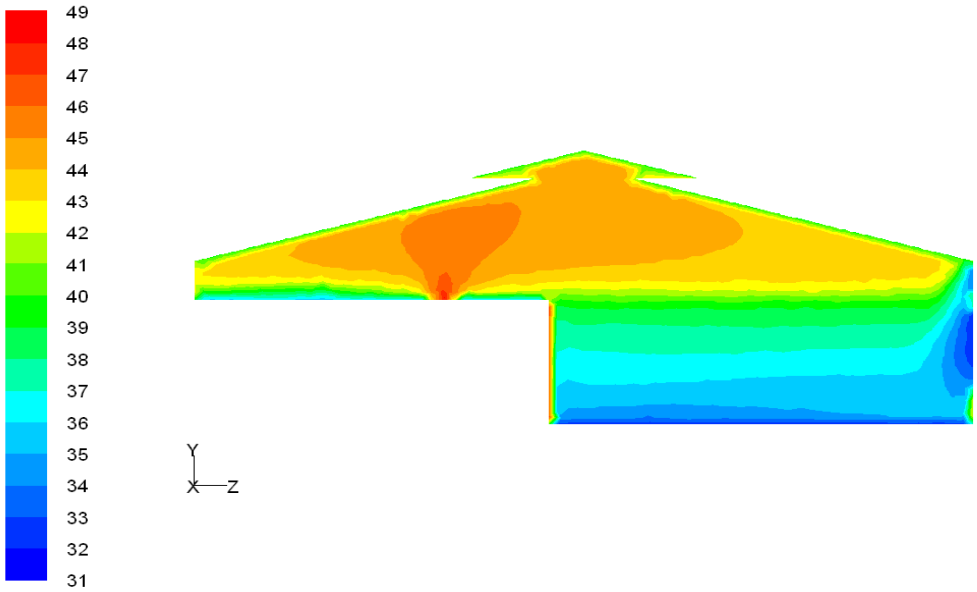

Fig 4.29 Contours of temperature at the plane cut across the center of B2 (improvement Case 2).

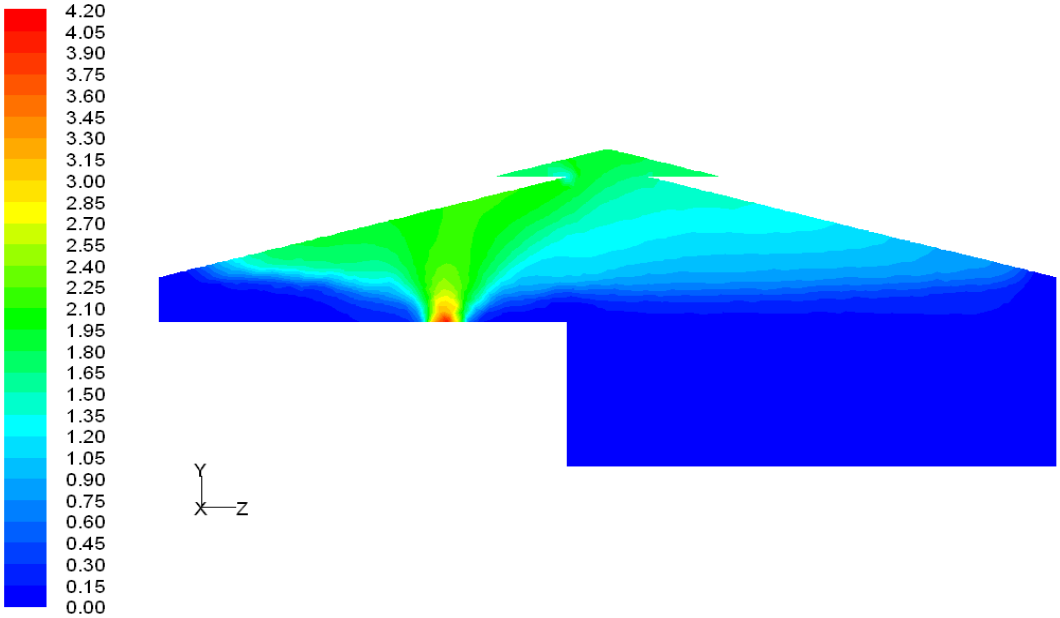

Fig 4.30 The contours of particle concentrations at the plane cut across the center of B2 (improvement Case 2).

Case 3

In this case the opening height in the vertical direction (*b*) and the span (*c*) are the same as Case 1, while opening *a* is reduced from 3 m to 2 m as given in Table 4.5. The calculation was converged after 480 iterations. The residual of the convergent case is shown in Fig 4.31. The velocity profile (Fig 4.32) shows the same behavior as in the previous cases. However, the velocities at the centers of roof openings on the left (point *M*) and right (point *N*) sides are 0.06 and 0.12 m/s, respectively. The velocity at the center of span *a* (point *L*) is 0.16 m/s. The temperature at the center of the span *a* (point *L*) is 40.3^{o}C while the contour plot is same as in Case 1 (Fig 4.33). The particle concentration at position *L* is 0.976 mg/m^3, while the concentration at P1, P2 and P3 are 0.062, 0.080 and 0.294 mg/m^3, respectively (Fig 4. 34).

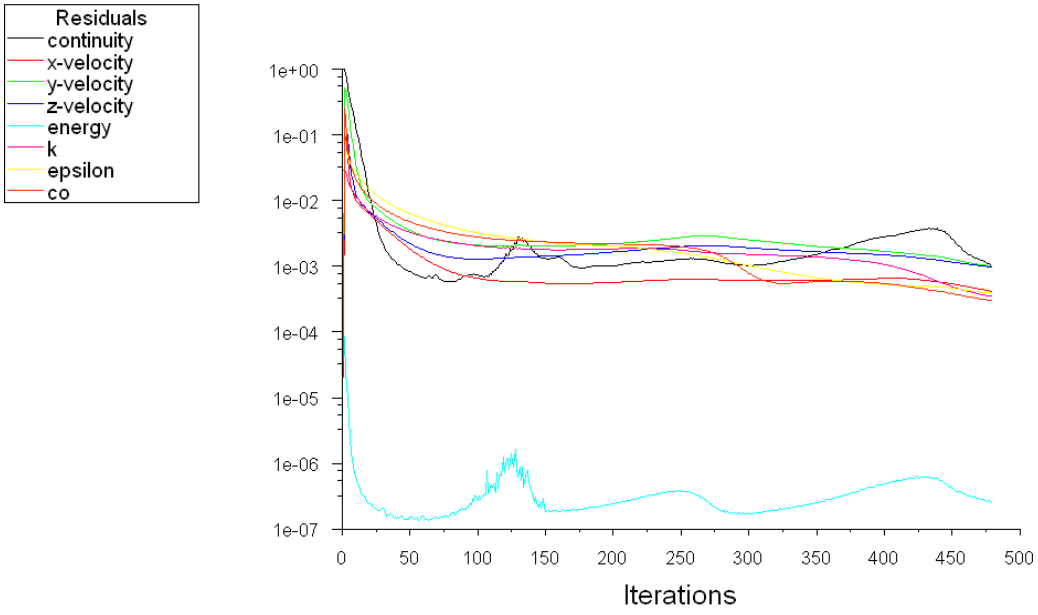

Fig 4.31 Scaled residuals of the calculation after convergence for 480 iterations (improvement Case 3).

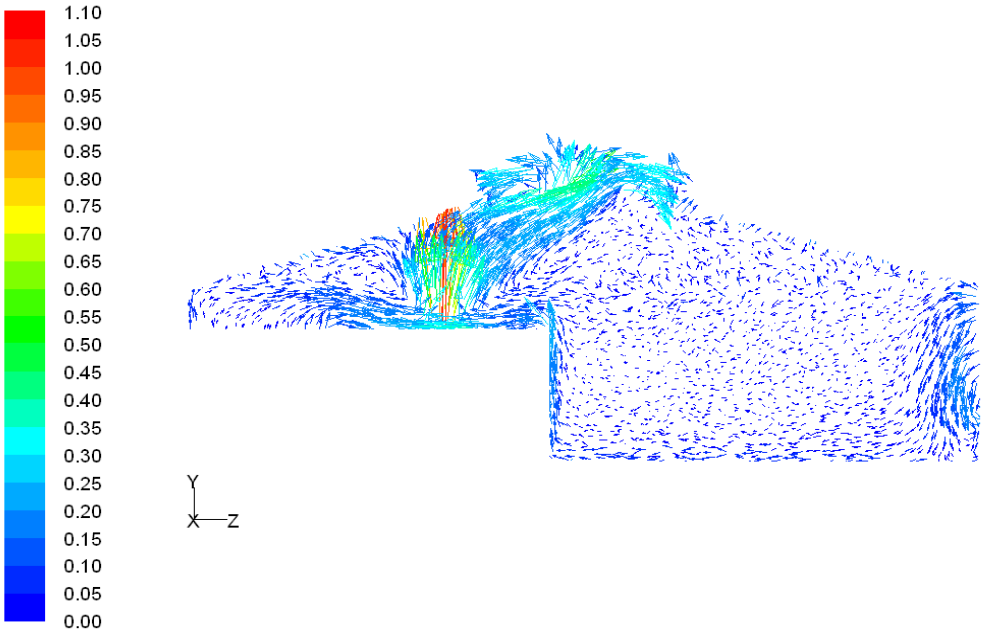

Fig 4.32 Vector of velocity magnitude at the plane cut across the center of B2 (improvement Case 3).

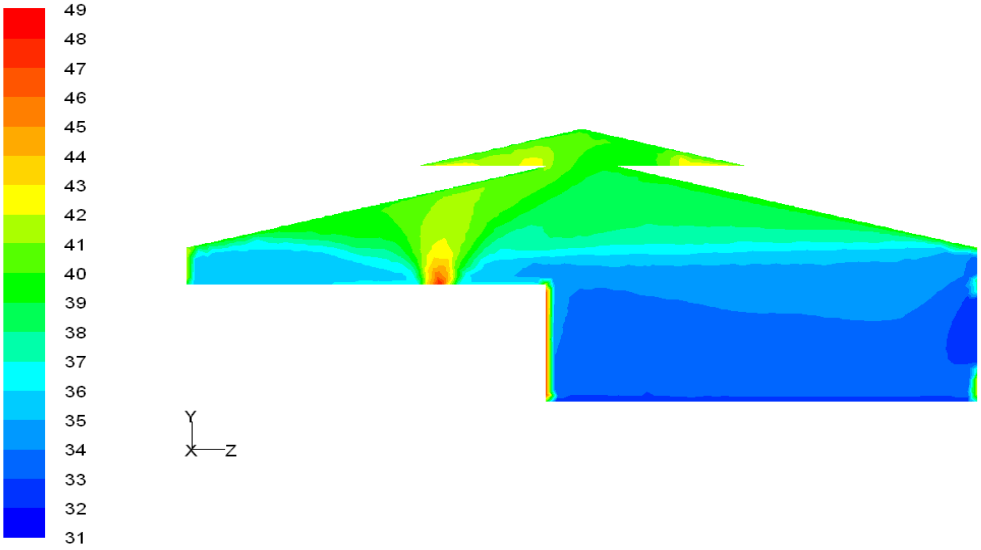

Fig 4.33 Contours of temperature at the plane cut across the center of B2 (improvement Case 3).

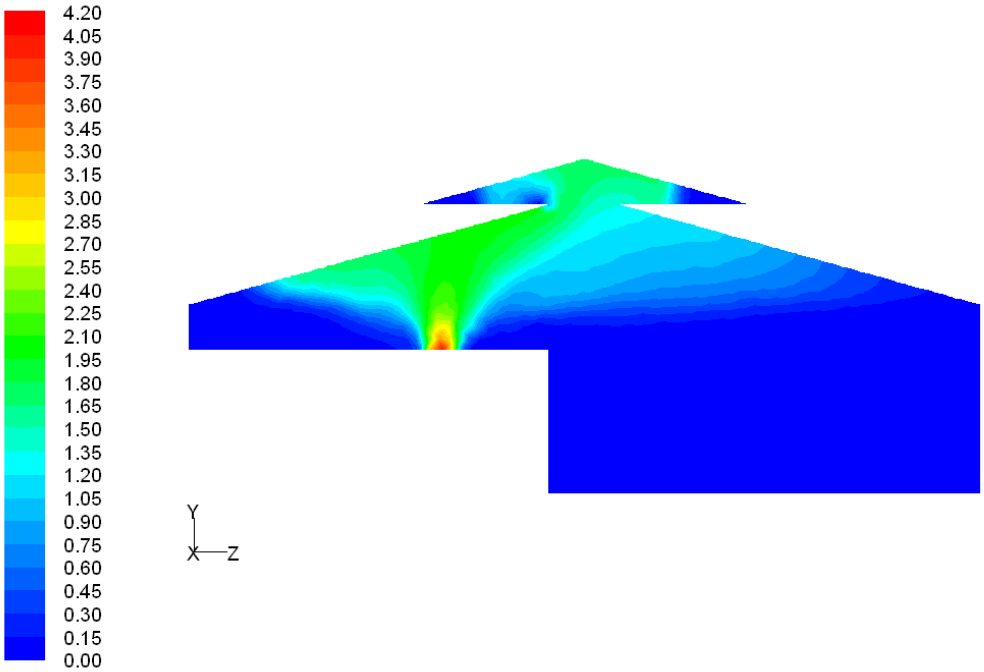

Fig 4.34 The contours of particle concentrations at the plane cut across the center of B2 (improvement Case 3).

Case 4

In this case, the opening height in the vertical direction (*b*) and the span (*c*) are the same as Case 2, while opening *a* is reduced from 3 m to 2 m, as given in Table 4.5. The calculation was converged after 474 iterations. The residual of the convergent case is shown in Fig 4.35. The velocity vectors in Fig 4.36 show that a major part of the smoke released from a ventilating lid escapes the cooperative through the opening on the roof top as in previous cases while their velocities in this case are highest. Velocities at the centers of roof openings on the left (point *M*) and right (point *N*) sides are 0.35 and 0.38 m/s, respectively. The velocity at the center of span *a* (point *L*) is 0.18 m/s. A small part of the smoke escapes via the opening on the back side (left

side of the figure, IO6). Some fresh air induced to the cooperative via the opening IO4 (upper right), moves along the ground to the front door surface of the smoke room and leave the cooperative via the opening on the roof top along with the smoke particles as in previous cases. The temperature at the center of the span *a* (point *L*) is 40.3^{o}C which is lower than Case 1 (Fig 4.37). The particle concentration at this position is 1.760 mg/m^{3}, while the concentration at P1, P2 and P3 are 0.075, 0.113 and 0.688 mg/m^{3}, respectively (Fig 4.38).

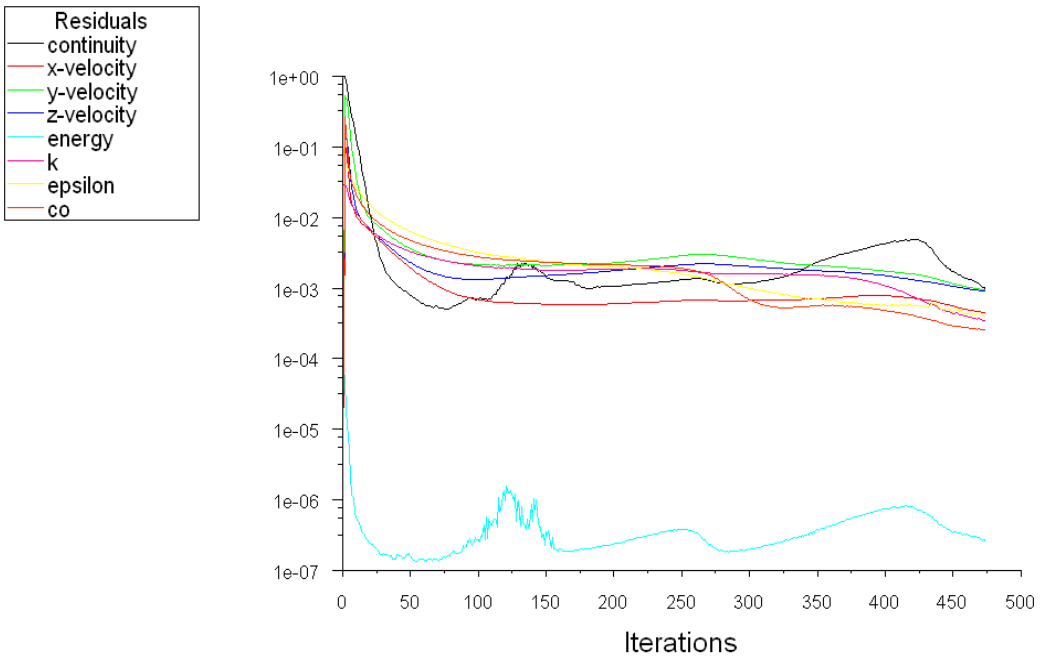

Fig 4.35 Scaled residuals of the calculation after convergence for 474 iterations (improvement Case 4).

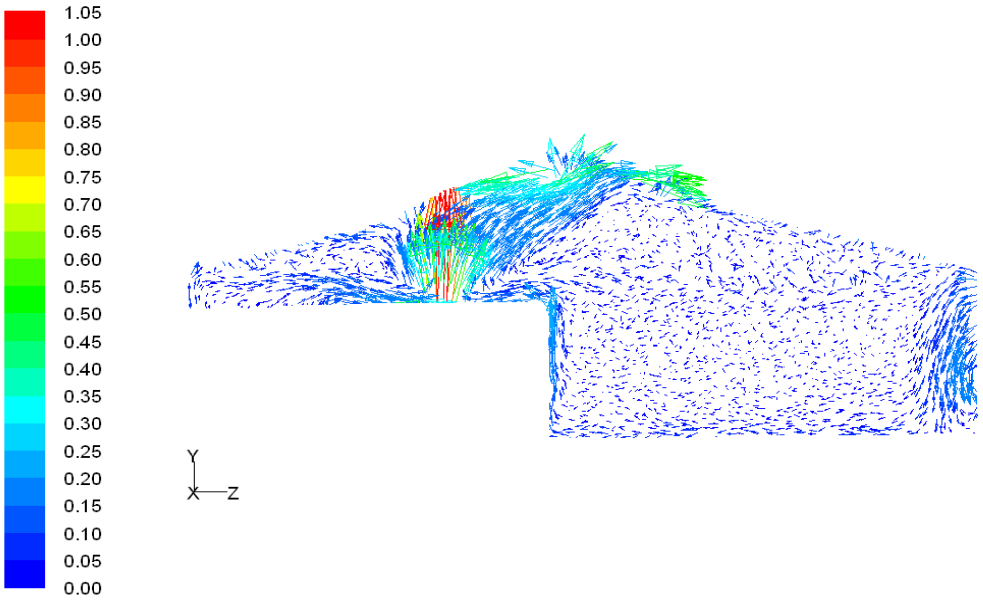

Fig 4.36 Vector of velocity magnitude at the plane cut across the center of B2 (improvement Case 4).

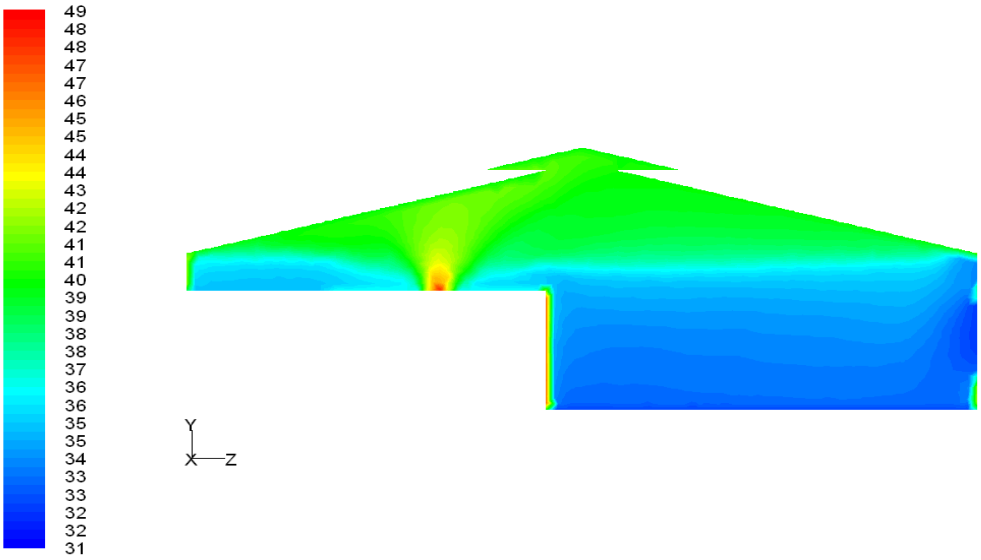

Fig 4.37 Contours of temperature at the plane cut across the center of B2 (improvement Case 4).

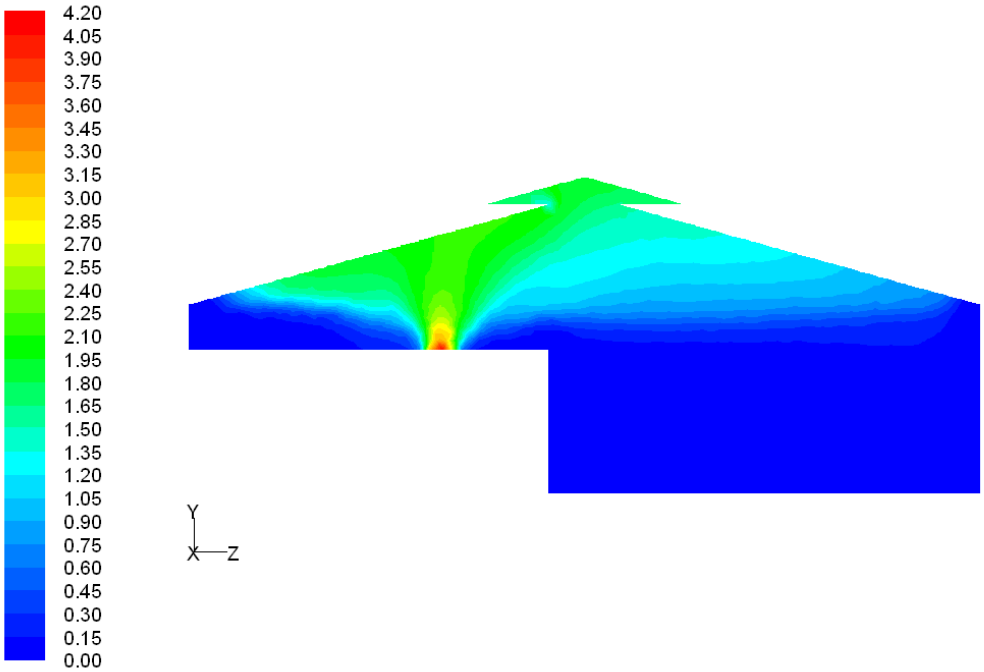

Fig 4.38 The contours of particle concentrations at the plane cut across the center of B2 (improvement Case 4).

Summary for improvements

Comparison of velocity, temperature, and aerosol concentrations at several positions are summarized in Table 4.6. For the velocity vector after improvement based on velocities at the centers of roof openings on the left (point *M*), the right (point *N*) and the span *a* (point *L*) Cases 1 and 4 result in the highest values while the temperature are practically the same for all cases. However the concentrations of aerosol in the workplace area (positions P1, P2 and P3) are higher than Cases 1 and 3. The best case seems to be Case 1 where the concentrations are lowest. This is confirmed for all workplace area as shown in the concentration contours plots. This is due to the largest openings of the improved roof top. The openings can be larger to

reduce the aerosol concentrations but at these values, the workplace contamination by smoke particles is significantly reduced to safe values compared to guidelines for ambient air concentration of dust < 0.330 mg/m^3 (Tekasakul et al., 2008; Thailand Pollution Control Department, 2009).

Table 4.6 Comparison of velocity, temperature and aerosol concentration for all cases.

Case	Velocity (m/s)			Temperature (^{o}C)	Concentration (mg/m^3)			
	L	*M*	*N*	*L*	*L*	P1	P2	P3
1	0.17	0.20	0.38	39.5	1.463	0.024	0.023	0.060
2	0.07	0.00	0.09	44.1	1.681	0.074	0.493	0.654
3	0.16	0.06	0.12	40.3	0.976	0.062	0.080	0.294
4	0.18	0.35	0.38	40.3	1.760	0.075	0.113	0.688
Unimproved	-	-	-	41.1	1.966	0.116	0.608	1.097

From all cases of improvements, in term of the objective to lessen risk of workers exposes to a large portion of smoke aerosol particles, it can be recommended for the owner or the RSS entrepreneurs to improve the workplace environment workplaces inside of the ribbed smoked sheet rubber cooperative by:

1. to modify the roof top of the cooperative with dimension of Case 1 in order to reduce the aerosol concentrations to safe values.

2. or if the budget is limited, to close the opening between the ceiling of the smoke room and the workplace area so that no smoke particle can leak to the workplace as an alternative to vent out the smoke to the back side (shown in Fig 4.39). Ventilating turbines may be installed on the roof to enhance the ventilation capacity.

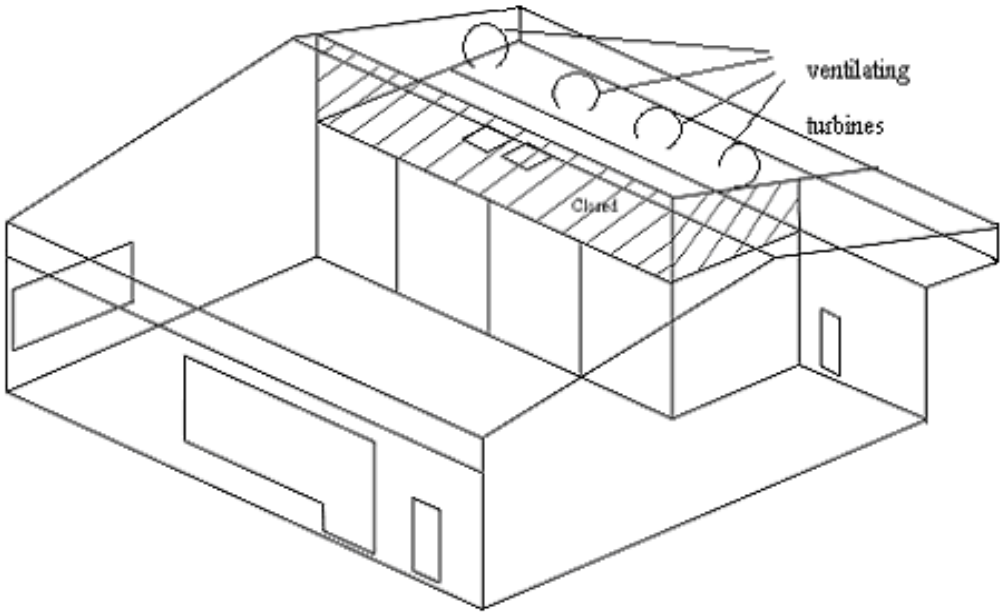

Fig 4.39 An alternative to improve ventilation of the smoke particles from the rubber sheet smoke room.

Chapter 5

Conclusions

The main objectives of this research are (i) to investigate the pattern of fluid flow and smoke particle concentration inside a ribbed smoked sheet rubber (RSS) cooperative and (ii) to improve the ventilation of the smoke. Smoke resulted from rubber-wood burning enters the workplace area of the cooperative via ventilating lids on the ceiling of the smoking rooms and exits through open spaces around the cooperative. One full batch operation of rubber sheet smoking takes about four days. Since the airflow contains thick clouds of smoke, it directly affects the health of workers exposed to these smoke particles. CFD simulation result shows air flow pattern containing smoke, temperature contours, particle trajectory and aerosol concentration inside the cooperative. Airflow pattern after improvement was also simulated. In the simulation, the flow was assumed to be steady. However, in general, the flow in the smoking room is difficult to control and unsteady effect dominates (Promtong and Tekasakul, 2007).

Results show that locations of the highest velocity and temperature and particle concentration are at the ventilating lid exits because these are the inlets of the system domain where smoke particles from the source enters the workplace area. Air (and smoke) from the ventilating lids generally flows upward to the roof of the cooperative. It then divides in all direction. Part of it is vented out of the workplace area while the remaining circulates inside. This is a major part and it causes contamination of air with smoke particles which is possible hazardous to workers'

health. Agreement between the measurement and the simulation results is good with errors of velocity, temperature and particle concentration lies in the range of 0 – 62.50 % (average 21.14 %), 1.24 – 9.43 % and 4.73 – 55.38 % (average 30.04 %), respectively, considering that the experiments in real condition were uncontrollable.

Particle concentration is high in the vicinity near the ventilating lids of rubber smoking room and the roof of the cooperative. It is reduced along the height in downward direction. Though the concentration in the workplace area is not extremely high, improvement of ventilation of smoke particles is necessary. This is because when all the smoking rooms is used for RSS production, concentration of aerosol particles can become much higher.

Improvements of ventilation by using natural ventilation via roof ridge vent have been simulated for four cases. Case-by-case improvement was performed in the form of velocity vectors, contours of temperature, and particle concentration. Based on the objective of the thesis work to lessen risk of workers exposed to a high concentration of smoke aerosol particles, improvement Case 1 is the best choice. Concentration of smoke particles is significantly reduced to a safe level of < 330 μg/m^3 (Tekasakul et al., 2008; Thailand Pollution Control Department, 2009). An alternative approach for smoke contamination reduction is to close the opening between smoke room ceiling and workplace area. Ventilating turbines may be installed on the roof to enhance the ventilation capacity.

References

Anderson W. K., Gropp W. D., Kaushik D. K., D. E. Keyes, and Smith B. F., "Achieving high sustained performance in an unstructured mesh CFD application", *Proceedings of SC'99*, 1999.

ANSYS FLUENT, *FLUENT 6.3 Documentation*, Fluent Inc., Lebanon, NH, March 2006.

BS4422: 1987, *Part 1: Terms Associated with Fire*, London, UK: British Standard Institution, 1987.

CNBP Transport and Fate Team, [Online]. Available: http://www.lanl.gov/orgs/d/d4/pdf/air/model_review.pdf.

Choosong T., Furuuchi M., Tekasakul P., Tekasakul S., Chomanee J., Jinno T., Hata M., and Otani Y., "Working Environment in a Rubber Sheet Smoking Factory Polluted by Smoke from Biomass Fuel Burning and Health Influences to Worker", *J. Ecotechnology Research*, vol. 13, no. 2, 2007, pp.91-96.

Chow W. K., and Yin R., "Smoke Movement in a Compartmental Fire", *Journal of FIRE SCIENCES,* vol. 24, November 2006, pp. 445-463.

Costa A.M.S., Mareze P.H., and Drugovich A.B., Introduction to finite volume method for Computational fluid dynamic-II-Solving one dimensional flow field", Maringa State University, Maringa PR., 2005, Brazil. [Online]. Available: http://www.geocities.com/desouzadacosta [Accessed 2007].

Einberg G., "Air Diffusion and Solid Contaminant Behaviour in Room Ventilation – a CFD Based Integrated Approach", PhD thesis, Royal Institute of Technology (KTH Industrial Engineering and Management), Stockholm, June 2005.

Fluent Inc., *GAMBIT 2.2 Tutorial Guide*, Fluent Incorporated, 2004.

Fluent Inc., *Tgrid 3 User's Guide,* First Edition, Fluent Inc., Centerra Resource Park, Lebanon, June 1997.

Furuuchi M., Tajima N., Sekiguchi K., Otani Y., Fukumoto M., Yoshikawa F., Bai Y., and Hata M., "Characteristic of Aerosol Nano-particles Sampled at Road Tunnel and Roadside in Kanazawa Outer Ring", *Departmental Bulletin Paper, Kanazawa University Repository for Academic resource (KURA)*, Japan, 2008. [Online]. Available: http://dspace.lib.kanazawa-u.ac.jp/dspace [Accessed 2009].

Gant S.E., Kelsey A., Gobeau N., and Ivings M. J., "Factors influencing the indoor transport of contaminants and modelling implications", *Health and Safety Laboratory Crown*, HSL, vol. 29, 2006.

Henkes R. A. W. M., van der Flugt F. F., and Hoogendoorn C. J., "Natural Convection Flow in a Square Cavity Calculated with Low-Reynolds-Number Turbulence Models", *Int. J. Heat Mass Transfer*, vol. 34, 1991, pp. 1543-1557.

Hinds W.C., *Aerosol Technology Properties, Behavior, and Measurement of Airborne Particles*, 2nd ed., Canada: John Wiley and Sons, 1999.

Hussein T., Korhonen H., Herrmann E., H¨ameri K., Lehtinen K.E.J., and Kulmala M., "Emission Rates Due to Indoor Activities: Indoor Aerosol Model Development, Evaluation, and Applications", *Aerosol Science and Technology*, vol. 39, 2005, pp. 1111–1127.

ISO 8421-1: 1987, *Fire Protection Part 1: General Terms and Phenomena of Fire*, Geneva, Switzerland: International Organization for Standardization, 1987.

Kalasee W., Tekasakul S., Otani Y., and Tekasakul P., "Characteristics of soot particles

produced from rubberwood combustion", *Proceeding of the Second Asian Particle Technology Symposium*, Penang, Malaysia, 2003, pp. 103-108.

Kanaoka C., Furuuchi M., Myojo T., Inaba J., and Ohmata K., "Numerical Investigation of Flow and Dust Concentration Distributions in the Work Area of a Mountain Tunnel Currently under Construction", *Aerosol and Air Quality Research*, vol. 6, no. 3, 2006, pp. 231-246.

Kickinger R., Gittler P., Juvarek M., and Lehner J., "Ventilation and dedusting of melting shop", *Second International Conference on CFD in Minerals and Process Industries*, Melbourne, Australia, 6-8 December 1999.

Kleven M., Melaaen M. C., Reimers M., Rotnes J. S., Aurdal L., and Djupesland P. G., "Using computational fluid dynamics (CFD) to improve the bi-directional nasal drug delivery concept", *Food and Bioproducts Processing,* vol. 83, Issue 2, 2005, pp. 107-117.

Launder B. E., and Spalding D. B., *Lectures in Mathematical Models of Turbulence*. London, England, Academic Press, 1972.

Loomans M., and Lemaire T., "Particle concentration calculations using CFD – a comparison", *Proceedings of Indoor Air*. Edinburgh, Scotland, 2002, pp. 153–156.

Lu W., and Howarth A.T., "Numerical analysis of indoor aerosol particle deposition and distribution in two-zone ventilation system", *Building and Environment*, vol. 31, no. 1, 1996, pp. 41-50.

Lu W., Howarth A.T., Adam N., and Riffat S.B., "Modelling and measurement of airflow

and aerosol particle distribution in a ventilated two-zone chamber", Pergamon, *Building and Environment*, vol. 31, no. 5, 1996, pp. 417-423.

Ministry of Commerce Thailand, http://www.ops2.moc.go.th/meeting/XcomB10b.xls, accessed January 2007.

Nazaroff W.W., "Indoor Particle Dynamics", *Indoor Air*, 2004, 14 (Supplement 7), pp. 175–183.

Occupational Safety & Health Administration, *Technical Manual, Chapter 3: Ventilation Investigation.* Occupational Safety & Health Administration. [On Line]. Available: http://www.osha.gov/dts/osta/otm/otm_iii/otm_iii_3.html.

Patankar S.V., *Numerical Heat Transfer and Fluid Flow*, USA: Hemisphere Publishing Corporation, 1980.

Promtong M., and Tekasakul P., "CFD study of flow in natural rubber smoking-room: I. Validation with the present smoking-room", *Applied Thermal Engineering*, vol. 27, 2007, pp. 2113–2121.

Purba L. P., Tekasakul P., Maliwan K., and Furuuchi M., "CFD study of flow in a natural rubber smoking cooperative: Turbulence free-convection airflow", *Proceeding of The 22nd Mechanical Engineering Networks of Thailand, MENETT22*, 15th – 17th October 2008, Rangsit, Bangkok, Thailand.

Seinfeld H. S., and Pandis S. N., *Atmospheric Chemistry and Physics: From Air Pollution to Climate Change,* 2nd ed., John Wiley & Sons: New York, 1998.

Sohn C. W., Solberg A., and Gonsoulin T., "Analysis of Numerical Models for Dispersion of Chemical/Biological Agents in Complex Building Environments", 2004. Construction Engineering Research Laboratory, ERDC/CERL TR-04-25.

Sohn M.D., Apte M.G., Sextro R.G., and Lai A.C.K., "Predicting size-resolved particle behaviour in multizone buildings", *Atmospheric Environment*, vol. 41, no. 7, 2007, pp. 1473-1482.

Stratman F., Laakso L., and Herrman E., "Modeling Fluid Flow, Heat/Mass Transfer and Particle Dynamics using FLUENT together with the FPM", Autumn 2006, [Online]. Available: http://www.atm.helsinki.fi/~eherrman/fluent2006/ [Accessed 2007].

Thailand Pollution Control Department (PCD), http://www.pcd.go.th, accessed January 2009.

Tekasakul P., and Promtong M., "Energy efficiency enhancement of natural rubber smoking process by flow improvement using a CFD technique", *Applied Energy*, vol. 85, 2008, pp. 878-895.

Tekasakul P., Furuuchi M., Tekasakul S., Chomanee J., and Otani Y., "Characteristics of PAHs in the Atmospheric Environment of Hat Yai City, Thailand, and Relationship with Rubber-wood Burning in Rubber Sheet Production", *Aerosol and Air Quality Research*, vol. 8, no. 3, 2008, pp.265-278.

Whitby K. T., "The Physical Characteristics of Sulfur Aerosols", *Atmospheric Environment*, vol. 12(1-3), 1978, pp. 135-159.

White F.M., *Fluid Mechanics*, 2nd ed., Singapore: McGraw-Hill Book Company, 1988.

Xu L., "*Effectiveness of Hybrid Air Conditioning System in a Residential House*", PhD thesis, Waseda University, Japan, 2003.

Vincent J.H., *Aerosol Science for Industrial Hygienists*, Great Brittain: Elsevier, 1995.

Zhang Z., and Chen Q., "Experimental measurements and numerical simulations of

particle transport and distribution in ventilated rooms," *Atmospheric Environment*, vol. 40, no. 18, 2006, pp. 3396-3408.

Appendix A.

- **Form Data Collections of Thesis Work**

Table A.1 Log sheet of measurement concentration of smoke particles in a ribbed smoked sheet rubber cooperative

Date ___/_____/_____ Time_____ to_____ Weather _____ AM PM

concentration

Loc.	Filter No	Flow (lpm)	Filter weight (mg) Before	After	Collected	Time (min)	C (mg/m^3)	Wood M/C (%lb)
SA								
SB								
SC								
SD								
P1								H = 1.5 m
P2								H = 3.0 m
P3								H=4.5 m

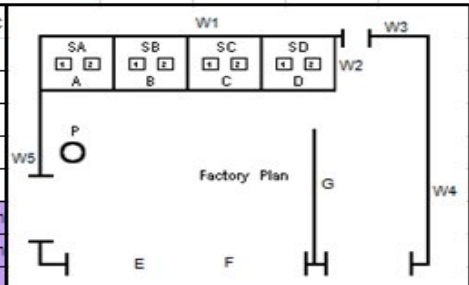

Fuel wood consumption

Room	
Date begin	_____/_____/_____
Date finish	_____/_____/_____
wood prepared	_____kg
wood remained	_____kg
wood used	_____kg
Dry RSS	_____kg

Velocity (m/sec)

Loc.	V1	V2	V3	V4	V5	V6	V7	V8	V9	V10	V11	V12	Vavg
P													
A1													
A2													
B1													
B2													
C1													
C2													
D1													
D2													
E													
F													
G													

Remarks

Wood M/C

Sample	Before	After	Collected
1			0
2			0
3			0
4			0

*Flow Rate >>>at 150 L/min >> A1 = 20.32 cm , A2 = 22.75 cm , A3 = 20.03 cm >>at 150 L/min >> AS = 14.12 cm

Appendix B.

- **Values of velocity from measurement at various locations (measured in m/s)**
- **Values of temperature from measurement at various locations (measured in ^{o}C)**
- **Values of concentration from measurement**
- **Coordinates of the locations for data measurement and simulation**

Table B.1 Values of velocity from measurement at various locations (measured in m/s).

Locations	#1	#2	#3	#4	#5	#6	#7	#8	#9	#10	Vavg	Min	Max	S.D.
P	0.15	0.13	0.14	0.12	0.13	0.13	0.13	0.14	0.14	0.14	0.14	0.12	0.15	0.01
G	0.03	0.02	0.03	0.03	0.02	0.02	0.02	0.02	0.02	0.03	0.02	0.02	0.03	0.01
B1	1.02	1.03	0.90	1.19	1.03	1.08	1.02	1.12	1.03	0.86	1.03	0.86	1.19	0.10
B2	1.01	1.02	1.00	1.00	1.02	1.07	1.02	1.11	1.02	0.96	1.02	0.96	1.11	0.04
IO1	0.78	0.79	0.76	0.80	0.80	0.70	0.98	0.76	0.79	0.70	0.79	0.70	0.98	0.08
IO2	0.49	0.49	0.70	0.40	0.49	0.49	0.51	0.45	0.45	0.45	0.49	0.40	0.70	0.08
IO3.1	0.11	0.15	0.21	0.16	0.12	0.10	0.21	0.12	0.15	0.18	0.15	0.10	0.21	0.04
IO3.2	0.23	0.04	0.12	0.04	0.24	0.23	0.22	0.13	0.04	0.23	0.15	0.04	0.24	0.09
IO3.3	0.25	0.35	0.28	0.27	0.34	0.22	0.54	0.22	0.22	0.33	0.30	0.22	0.54	0.10
IO3.4	0.30	0.33	0.22	0.24	0.24	0.01	0.26	0.30	0.24	0.29	0.24	0.01	0.33	0.09
IO3.5(E)	0.41	0.13	0.43	0.16	0.10	0.44	0.19	0.29	0.03	0.23	0.24	0.03	0.44	0.15
IO3.6	0.65	0.73	0.63	0.68	0.72	0.66	0.66	0.76	0.66	0.71	0.69	0.63	0.76	0.04
IO3.7	0.24	0.23	0.33	0.29	0.21	0.24	0.10	0.26	0.23	0.23	0.24	0.10	0.33	0.06
IO3.8	0.31	0.26	0.22	0.13	0.28	0.19	0.26	0.23	0.25	0.24	0.24	0.13	0.31	0.05
IO3.9	0.65	0.71	0.62	0.69	0.60	0.80	0.71	0.68	0.68	0.71	0.69	0.60	0.80	0.06
IO3.10	0.42	0.16	0.23	0.13	0.16	0.19	0.18	0.14	0.06	0.16	0.18	0.06	0.42	0.09
IO3.11(F)	0.23	0.16	0.20	0.14	0.12	0.19	0.19	0.14	0.11	0.16	0.16	0.11	0.23	0.04
IO3.12	0.51	0.03	0.84	0.42	0.52	0.05	0.32	0.90	0.09	1.27	0.50	0.03	1.27	0.41
IO3.13	0.30	0.13	0.29	0.19	0.26	0.03	0.16	0.21	0.06	0.27	0.19	0.03	0.30	0.09
IO3.14	0.15	0.20	0.15	0.15	0.15	0.15	0.20	0.04	0.13	0.19	0.15	0.04	0.20	0.05
IO3.15	0.51	0.41	0.50	0.40	0.30	0.40	0.35	0.09	0.06	0.79	0.38	0.06	0.79	0.21
IO3.16	0.51	0.61	0.71	0.61	0.61	0.63	0.64	0.62	0.71	0.63	0.63	0.51	0.71	0.06
IO4.1	0.50	0.34	0.35	0.30	0.30	0.30	0.35	0.35	0.30	0.37	0.35	0.30	0.50	0.06
IO4.2	0.50	0.35	0.35	0.35	0.30	0.30	0.30	0.30	0.32	0.35	0.34	0.30	0.50	0.06
IO4.3	0.50	0.30	0.35	0.35	0.35	0.25	0.35	0.35	0.30	0.30	0.34	0.25	0.50	0.07
IO4.4	0.50	0.40	0.30	0.40	0.30	0.35	0.25	0.35	0.34	0.35	0.35	0.25	0.50	0.07
IO4.5	0.50	0.40	0.30	0.40	0.33	0.33	0.30	0.35	0.33	0.30	0.35	0.30	0.50	0.06
IO.5	0.40	0.35	0.30	0.35	0.35	0.37	0.35	0.37	0.35	0.33	0.35	0.30	0.40	0.03
IO6.1	0.02	0.01	0.02	0.01	0.02	0.01	0.02	0.01	0.01	0.01	0.01	0.01	0.02	0.01
IO6.2	0.01	0.01	0.00	0.00	0.00	0.00	0.00	0.01	0.01	0.00	0.00	0.00	0.01	0.01
IO6.3	0.01	0.01	0.00	0.00	0.00	0.00	0.00	0.00	0.01	0.01	0.00	0.00	0.01	0.01
IO6.4	0.01	0.01	0.00	0.00	0.00	0.00	0.00	0.00	0.01	0.01	0.00	0.00	0.01	0.01
IO6.5	0.01	0.02	0.01	0.02	0.01	0.02	0.01	0.02	0.01	0.01	0.01	0.01	0.02	0.01

Remarks: '#' = Measurement periode
'avg' = average
'1, 2, …, '10 = number of average data measurement from about three times of measurements
'Min' = Lower band
'Max' = Upper band
'S.D.' = Standard deviation

Table B.2 Values of temperature from measurement at various locations (measured in Celcius).

Location	#1	#2	#3	#4	#5	#6	#7	#8	#9	#10	Tavg	Min	Max	S.D.
P	31.1	32.7	34.6	34.0	30.3	34.1	32.7	32.7	32.7	32.0	32.7	30.3	34.6	1.33
G	33.2	25.7	31.7	31.4	29.2	33.0	43.8	42.8	33.8	33.0	33.8	25.7	43.8	5.59
B1	48.0	60.5	51.4	47.3	61.9	47.0	41.8	41.8	48.7	38.7	48.7	38.7	61.9	7.59
B2	47.0	60.1	52.1	47.2	62.2	46.9	35.8	35.8	48.6	49.5	48.5	35.8	62.2	8.59
IO1	29.2	32.0	30.3	29.7	34.3	35.3	29.7	30.6	31.5	32.1	31.5	29.2	35.3	2.03
IO2	30.0	33.2	28.9	33.8	32.8	31.8	30.1	28.9	31.6	34.8	31.6	28.9	34.8	2.08
IO3.1	30.0	34.4	29.6	34.3	34.4	32.9	29.4	28.9	32.0	33.8	32.0	28.9	34.4	2.29
IO3.2	32.1	32.2	32.1	32.2	32.2	32.1	32.1	32.3	32.4	32.4	32.2	32.1	32.4	0.12
IO3.3	30.2	30.0	30.0	30.3	29.3	30.4	30.4	30.0	29.8	30.0	30.0	29.3	30.4	0.33
IO3.4	30.1	30.2	30.3	30.4	30.8	30.2	30.1	29.0	30.1	29.2	30.0	29.0	30.8	0.54
IO3.5(E)	30.1	30.2	30.4	30.3	30.1	29.4	30.0	29.9	30.2	29.8	30.0	29.4	30.4	0.29
IO3.6	32.6	32.2	32.5	32.6	32.5	32.7	33.0	32.5	32.2	32.6	32.5	32.2	33.0	0.23
IO3.7	31.9	35.5	35.3	34.8	35.5	33.2	34.4	34.6	35.5	32.6	34.3	31.9	35.5	1.31
IO3.8	31.7	34.6	34.8	33.1	32.5	34.6	33.5	33.5	33.5	32.6	33.4	31.7	34.8	1.02
IO3.9	30.7	32.5	30.5	32.7	30.8	34.0	32.5	34.5	33.5	32.7	32.4	30.5	34.5	1.39
IO3.10	34.5	33.2	33.8	33.0	32.6	34.8	34.4	33.3	34.9	35.8	34.0	32.6	35.8	1.01
IO3.11(F)	28.1	34.0	34.0	31.7	32.9	33.5	33.2	32.2	35.0	33.3	32.8	28.1	35.0	1.90
IO3.12	32.1	36.5	32.4	31.6	31.9	33.0	33.0	31.4	32.9	33.0	32.8	31.4	36.5	1.44
IO3.13	31.4	33.0	35.3	32.1	36.2	33.4	29.6	30.0	33.2	33.4	32.8	29.6	36.2	2.09
IO3.14	28.5	32.5	29.9	31.3	29.2	33.4	29.4	28.9	44.8	32.0	32.0	28.5	44.8	4.80
IO3.15	28.5	32.9	29.9	31.6	31.2	33.4	33.0	31.6	31.5	31.5	31.5	28.5	33.4	1.47
IO3.16	34.4	32.5	34.3	33.9	35.2	35.1	34.4	33.7	33.9	31.4	33.9	31.4	35.2	1.16
IO4.1	32.1	34.2	32.0	31.2	33.2	33.4	33.6	35.5	33.2	33.6	33.2	31.2	35.5	1.21
IO4.2	33.4	32.9	35.0	32.0	35.4	35.5	34.6	35.5	35.5	35.8	34.6	32.0	35.8	1.32
IO4.3	34.4	32.7	36.2	31.0	33.7	35.8	33.9	32.5	34.3	34.5	33.9	31.0	36.2	1.55
IO4.4	33.5	34.4	35.6	35.0	35.6	33.6	34.0	33.7	35.5	34.6	34.6	33.5	35.6	0.84
IO4.5	34.3	32.7	32.8	32.0	33.5	33.8	34.8	30.6	33.8	33.7	33.2	30.6	34.8	1.24
IO.5	29.5	34.4	28.8	33.3	32.8	33.2	31.4	28.9	31.4	30.3	31.4	28.8	34.4	2.00
IO6.1	32.6	34.1	33.2	33.0	34.8	35.8	36.8	36.4	35.1	35.7	34.8	32.6	36.8	1.47
IO6.2	33.4	33.2	36.2	32.9	35.4	34.8	35.4	36.2	35.0	34.8	34.8	32.9	36.2	1.19
IO6.3	35.6	35.1	35.9	36.6	35.6	35.7	35.6	36.4	35.0	35.9	35.8	35.0	36.6	0.50
IO6.4	35.8	35.1	36.3	31.5	35.5	34.4	36.1	31.5	34.6	35.4	34.6	31.5	36.3	1.76
IO6.5	35.4	34.8	32.4	32.4	36.9	35.3	36.3	36.2	35.0	35.4	35.0	32.4	36.9	1.52

Remarks: '#' = Measurement periode
'avg' = average
'1, 2, …, '10 = number of average data measurement from about three times of measurements
'Min' = Lower band
'Max' = Upper band
'S.D.' = Standard deviation

Table B.3 Values of concentration from measurement.

Measurement Date	Concentration (mg/m3)		
	P1 (1.5 m)	P2 (3.0 m)	P3 (4.5 m)
21/11/2007	0.0345	0.0355	0.1150
15/12/2007	0.0845	0.1140	0.3410
8/1/2008	0.0895	0.1160	0.2760
16/1/2008	0.0733	0.1022	0.3000
22/1/2008	0.0750	0.1200	0.3300
28/2/2008	0.0750	0.1150	0.3630
29/2/2008	0.0760	0.1100	0.3080
29/2/2008	0.0785	0.1050	0.3670
AVERAGE	0.0733	0.1022	0.3000

Table B.4 Coordinates of the locations for data measurement and simulation.

Location	x (m)	y (m)	z (m)
E	9.36	-1.30	22.00
F	15.04	-1.30	22.00
G	20.00	-2.00	12.00
P	1.00	-3.00	12.00
P1	1.00	-2.50	12.00
P2	1.00	-1.00	12.00
P3	1.00	0.50	12.00
IO1	21.55	-2.80	4.00
IO2	22.20	-2.60	22.00
IO3.1	6.25	-0.50	22.00
IO3.2	6.52	-1.30	22.00
IO3.3	6.50	-2.10	22.00
IO3.4	9.36	-0.50	22.00
IO3.5	9.36	-1.30	22.00
IO3.6	9.36	-2.10	22.00
IO3.7	12.20	-0.50	22.00
IO3.8	12.20	-1.30	22.00
IO3.9	12.20	-2.10	22.00
IO3.10	15.04	-0.50	22.00
IO3.11	15.04	-1.30	22.00
IO3.12	15.04	-2.10	22.00
IO3.13	17.80	-0.50	22.00
IO3.14	17.80	-1.30	22.00
IO3.15	17.80	-2.10	22.00
IO3.16	17.80	-3.30	22.00
IO4.1	2.66	0.56	22.00
IO4.2	7.58	0.56	22.00
IO4.3	12.50	0.56	22.00
IO4.4	17.42	0.56	22.00
IO4.5	22.34	0.56	22.00
IO5	0.00	-1.75	20.15
IO6.1	2.66	0.00	1.00
IO6.2	7.58	0.00	1.00
IO6.3	12.50	0.00	1.00
IO6.4	17.42	0.00	1.00
IO6.5	22.34	0.00	1.00
L	8.30	3.90 (Case 1 and 2); 4.04 (Case 3 and 4)	11.00 (Case 1, 2, 3 and 4)
M	8.30		7.70 (Case 1 and 2); 9.10 (Case 3 and 4)
N	8.30		12.90 (Case 1 and 2); 14.30 (Case 3 and 4)

Appendix C.

- **Discretization by using Finite Volume Method**

Appendix C. Discretization by using Finite Volume Method

Discretization process of Eqs. 10 is explained below (Costa et. al., 2005). By integrating the Eqs. 5 over a cubic volume of dimensions Δx, Δy, Δz (only two-dimensional view is shown for convenience) and over time (interval between t and t + Δt) we obtain discretized equations. The integration process is called discretization. The discretization equation expresses the conservation principle for the variables inside the control volume, (Fig. C.1).

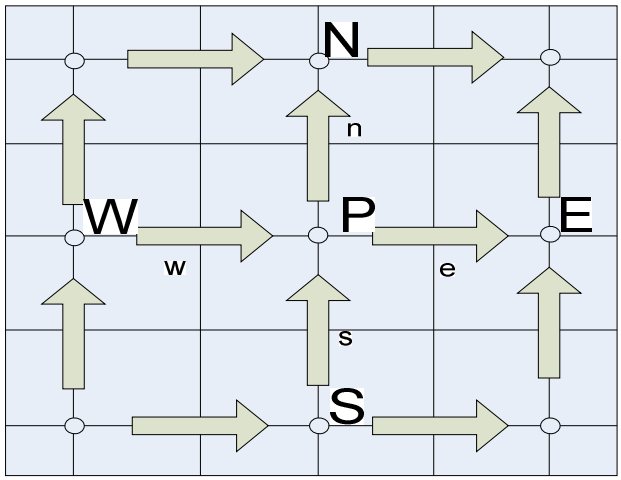

Fig. C.1 Representation of control volume to be treated by Finite Volume Method.

$$\int_{v,t}\frac{\partial}{\partial t}(\rho\Phi)dvdt+\int_{v,t}\frac{\partial}{\partial x}(\rho u\Phi)dvdt+\int_{v,t}\frac{\partial}{\partial y}(\rho v\Phi)dvdt+\int_{v,t}\frac{\partial}{\partial z}(\rho w\Phi)dvdt=$$
$$\int_{v,t}\frac{\partial}{\partial x}(\Gamma_\Phi\frac{\partial\Phi}{\partial x})dvdt+\int_{v,t}\frac{\partial}{\partial y}(\Gamma_\Phi\frac{\partial\Phi}{\partial y})dvdt+\int_{v,t}\frac{\partial}{\partial z}(\Gamma_\Phi\frac{\partial\Phi}{\partial z})dvdt+\int_{v,t}S_\Phi dvdt \qquad \text{(C1)}$$

Integration of Eqs. C1 results in:

$$\frac{M_P\Phi_P - M_P^o\Phi_P^o}{\Delta t} + \dot{M}_e\Phi_e^\theta - \dot{M}_w\Phi_w^\theta + \dot{M}_n\Phi_n^\theta - \dot{M}_s\Phi_s^\theta = D_1\left[\frac{\partial\Phi}{\partial x}\right]_e^\theta - D_1\left[\frac{\partial\Phi}{\partial x}\right]_w^\theta + D_2\left[\frac{\partial\Phi}{\partial y}\right]_e^\theta - D_2\left[\frac{\partial\Phi}{\partial y}\right]_w^\theta + D_3\left[\frac{\partial\Phi}{\partial z}\right]_e^\theta - D_3\left[\frac{\partial\Phi}{\partial z}\right]_w^\theta + L\left[S_\Phi\right]^\theta \quad \text{(C2)}$$

The process of integration described by Eqs. C1 and C2 is named discretization. Eqs. C2 and other similar equations obtained by this type of process are known as discretized equations. From Eqs. C2, we have

$$M_P = \rho\Delta x\Delta y\Delta z$$
$$M_P = \rho^o\Delta x\Delta y\Delta z \quad \text{(C3)}$$

$$\dot{M}_e = [\rho\Delta y\Delta z]_e$$
$$\dot{M}_w = [\rho u\Delta x\Delta y\Delta z]_w \quad \text{(C4)}$$

$$\dot{M}_n = [\rho v\Delta x\Delta z]_n$$
$$\dot{M}_s = [\rho v\Delta x\Delta z]_s \quad \text{(C5)}$$

$$D_{1e} = [\Gamma_\Phi\Delta y\Delta z]_e$$
$$D_{1w} = [\Gamma_\Phi\Delta y\Delta z]_w \quad \text{(C6)}$$

$$D_{2n} = [\Gamma_\Phi\Delta x\Delta z]_n$$
$$D_{2s} = [\Gamma_\Phi\Delta x\Delta z]_s \quad \text{(C7)}$$

From the previous equations the superscript "o" stands for the time t and no superscript stands for the time t + Δt. The superscript "θ" stands for a time between t and t + Δt. In this time the ϕ variable is weighted by θ value (between 0 and 1):

$$\Phi^\theta = \theta\Phi + (1-\theta)\Phi^o \quad \text{(C8)}$$

By referring to Eqs. C2, the volume face values are weighted by the adjacent volume values:

$$\Phi_e = (\frac{1}{2} + \alpha_e)\Phi_P + (\frac{1}{2} - \alpha_e)\Phi_E \tag{C9}$$

$$\Phi_w = (\frac{1}{2} + \alpha_w)\Phi_w + (\frac{1}{2} - \alpha_w)\Phi_P \tag{C10}$$

$$\Phi_n = (\frac{1}{2} + \alpha_n)\Phi_P + (\frac{1}{2} - \alpha_n)\Phi_N \tag{C11}$$

$$\Phi_s = (\frac{1}{2} + \alpha_s)\Phi_s + (\frac{1}{2} - \alpha_s)\Phi_P \tag{C12}$$

Similarly, the face gradient values for ϕ are weighted by the β variable:

$$[\frac{\partial \Phi}{\partial x}]_e = \beta_e(\frac{\Phi_E - \Phi_P}{\Delta x_e}) \tag{C13}$$

$$[\frac{\partial \Phi}{\partial x}]_w = \beta_w(\frac{\Phi_P - \Phi_W}{\Delta x_w}) \tag{C14}$$

$$[\frac{\partial \Phi}{\partial x}]_n = \beta_n(\frac{\Phi_N - \Phi_P}{\Delta y_n}) \tag{C15}$$

$$[\frac{\partial \Phi}{\partial x}]_s = \beta_s(\frac{\Phi_P - \Phi_S}{\Delta y_s}) \tag{C16}$$

The case for which α = 0 and β = 1 is named central difference scheme. This scheme is commonly employed for pure conduction problems. The case for which β = 0 and α = 0.5 or α = -0.5 is named upwind scheme for positive and negative

velocities, respectively. The last term from equation corresponds to the last integral on equation. We are going to assume that:

$$L[S_\Phi] = [S_P \Phi_P^o + S_C]\Delta V \tag{C17}$$

where Sp and Sc are coefficient defined according to Φ. ΔV is the volume $\Delta x\ \Delta y\ \Delta z$.

Using Eqs. C3 to Eqs. C17 and the discretized mass conservation equation (underlined below), Eqs. C2 becomes:

$$\begin{aligned}
&\frac{M_P \Phi_P}{\Delta t} + \Phi_P^\theta [\dot{M}_e(\frac{1}{2}+\alpha_e) - \dot{M}_w(\frac{1}{2}-\alpha_e) + \dot{M}_n(\frac{1}{2}+\alpha_n) - \dot{M}_s(\frac{1}{2}-\alpha_s) - \\
&S_P \Delta V + [\frac{D_1\beta}{\Delta x}]_e + [\frac{D_1\beta}{\Delta x}]_w + [\frac{D_2\beta}{\Delta y}]_n + [\frac{D_2\beta}{\Delta y}]_s - \\
&\underline{\frac{\mathrm{M_P} - \mathrm{M_P^o}}{\Delta \mathrm{t}} - \dot{\mathrm{M}}_\mathrm{e} + \dot{\mathrm{M}}_\mathrm{w} - \dot{\mathrm{M}}_\mathrm{n} + \dot{\mathrm{M}}_\mathrm{s} =} \\
&\Phi_E^\theta [-(\frac{1}{2}-\alpha_e)\dot{M}_e + [\frac{D_1\beta}{\Delta x}]_e] + \Phi_W^\theta [(\frac{1}{2}+\alpha_w)\dot{M}_w + [\frac{D_1\beta}{\Delta x}]_w] + \\
&\Phi_N^\theta [-(\frac{1}{2}-\alpha_n)\dot{M}_n + [\frac{D_2\beta}{\Delta y}]_n] + \\
&\Phi_S^\theta [(\frac{1}{2}+\alpha_s)\dot{M}_s + [\frac{D2\beta}{\Delta y}]_s] + \frac{M_P^o \Phi_P^o}{\Delta t} + S_C \Delta V
\end{aligned} \tag{C18}$$

Collecting the Φ coefficients:

$$\frac{M_P \Phi_P}{\Delta t} + A_P^* \Phi_P^\theta = A_e \Phi_E^\theta + A_w \Phi_W^\theta + A_n \Phi_N^\theta + A_s \Phi_S^\theta + \frac{M_P^o \Phi_P^o}{\Delta t} + S_C \Delta V \tag{C19}$$

where

$$A_P^* = A_e + A_w + A_n + A_s - S_C \Delta V - \frac{M_P}{\Delta t} + \frac{M_P^o}{\Delta t} \tag{C20}$$

$$A_e = -(\frac{1}{2}-\alpha_e)\dot{M}_e + [\frac{D_1\beta}{\Delta x}]_e \tag{C21}$$

$$A_w = (\frac{1}{2} + \alpha_w)\dot{M}_w + [\frac{D_1\beta}{\Delta x}]_w \tag{C22}$$

$$A_n = -(\frac{1}{2} - \alpha_n)\dot{M}_n + [\frac{D_2\beta}{\Delta y}]_n \tag{C23}$$

$$A_s = (\frac{1}{2} + \alpha_s)\dot{M}_s + \left[\frac{D_2}{\Delta y}\right]_s \tag{C24}$$

The Eqs. C19 for $\theta = 0$ (explicit formulation) becomes:

$$\frac{M_P\Phi_P}{\Delta t} = \Phi_P^o\left(\frac{M_P^o}{\Delta t} - A_P^*\right) + \sum A_{nb}\Phi_{NB}^o + S_C\Delta V \tag{C25}$$

And for $\theta = 1$ (fully implicit):

$$A_P\Phi_P = \sum A_{nb}\Phi_{NB} + \frac{M_P^o\Phi_P^o}{\Delta t} + S_C\Delta V \tag{C26}$$

where

$$A_P = \sum A_{nb} - S_P\Delta V + \frac{M_P^o}{\Delta t} \tag{C27}$$

Appendix D.

- **Step by step calculation of particle concentration distribution in side of ribbed smoked sheet rubber cooperative (SPE Simulation)**

Appendix D.

Step by step calculation of particle concentration distribution in side of ribbed smoked sheet rubber cooperative (SPE Simulation)

SECTION 1.

Step 1: Preparation for Grid profile.

1.Create file:

2007.12.14_PATRON.GEOVersion02.2008.02.08_fullscaled_b_TetHybrid_TGrid_0.1.dbs and

2007.12.14_PATRON.GEOVersion02.2008.02.08_fullscaled_b_TetHybrid_TGrid_0.1.msh in GAMBIT.

Step 2: Preparation for FLUENT Calculation

With the

2007.12.14_PATRON.GEOVersion02.2008.02.08_fullscaled_b_TetHybrid_TGrid_0.1.dbs file creation completed, SPE model of FLUENT is used and predict particle concentration distribution in the ribbed smoked sheet rubber cooperative.

1. Copy the file

2007.12.14_PATRON.GEOVersion02.2008.02.08_fullscaled_b_TetHybrid_TGrid_0.1.msh GAMBIT to working directory.

The mesh file

2007.12.14_PATRON.GEOVersion02.2008.02.08_fullscaled_b_TetHybrid_TGrid_0.1.msh is a tetrahedral mesh describing the ribbed smoked sheet rubber cooperative system

geometry. Mesh file had been created by GAMBIT, which is a software package designed to help analysis and designers build and mesh models for computational fluid dynamics (CFD).

2. Start the 3DDP version of FLUENT.

Step 3: Grid check and validation

1. Read the grid file 2007.12.14_PATRON.GEOVersion02.2008.02.08_fullscaled_b_TetHybrid_TGrid_0.1.msh into FLUENT. As FLUENT reads the grid file, messages will appear in the console window reporting progress and information about the mesh. The meshes volume type was tetrahedral fluid cells.

2. Check the grid.

3. Display the grid.

SECTION 2.

Step 4: Models

1. Click Define – Model – Solver - Pressure Based Solver.

2. Activate the Energy conservation by Click: Define – Model – Energy – enabled Energy - OK.

3. Turn on the $k - e$ 2 equations turbulence model by click:

Define – Model – Viscous – k-epsilon (2 eqn) and the Model Constants are (by default of FLEUNT based on Launder and Spalding: Cmu = 0.09, C1-Epsilon = 1.44, C2-Epsilon = 1.92, TKE Prandtl number = 1, TDR Prandtl number = 1.3, Energy Prandtl

Number = 0.85, Wall Prandtl Number = 0.85; Model: Standard; Standard Wall Function for Near-Wall Treatment.

4. Enable Species Model of FLUENT to display particle or aerosol particle concentration distribution and or Discrete Phase Model.

Step 5a: Materials (fluid)

1. Select Materials: air in the drop down list of Density and use the default material properties as of FLUENT database [1.225 for Density (kg/ m^3), 0.0242 for Thermal Conductivity (w/m-K), 1.7894e-05 for Viscosity (kg/m-s)].

2. Click the Change/Create button.

Here, all material properties are assumed to be constant values for air because the incompressible fluid flow modeling and that is adequate since the fluid flow is turbulent flows.

Step 5b: Materials (mixture: carbon-monoxide-air)

1. Click edit for Mixture species: co and air.

2. Use all material properties as of FLUENT database. [Density (kg/m3): incompressible-ideal-gas, Cp(j.kg-j): mixing-law, Thermal conductivity (w/m-k): 0.0454, Viscosity (kg/m-s): 1.72e-05, Mass diffusivity(m2/s) : constant-dilute-appx].

3. Click the Change/Create button.

Step 6: Operating Conditions

1. Click Define – Operating Condition to define Operating Conditions of the Numerical Calculation.

2. Pressure: Operating Pressure (pascal) = 101325.

3. Gravity: Enter -9.81 for Y(m/s^2) and leave 0 for X(m/s^2) and Z(m/s^2), because influence of gravity is only for Y direction.

4. Enter 40.1 for Operating Temperature (C) of Boussinesq Parameter after enabled Gravity. This value is derived by summation of the maximum temperature (48.7 C) and the minimum temperature (31.5 K) from available data measurement devided by two.

5. Enter 22.2 for X(m), -1.25 for Y(m), and 22 for Z(m) for the Reference Pressure Location. Because the fluid that want to models are incompressible fluid [air (gas) flows, and smoke particles flows], and that is why do not involved any pressure boundaries so the adjustment of Reference Pressure Location is needed. The default values of Reference Pressure Location are zeros.

6. Click OK.

Step 7: Boundary Conditions

Select each boundary zone and click the Set... button to define boundary conditions, as detailed belows.

1. Set the velocity-inlet following conditions for velocity_inlet.7 to define B1. Then enter 1.03 for Y-Velocity (m/s) of Momentum drop down list, and enter 48.7 for Temperature (C) of Thermal drop down list, Enter 3.41e-06 for Species Boundary (Species mass fractions).

2. Set the velocity-inlet following conditions for velocity_inlet.8 for defined B2. Then enter 1.02 for Y-Velocity (m/s) of Momentum drop down list, and enter 48.5 for Temperature (C) of Thermal drop down list, Enter 3.41e-06 for Species Boundary (Species mass fractions).
3. Set the pressure-outlet following conditions for IO1 until IO6 to define Thermal boundaries by enter 31.5 for Temperature (C) of Thermal drop down list of IO1, 31.6 for Temperature (C) of Thermal drop down list of IO2, 32.3 for Temperature (C) of Thermal drop down list of IO3, 33.9 for Temperature (C) of Thermal drop down list of IO4, 31.4 for Temperature (C) of Thermal drop down list of IO5, and 35.0 for Temperature (C) of Thermal drop down list of IO6. For Species boundary: zero.
4. Set stationary wall for the wall motion and no slip for shear condition in the Momentum drop down list. For Thermal dropdown list of W1 enter 46.8 for Temperature (C), W2 enter 44.1for Temperature (C), W3 enter 33.9 for Temperature (C), W4 enter 42.2 for Temperature (C), W5 enter 32.1 for Temperature (C), WB enter 36.4 for Temperature (C), Wfloor enter 32.5 for Temperature (C), and Wroof enter 39.8 for Temperature (C). For species boundary by default: Zero Diffusive Flux.
5. Note: need to set TDR and TKE for both boundaries Velocity-inlet and Pressure-outlet. Set as default of FLUENT.

Step 8: Solution Controls

1. Flow, Turbulence, and Energy are solved simultaneously.

2. Under-Relaxation Factors as Pressures = 0.3, Density = 1, Body Forces = 1, Momentum = 0.05, Turbulent Kinetic Energy = 0.8, Turbulent Dissipation Rate = 0.8, Turbulent Viscosity = 1, co = 0.8, Energy = 1.
3. SIMPLE is selected from drop down list of Pressure-Velocity Coupling.
4. Set Standard for Pressure but First Order Upwind for -Momentum, -Turbulent Kinetic Energy, -Turbulent Dissipation Rate and -Energy in the Discretization drop down list.

Step 9: Solution Initialization

1. Select B1 in the Compute From list (optional)
2. Enter 0.09 for Y-Velocity (m/s).
3. Enter 31.8 for Temperature (C).
4. Click Init to initialize the flow field and OK.

Step 10: Residual Monitors

Enable the plotting of residuals during the calculation, retaining the default Convergence criteria.

1. Enable Plot under Options and then click OK.

Step 11: Save, Start Calculation

1. Save the case file (PATRON.GEO.02_2008.05.06_Thesis lasman airflow in a RSSC_ST4_0370convergent.cas).

2. Start the calculation by requesting 2000 iterations.

3. The solution converged in about 370 iterations. Save the case and data files (PATRON.GEO.02_2008.05.06_Thesis lasman airflow in a RSSC_ST4_0370convergent.cas). (PATRON.GEO.02_2008.05.06_Thesis lasman airflow in a RSSC_ST4_0370convergent.dat).

Step 12: Postprocessing

1. Display the airflow contains smoke particles simulation (mainly for contour or image of particle concentration distribution in the ribbed smoked sheet rubber cooperative). As an optional: this FLUENT model also possible to display flow pattern, temperature distribution, and particle trajectories.
2. Export ASCII file to the EXCELL file to find the values of source of concentration at B1, B2 and workplaces concentrations at P1, P2, and P3 of simulation in order to compare with the available data measurements (from range of values and or from exact values which indicated by the exact coordinates).
3. Make conclusion after performs the simulation result.

Appendix E.

- **Meshing of the geometry**

Appendix E: Meshing of the geometry

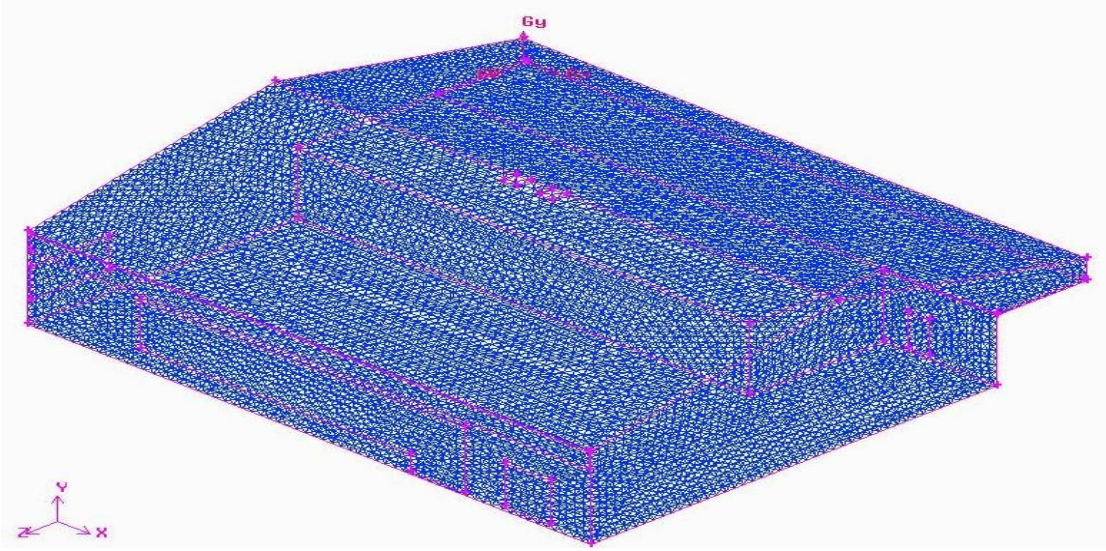

Fig E.1 The meshing of the ribbed smoked sheet rubber cooperative geometry using GAMBIT: isometric view.

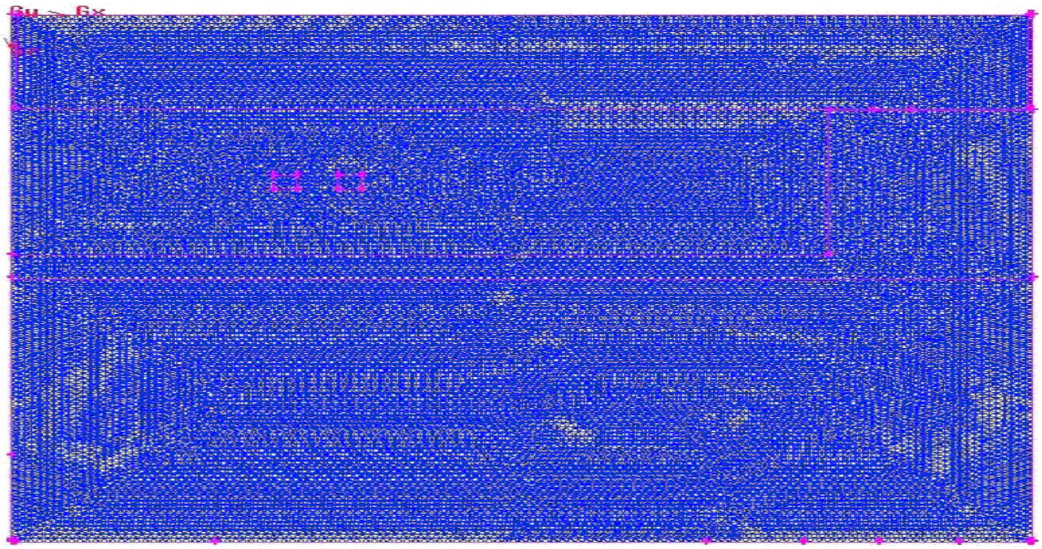

Fig E.2 The meshing of the ribbed smoked sheet rubber cooperative geometry using GAMBIT: top view.

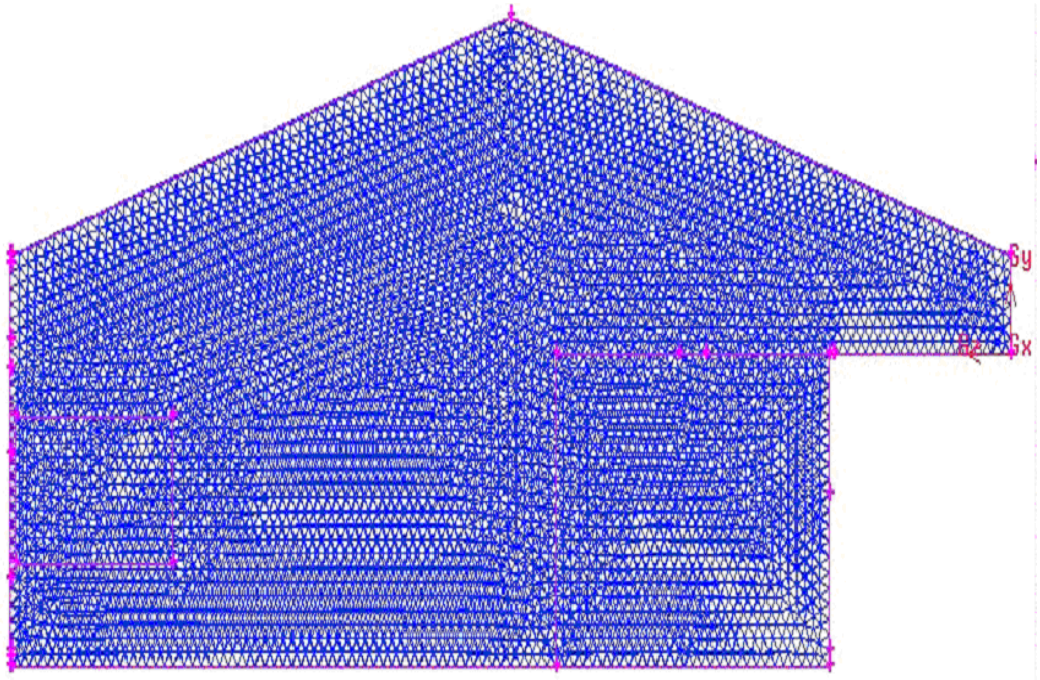

Fig E.3 The meshing of the ribbed smoked sheet rubber cooperative geometry using GAMBIT: view from direction-c.

Table E.1 Result of geometry history design and boundary conditions in GAMBIT.

elements	type	smoother	spacing	sources	Results	Possibility of Solutions
HEX	MAP	None	0.6	NA	ERROR: Entity V.5 can not be mesh on lower entity f.79	done
			0.15	NA	f.77	done
			0.1; 1.0; 1.0	NA	f.75; f68; f67	done

Hex	Sub map	NA	1.0; 0.6	NA	F67; F62	done
Hex	Tet primitive	NA	0.6	NA	Connectivity for v.5 does not allow meshing using the tetrahedral primitive scheme	done
Hex	cooper	NA	0.6; 1.0	F.63; 67; 68; 69 = all from 4th ventilating lids	F38, 37, 57, 5, 42, 53, 24, 22 is Not appropriate for use as a face to project along. Either it is not sub mapped or the choice of source faces is incorrect	done
HEX	STAIRSTEP	NA	1.0; 0.6; 2.0	NA	Successfully meshed V.5. Created faceted volume (s). F_volume.6 with mesh volumes = 5564	not as a real geometry of the RSC
HEX/wedge	cooper	NA	0.6	NA	F38, 37, 57, 5, 42, 53, 24, 22 is Not appropriate for use as a face to project along. Either it is not sub mapped or the choice of source faces is incorrect	done
Tet/hybrid	hexcore	NA	0.6	NA	Mesh generated for v.5: mesh volumes = 47457. Contains 16 highly skewed	done

					element (EQUISIZE SKEW > 0.97)	
Tet/hybrid	tgrid	na	0.6; 1	NA	Mesh generated for v.5: mesh volumes = 51780. Contains 11 highly skewed element (EQUISIZE SKEW > 0.97)	done
…	…	…	…	…	…	…
Tet/hybrid	tgrid	na	0.2	NA	Mesh generated for v.10: 2,159,347	done
Tet/hybrid	tgrid	na	0.25	NA	Mesh generated for v.10: 712,469	done
Tet/hybrid	tgrid	na	0.3	NA	Mesh generated for v.10: 629,202	done
Tet/hybrid	tgrid	na	0.4	NA	Mesh generated for v.10: 141,145	done

VITAE

Name Mr. Lasman Parulian Purba

Student ID 4910120113

Educational Attainment

Degree	Name of Institution	Year of Graduation
ST (Ina) = B.Sc (Eng)	Sepuluh Nopember Institute of Technology Surabaya, ITS Surabaya, Indonesia	2000

Scholarship Awards during Enrollment

The NRCT-JSPS (National Research Council of Thailand - Japan Society for the Promotion of Science) Joint Research Program.

Work – Position and Address (If Possible)

Research Assistant in the field of CFD Simulation of an Empty Rubber Sheet Smoking Room (RSSR) Model Dryer with Heaters Off and with Heaters On; Workshop of Energy Engineering Research, Mechanical Engineering Department, Engineering Faculty, Prince of Songkla University, THAILAND

List of Publication and Proceeding

[1]. Purba L. P., Tarigan E., "Airflow Modeling: Effort to find better models for building air quality simulation", *Proceedings: International Conference on Risk Technology & Management, RISKTech2007*, 20th – 22nd March 2007, Bandung, Indonesia.

[2]. Purba L. P., Tekasakul P., Maliwan K., and Furuuchi M., "CFD study of flow in a natural rubber smoking cooperative", *Poster Session of The 6-th PSU Engineering Conference (PEC-6)*, 08th – 09th May 2008, Hat Yai, Thailand.

[3]. Purba L. P., Tekasakul P., Maliwan K., and Furuuchi M., "CFD study of flow in a natural rubber smoking cooperative: Turbulence free-convection airflow", *Proceeding of The 22nd Mechanical Engineering Networks of Thailand, MENETT22*, 15th – 17th October 2008, Rangsit, Bangkok, Thailand.

[4]. Purba L. P., and Tekasakul P., "CFD study of flow in a ribbed smoked sheet rubber cooperative: I. Validation with the present natural ribbed smoked sheet rubber cooperative", In Process.